



Catalysis Reviews

Science and Engineering

ISSN: (Print) (Online) Journal homepage: www.tandfonline.com/journals/lctr20

Recent advances in Fischer-Tropsch synthesis using cobalt-based catalysts: a review on supports, promoters, and reactors

Zahra Gholami, Zdeněk Tišler & Vlastimil Rubáš

To cite this article: Zahra Gholami, Zdeněk Tišler & Vlastimil Rubáš (2021) Recent advances in Fischer-Tropsch synthesis using cobalt-based catalysts: a review on supports, promoters, and reactors, *Catalysis Reviews*, 63:3, 512-595, DOI: [10.1080/01614940.2020.1762367](https://doi.org/10.1080/01614940.2020.1762367)

To link to this article: <https://doi.org/10.1080/01614940.2020.1762367>



Published online: 18 May 2020.



Submit your article to this journal [↗](#)



Article views: 4527



View related articles [↗](#)



View Crossmark data [↗](#)



Citing articles: 89 View citing articles [↗](#)



Recent advances in Fischer-Tropsch synthesis using cobalt-based catalysts: a review on supports, promoters, and reactors

Zahra Gholami , Zdeněk Tišler, and Vlastimil Rubáš

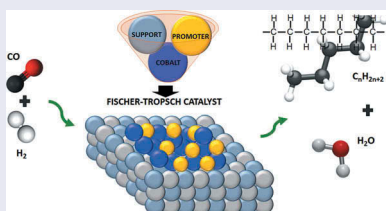
Unipetrol Centre of Research and Education, Litvínov, Czech Republic

ABSTRACT

Fischer–Tropsch (FT) process is a promising method for producing liquid fuels and other valuable chemicals through CO hydrogenation. The catalyst activity and product selectivity can be strongly affected by different parameters such as support and promoters. The physicochemical and textural properties of the support affect the metal–support interaction, crystallite size, metal dispersion, mass transfer of reactants/products, mechanical strength, and thermal stability of the catalyst. Promoters can also be used as structural, textural, electronic modifier, stabilizers, and catalyst-poison-resistant, which can improve the catalytic performance. According to the parameters mentioned above, this paper reviews the brief history of the FT process, the effect of different supports and promoters on the catalytic performance of cobalt-based catalysts. In addition to the catalyst properties, the reactor must also be designed appropriately to handle the heat of this highly exothermic reaction. The reactor types have also been reviewed and compared as a crucial part of the catalytic reactions.

KEYWORDS

Fischer–Tropsch; cobalt catalyst; support; promoter; reactor

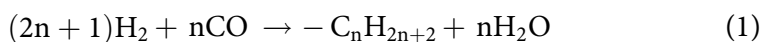


1. Introduction

The impending depletion of fossil fuel sources and the increasing demand for energy resources due to the increasing population and economic development have led to new approaches for producing of renewable liquid fuels. Fossil fuel consumption is the main reason for environmental issues, such as global warming and climate change. The high level of local air pollution is also caused by the high consumption of fossil fuels, especially by power plants and motor vehicles.^[1,2] In

CONTACT Zahra Gholami  Zahra.Gholami@unicre.cz  Unipetrol Centre of Research and Education, a.s, Areál Chempark 2838, Záluží 1, 436 70 Litvínov, Czech Republic

recent years, the production cost has gradually decreased with the increase of available technologies for producing renewable energy.^[3] Researchers in industry and academia are attempting to find an alternative and clean energy. The X to liquid (XTL) technologies for converting different carbon-containing sources, such as natural gas (GTL), coal (CTL), biomass (BTL), and waste/oil residues (WTL), to liquid fuels have been studied extensively to achieve this goal.^[4] Carbonaceous resources are transformed into syngas (H_2 and CO) through one of these technologies and then converted to a wide range of hydrocarbons; these hydrocarbons are refined to obtain the final products, including liquefied petroleum gas (LPG), gasoline, jet fuel, distillate, diesel, and wax.^[5] Fischer–Tropsch synthesis (FTS) is a well-known process for the catalytic conversion of syngas into higher hydrocarbons and oxygenates, which are finally upgraded to sulfur and aromatic free transportation fuels and chemicals.^[6,7] FTS, which is a strongly exothermic catalytic gas liquefaction process, plays an important role in the production of sustainable and clean liquid fuels.^[8] Syngas is transformed into liquid fuel through catalytic–polymerization, which results in a wide range of products such as paraffins, olefins, alcohols, and aldehydes. The primary products of FTS are linear olefins with terminal double bonds and linear paraffins [eq. (1) and (2)].



The FT reaction, as surface polymerization reaction, follows these steps: 1) reaction initiation, 2) chain growth, and 3) chain termination. Two different mechanisms (CO insertion chain growth and carbide) are suggested for the FT reaction steps.^[9–11] In the CO insertion chain growth mechanism (Figure 1), CO molecule

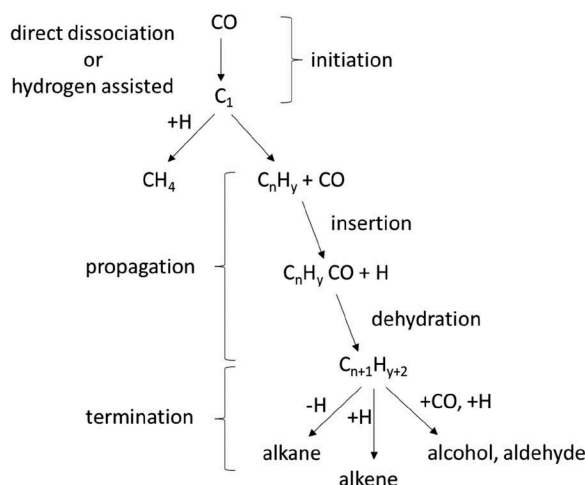


Figure 1. Reaction scheme of the Fischer–Tropsch reaction according to CO insertion chain growth mechanism.^[10]

is first adsorbed on the surface of the catalyst, and chain-growth is initiated by the initial dissociation of a CO molecule, followed by the hydrogenation of the dissociated CO molecule to form CH_x , and continued by the insertion of another CO into the CH_x species that has been formed. After the cleavage of the C–O bond of the inserted CO, an initial C_2H_y species is formed, and the chain growth step occurs consecutively. Chain termination may occur any time during the chain growth step to form α -olefin or n-paraffin once the product desorbs.

The relation between the FT activity and the active metals that readily dissociate CO is already known. However, the activation energy of CO dissociation, which is adsorbed on Co particles, is decreased by the addition of H_2 ; on less reactive surfaces, H-activated CO bond dissociation via formation of formyl intermediate has a lower barrier than the direct CO cleavage.^[10] In the carbide mechanism (Figure 2), the methylene ($-\text{CH}_2-$) species is the initiating monomer. H_2 and CO are assumed to be adsorbed and dissociated and are incorporated into the chain growth. Thus, several CH_x species, such as $-\text{CH}_2-$ and $-\text{CH}_3$, can be formed. Chain growth occurs by the insertion of the monomer in a growing alkyl species, and $-\text{CH}_2-$ monomers can be polymerized to long-chain hydrocarbons. Then, termination occurs by the addition of a $-\text{CH}_3$ species or hydrogen to form paraffin or the loosening of hydrogen to form an olefin.^[11]

Given the importance of the FT reaction in the production of clean liquid fuels, this review aims to present information about the history of FT synthesis and commercially available FT plants. It also provides a summary of cobalt-based catalysts for FT reaction and discusses the effect of support

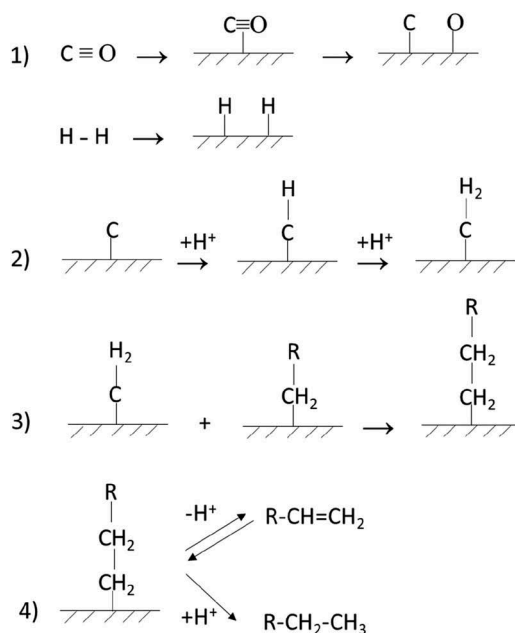


Figure 2. Reaction scheme of the Fischer–Tropsch reaction according to carbide mechanism.^[11]

and promoters on the catalytic activity and product selectivity. Furthermore, different types of reactors, including fluidized-bed, slurry bubble column, and fixed-bed reactors along with the recently developed FT reactors, have been discussed.

2. History of Fischer–Tropsch synthesis

The catalytic methanation reaction between hydrogen and carbon dioxide over nickel catalysts was first reported by Sabatier and Senderens in 1902.^[12] Friedrich Bergius in Rheinau-Mannheim is known as the German drive for energy independence due to his invention and early development of high-pressure coal hydrogenation in the period of 1910–1925.^[13] In 1913, Baden Aniline and Soda Factory (BASF) patented a process for carbon monoxide hydrogenation to produce hydrocarbons other than methane, acids, ketones, and alcohols. However, BASF did not continue its hydrocarbon synthesis because of World War I and the priority of ammonia and methanol synthesis.^[12] Germany as one of the pioneer industrialized nations was also working on petroleum synthesis when Friedrich Bergius (1884–1949) in Rheinau-Mannheim in 1913 and Franz Fischer (1877–1947) and Hans Tropsch (1889–1935) at the Kaiser Wilhelm Institute for Coal Research (KWI) in Mülheim, Ruhr, in 1925–1926 invented processes for converting coal to petroleum which is known as Fischer–Tropsch synthesis (FTS).^[14] In 1923, Fischer and Tropsch showed that syngas can be converted to an oily liquid product using an alkali–iron catalyst at 325 °C–425 °C and 100–150 atm. This product was called synthol and contained alcohols, acids, aldehydes, ketones, esters, and hydrocarbons. However, they found that a very low yield of oil was obtained at low pressure (approximately 7 atm), but the product is almost completely paraffinic and contained only a small fraction of oxygenated organic compounds.^[15] Later, in 1925, oxygenated compounds were eliminated using a cobalt–iron catalyst, at 250 °C–300 °C and 1 atm, and the product contained only hydrocarbon gases and liquids. The cobalt-based catalyst (100Co-5ThO₂-8MgO-200 Kieselguhr) developed by Ruhrchemie chemist Otto Roelen from 1933 to 1938 became the standard FT catalyst due to its high activity, low reaction temperature (180 °C–200 °C), and low/medium pressure (1–15 atm) it. Given the expensive preparation cost of this catalyst, cobalt and thorium were recovered from the spent catalyst and reused in preparing of fresh catalyst after treatment by nitric acid and hydrogen gas.^[11] In 1936, the Steinkohlen–Bergwerk Rheinpreussen plant was completed as the first commercial-size FT plant in Ruhr, Germany. The annual capacity of this plant was 25,000–30,000 metric tons of primary oils (gasoline and diesel oil) and paraffin wax. Further studies on FT reaction revealed that a slight increase in pressure resulted in a higher yield of primary oils and also increased the heavier hydrocarbons (soft and hard wax) for lubricating oil and chemicals. In addition, the lifetime of the catalysts increased from 4–7 months to 6–9 months without any reactivation. Several FT plans were

constructed and operated in Germany, while they were working at atmospheric and medium pressure, 180 °C–200 °C, with the standard FT catalyst; the products were mainly primary oils (gasoline and diesel oil) (Table 1).^[16]

By the outbreak of World War II (1939–1945), the construction of FT plants stopped. However, research continued to find cheaper catalysts, such as iron-based catalysts, due to the limitation of cobalt compound supplies during wartime and higher price of cobalt. After the war, and during the closing months of the war, different teams from other countries, such as the British Intelligence Objectives Subcommittee (BIOS) and the United States Technical Oil Mission (TOM), went to Germany to obtain and examine technical reports and interview German synthetic fuel scientists. Then, the Combined Intelligence Office Subcommittee (CIOS), BIOS, TOM and Field Intelligence Agency Technical (FIAT) printed and released more than 1400 reports on German synthetic fuel plants.^[13,16] Gradually, other countries started to construct and operate their FT plants. One of these released reports is the “report on the petroleum and synthetic oil industry of Germany” by the Ministry of Fuel and Power.^[17] Another comprehensive source is The Fischer–Tropsch and Related Syntheses by Henry et al.^[18] It also relies heavily on the captured German World War II synthetic fuel documents. These are some of the best and most comprehensive sources. Some important sources can be found in other published books.^[19–21]

Table 2 shows a summary of commercially established FT synthesis plants.^[22–28] In 1955, South Africa Coal and Oil (Sasol 1) in Sasolburg, developed a large-scale FT plant using circulating fluidized bed (CFB)

Table 1. Earliest Fischer–Tropsch plants in Germany.^[16]

Year	Plant/location	Catalyst	Pressure	Annual capacity (metric tons)	Products
1936	Steinkohlen-Bergwerk Rheinpreussen/Ruhr, Germany	*standard FT catalyst	Atmospheric (1atm)	25,000–30,000	Gasoline, diesel oil, paraffin wax
1937	Ruhrbenzin AG/Ruhr, Germany	standard FT catalyst	Atmospheric and medium (5–15 atm)	62,200	Gasoline, diesel oil, lubrication oil
1936	Wintershall AG/Ruhr, Germany	standard FT catalyst	Atmospheric	30,000–40,000	Gasoline, diesel oil
1937	Brabag II, Ruhland-Schwarzheide/Germany	standard FT catalyst	Atmospheric	200,000	Gasoline, diesel oil
1938	Mitteldeutsche Treibstoff, Lutzkendorf, Germany	standard FT catalyst	Atmospheric	30,000	Gasoline, diesel oil
1938	Krupp Treibstoffwerk GmbH/Wanne-Eickel, Germany	standard FT catalyst	Atmospheric and medium	130,000	Gasoline, diesel oil
1939	Essener Steinkohl/Dortmund, Germany	standard FT catalyst	Atmospheric	86,500	Gasoline, diesel oil
1939	Hoesch-Benzin GmbH/Dortmund, Germany	standard FT catalyst	Medium	51,000	Gasoline, diesel oil
1939	Schaffgotsch Benzin/Germany	standard FT catalyst	Medium	80,000	Gasoline, diesel oil

*standard FT catalyst: 100Co-5ThO₂-8MgO- 200 Kieselguhr

Table 2. Current commercial plants of Fischer–Tropsch synthesis.^[22–28]

Company/location	Feedstock	Reactor type	Catalyst type	Start-up date
Sasol/Sasolburg, South Africa	Coal (initially), natural gas (current)	HTFT circulating fluidized bed	Fused Fe/K	1955
		LTFT multitubular fixed-bed	Precipitated Fe/K	1955
		LTFT slurry phase	Precipitated Fe/K	1993
Sasol/Secunda, South Africa	Coal, natural gas	HTFT circulating fluidized bed	Fused Fe/K	1980
Shell/Bintulu, Malaysia	Natural gas	HTFT SAS reactor	Fused Fe/K	1995
		LTFT multitubular fixed-bed	Co/TiO ₂ , Co/SiO ₂	1993
PetroSA/Mosselbay, South Africa	Natural gas	HTFT circulating fluidized bed	Fused Fe/K	1993
Sasol-QP (Oryx)/Ras Laffan, Qatar	Natural gas	LTFT slurry phase	Co/Al ₂ O ₃	2006
Synfuels China, Taiyuan, Shanxi, China	Coal	HTFT slurry-bed	Fe	2006
NiQUAN GTL/Trinidad (Pointe-à-Pierre)	Natural gas	LTFT multitubular fixed bed (Compression two fixed-bed reactors with catalyst filled tubes)	Co	2008
Yitai CTL Plant/Inner Mongolia, China	Coal	MTFT slurry-bed	Fe	2009
Shenhua ICL/China	Coal	HTFT slurry-bed	Fe	2009
Shanxi Lu'an/Shanxi, China	Coal	HTFT fixed-bed	Fe, Co	2010
Shell (Pearl)/Ras Laffan, Qatar	Natural gas	LTFT multitubular fixed-bed	Co/TiO ₂	2011
Sasol-Chevron/Escravos, Nigeria	Natural gas	LTFT slurry-bed	Co/Al ₂ O ₃	2013
Synfuels China, Ningdong Energy, Ningxia, China	Coal	MTFT slurry-bed	Fe	2016

reactors over fused Fe/K catalyst for petrol production using high-temperature FT (HTFT, 320 °C–350 °C). Low-temperature FT (LTFT, 200 °C–250 °C) technology was also used for the production of waxes using precipitated Fe/K catalyst in a multitubular fixed-bed reactor (in 1955) and slurry reactor (later in 1993). The carbon feedstock for these plants was initially coal and then shifted to natural gas. Other plants by Sasol (Sasol 2 and 3) were also constructed in Secunda, South Africa by Sasol, in 1980 and 1983^[25,26] using fused Fe/K catalyst in CFB reactors and HTFT process. However, in 1995, the initially developed CFB reactors were replaced by Sasol Advanced Synthol (SAS) reactors for the HTFT process. In 1993, Shell commenced the first facility using natural gas as feedstock and cobalt-based catalysts (Co/SiO₂, Co/TiO₂) based on the LTFT technology in a multitubular fixed-bed reactor on the Shell middle distilled Synthesis (SMDS) process in Bintulu, Malaysia. In this plant, heavy paraffins are produced in the FT process and then converted to middle distillates by hydroprocessing.^[25] In 1993, another FT plant based on HTFT synthol

technology, CFB reactor, and iron-based catalysts (fused Fe/K) was operated by Petro SA in Mosselbay, South Africa. Natural gas is used as feedstock in this plant for the production of hydrocarbons (mainly gasoline).^[25,26] In 2006, the Sasol1 Oryx GTL (Sasol-QP (Oryx)) plant was constructed in Las Raffan, Qatar using cobalt-based catalysts (Co-Al₂O₃) and based on LTFT Sasol technology and slurry phase reactors. Using natural gas as feedstock, this plant has been producing diesel fuel as the main product and naphtha as a by-product.

The high-temperature slurry FT process (HTSFTP) was developed in China in 2009. An iron-based catalyst is used in this process within a slurry-bed reactor, which is operated at 270 °C; thus, it is a medium-temperature FT (MTFT, 270 °C–300 °C) process.^[27] In 2011, the GTL plant (Qatar Petroleum, Pearl GTL development) based on the SMDS process, cobalt-based catalyst (Co-TiO₂), and LTFT technology in a multitubular fixed-bed reactor using natural gas as feedstock was constructed at Las Raffan, Qatar (Shell (Pearl)).^[25–29] Chevron–Sasol developed an FT plant in Escravos, Nigeria in 2013. The plant uses the LTFT technology, slurry phase reactor and cobalt-based catalyst (Co/Al₂O₃), and the feedstock is natural gas.^[26] About more or less the same time, other countries such as China, Indonesia, and Iran are also considering plants to produce FT liquid fuels.^[2] The medium-temperature slurry-bed FT process (MTSFTP) technology for the production of high-quality clean liquid fuels, such as gasoline and diesel, was developed by Synfuels China in 2016. The MTSFTP technology contains FT synthesis technologies, including its proprietary iron-based FT synthesis catalysts and slurry-bed FT reactor, and product upgrading technologies.^[22,28]

3. Fischer–Tropsch catalysts

The catalytic performance of the FT catalysts is directly affected by the chemical composition of the catalysts. Other physical properties, such as high surface area and porosity, are also essential to achieve a high activity. The catalyst should have some specific characterization to be active in the FT reaction. The catalyst required to be able to adsorb and dissociate the C–O bond, and at the same time, should have a good capacity for adsorption of H₂. Obtained O atoms detached from the surface by the formation of water and carbon dioxide. Easy reducibility of the catalyst is an important parameter. The enhanced reducibility causes an increase in the CO and H₂ chemisorption, as well as the number of active sites. Subsequently, leads to an increase in the CO conversion and affect the product selectivity.^[2,30,31] Due to their excellent ability for adsorption and dissociation of CO and H₂, the elements of group 8–10 of the periodic table are the most commonly used and reported elements for the FT reaction.^[32,33] Fe and Co are the active metals with enough activity toward hydrocarbons for commercial applications.

Iron is inexpensive and readily available, but it has more tendency for the water-gas shift reaction (WGS, $\text{CO} + \text{H}_2\text{O} \rightarrow \text{CO}_2 + \text{H}_2$), and it is useful for the low H_2/CO ratio syngas. Cobalt shows high activity, especially for the production of heavy hydrocarbons, including diesel fuel and wax, while iron-based catalysts are suitable for gasoline production.^[32,34] Co catalysts possess a very low intrinsic WGS activity, and it is more suitable for syngas with a high H_2/CO ratio.^[34,35] Nickel catalysts are useful for the selective methane production. Despite its higher activity than cobalt and iron, due to the high price (~50,000 times higher than iron), ruthenium is not economically preferred for commercial FT production, and it is usually used as a reduction promoter, mostly for cobalt-based FT catalysts.^[3,32]

In order to have a cost-effective and more efficient, cobalt is required to be well dispersed on the support to maximize its activity. Increasing the dispersion leads to higher selectivity of liquid hydrocarbon; however, selectivity to liquid hydrocarbons could be decreased by an excessive increase in the Co loading.^[36,37] Iglesias et al.^[37–39] reported a severe decrease in the reaction rate by decreasing the crystallite size of cobalt catalysts ($d < 10\text{nm}$), and they found a linear correlation between the metal dispersion and the FTS reaction rate. Yang et al.^[40] also found that increasing the cobalt particle size leads to an increase in the turnover frequency (TOF) for CO conversion, which could be due to the increased site coverage of CO. The effect of cobalt particle size on FT catalysts has been studied extensively.^[41–46] The catalytic activity increased by increasing the particle size, while the morphological characteristics have remained constant. At smaller particle sizes, the selectivity to C_{5+} decreased, though selectivity to CO_2 and CH_4 were increased. Higher coverage of irreversibly bonded CO was observed for the small cobalt particles ($<6\text{ nm}$), which can block the surface and decrease the catalyst activity. On the contrary, an increase in H coverage was found for these small cobalt particles, which led to higher methane production. The low metal-support interactions and chain-growth probability would be enhanced with large particle size, thus resulted in improved reducibility. The cobalt particle size also affected by the nature of cobalt precursor (such as nitrate, chloride, acetate, citrate, carbonyl, etc.), which could be due to the changes in Co^0 dispersion and metal-support interaction. The effect of different parent cobalt compounds on the physicochemical properties of the Co/SiC catalyst and also its effect on the FT catalytic performance was studied by De la Osa et al.^[44] An increase in both basicity and average Co particle size of the catalyst was observed in the following order: $\text{Co}(\text{citrate})/\text{SiC} < \text{Co}(\text{acetate})/\text{SiC} < \text{Co}(\text{chloride})/\text{SiC} < \text{Co}(\text{nitrate})/\text{SiC}$. Nitrate source catalyst showed the highest basicity, degree of reduction, and particle size, which resulted in a higher FTS activity, with lower CH_4 selectivity and higher selectivity toward C_{5+} hydrocarbons (kerosene-diesel fraction). The diesel yield over Co(nitrate) was doubled compared to that produced by Co(citrate) catalyst. Larger cobalt particles with weaker interaction with the support resulted in higher activity in FTS.^[47] However, the higher concentration of cobalt species (silicate or

aluminate) with poor reducibility (for the catalyst with smaller Co particles), resulted in a lower catalytic activity and higher selectivity to low molecular weight hydrocarbons. Different parameters are affecting the FT catalyst performance, and it is essential to have a catalyst with the optimized properties based on the desired product and reaction condition. The following sections provide some information about the role of supports such as alumina, titania, and zeolite, as well as promoters including noble metals, transition metals, alkali, and alkaline earth metals in the catalytic performance of cobalt-based catalysts for FT synthesis.

3.1. Support materials for the cobalt-based Fischer–Tropsch catalyst

Catalyst support could facilitate the crystallization and stabilization of the active metals on its texture. Physicochemical and textural properties of the support material affect the metal-support interaction, crystallite size, metal dispersion, mass transfer of the reactants/products, mechanical strength, and thermal stability of the catalyst. Therefore, the selection and synthesis of proper support material with distinct physicochemical composition, well-defined surface chemistry, large surface area, and appropriate pore size/volume is critical for designing an efficient catalyst.^[48,49] The catalytic performance of cobalt-based catalysts for FT synthesis is highly related to the support properties.^[50] The metal-support interactions influence the structure and electron density of the metal particles, and cobalt-support mixed compounds could be formed due to this interaction. The metal dispersion and reducibility, and thus the catalytic activity and selectivity significantly depend on the surface properties of the support, such as surface area, pore size, and pore volume. The support can also enhance the heat dissipation and reduce the temperature gradient in a fixed-bed reactor.^[51]

During FT synthesis, liquid products, heavier hydrocarbons, and waxes, fill the pores and results in diffusion limitation for the reactants and products and affect the reaction rate.^[52] The reactants (H_2 , CO) could dissolve in the waxes on the catalyst surface and then diffuse inside the pores. It has been reported that the diffusion significantly reduced in large pellet catalysts, which is more evident for CO than for H_2 , due to their different diffusion coefficients.^[53] H_2 diffuses much faster than CO; therefore, dissolution and diffusion of reactants into the pore result in a higher hydrogen concentration inside the porous catalyst and increase the H_2/CO ratio, which facilitates the chain termination step and affects the product selectivity and often resulted to high CH_4 selectivity.^[54] In addition, support can alter the size and charge of the metal particles, crystallographic structure, and the formation of active sites.^[55] In order to retain the desired pressure drop and heat transfer in many fixed-bed reactors for FT reaction, usually, the Co catalysts with large pellet size (1 to 3 mm) are used, which resulted in severe diffusion limitations.^[56] Merino et al.^[57] reported that the diffusion decreased by increasing the particle size, and an increase in CH_4 selectivity and

decrease in C_{5+} selectivity were observed for Co–Re/AC70 catalyst. In addition, the effect of diffusion limitations of the reactants and products over the catalyst pores was found to be lower for catalysts with high mesoporosity (20–50 nm). The influence of diffusion limitations was even much lower for the catalysts with more macroporous structure (100–1000 nm), due to the improved transportation of the reactants and products between the active sites and gaseous phase.^[57,58]

Several types of materials such as zeolite, aluminum oxide, titanium dioxide, silicon oxide, and carbonaceous materials have been widely used as support for the Co catalyst in FT synthesis^[4,59–64] Different support materials used for the cobalt-based FT catalysts, their properties, effect on the catalyst activity, and product selectivity are discussed in this section.

3.1.1. Al_2O_3

Alumina is one of the most commercially used supports for cobalt-based FT catalysts. Improvement of the textural properties (surface area, pore size, pore volume) of conventional alumina enhances the loading of active metals and increases the availability of active sites. Alumina is widely used as support for cobalt-based catalysts, because it shows several attractive features, such as excellent mechanical properties, high attrition resistance, adjustable pore structure, and intermediate strength of the Co-support interaction.^[65–67] Due to its effect on catalytic activity, selectivity, and stability of supported catalysts in FT synthesis, it is essential to optimize the pore diffusional transport.^[4,68] Mesoporous materials with a pore size of 10–15 nm could provide a proper texture for the formation of cobalt crystallites^[26,69–71] The larger pore size of support resulted in the formation of larger cobalt crystallites, which leads to faster sintering of the cobalt particles. In comparison, the smaller pore size leads to the formation of smaller particles, which causes strong metal-support interaction and lower reducibility. Several studies have been done to develop novel alumina, and other metal oxide supports with the enhanced properties to attain high activity, selectivity, and stability for the cobalt-based FT catalysts.^[4,45,70,72,73] The catalytic activity of different alumina supported cobalt-based catalysts in the FT reaction are summarized in [Table 3](#).

Alumina nanofibers supported catalysts, with stable, large, and interconnected pore structure, revealed an enhanced catalytic performance and stability.^[86] However, it seems to be challenging to achieve a homogeneous Co particle size distribution using the conventional impregnation method. A practical method for the preparation of cobalt catalysts supported on alumina nanofibers with narrow crystallite size has been investigated by Liu et al..^[67] The prepared Co_3O_4 nanoparticles and alumina nanofibers were mixed and rearranged successfully by an ultrasonication assisted mixing method. The obtained catalyst revealed a more homogeneous dispersion of cobalt nanoparticles, enhanced reducibility, and interconnected porous structure. Consequently, the presence of more Co^0 active sites led to higher catalytic activity and C_{5+} selectivity, and the stability of catalyst


Table 3. The catalytic activity of different alumina supported cobalt-based catalysts in the FT reaction.

No	Catalyst	Preparation method	T (°C)	P (MPa)	H ₂ /CO	In-situ reduction	CO conv. %	Main product	Sel. %	Ref
1	15%Co/Al ₂ O ₃	ultrasonication assisted mixing	230	1	2	450 °C, 10 h, H ₂	79.2	C ₅₊	77.6	[67]
2	15%Co/Al ₂ O ₃ (nanofiber)	impregnation (Imp)	230	1	2	450 °C, 10 h, H ₂	51	C ₅₊	74.4	[67]
3	15%Co/meso-Al ₂ O ₃	incipient wetness impregnation (IWI)	230	2.75	2	400 °C, 18 h, H ₂	74.5	C ₅₊	83.9	[4]
4	15%Co/α-Al ₂ O ₃	IWI	210	2	2	350 °C, 16 h, H ₂	46	C ₅₊	83.9	[45]
5	20%Co/Al ₂ O ₃	combustion	230	3	2.3	320 °C, 16 h, H ₂	40	C ₅₊	83	[74]
6	CoDEG/Al ₂ O ₃	Imp	200	2.5	2	400 °C, 17 h, H ₂	30	C ₅₊	77	[75]
7	Co/γ-Al ₂ O ₃	Imp	200	2.5	2	400 °C, 17 h, H ₂	19	C ₅₊	79	[75]
8	Co/γ-Al ₂ O ₃	Imp	230	0.1	2	400 °C, 12 h, H ₂	42	C ₅₊	32	[76]
9	Co/γ-Al ₂ O ₃	atomic layer deposition	230	0.1	2	400 °C, 12 h, H ₂	57	C ₅₊	39	[76]
10	12wt.%Co/γ-Al ₂ O ₃	IWI	210	2	2	350 °C, 16 h, H ₂	45	C ₅₊	82.8	[77]
11	12wt.%Co/δ-Al ₂ O ₃	IWI	210	2	2	350 °C, 16 h, H ₂	47	C ₅₊	85.9	[77]
12	12wt.%Co/θ-Al ₂ O ₃	IWI	210	2	2	350 °C, 16 h, H ₂	46	C ₅₊	83.1	[77]
13	12wt.%Co/α-Al ₂ O ₃	IWI	210	2	2	350 °C, 16 h, H ₂	46	C ₅₊	88.5	[77]
14	15%Co/Al ₂ O ₃ -FSM16	Imp	220	2	2	400 °C, 12 h, H ₂	75	C ₅₊	82	[78]
15	15%Co/meso-Al ₂ O ₃	Imp	220	2	2	400 °C, 12 h, H ₂	53	C ₅₊	77	[78]
16	15%Co/Al ₂ O ₃	Imp	220	2	2	400 °C, 12 h, H ₂	61	C ₅₊	77	[78]
17	20%Co-0.5%Re/α-Al ₂ O ₃	IWI	210	2	2	350 °C, 16 h, H ₂	44	C ₅₊	85	[79]
18	10%Co/SiO ₂ -Al ₂ O ₃	IWI	240	1	2	400 °C, 10 h, H ₂	38.9	NA	NA	[80]
20	1.2%Ag-20%Co/AlSi	solvent deficient precipitation	220	2	2	420 °C, 4 h, 10% H ₂ in He	66	C ₃₊	82.1	[81]
21	1.2%Ag-20%Co/AlSi	solvent deficient precipitation	220	2	2	420 °C, 4 h, 10% H ₂ in He	60	C ₃₊	81.3	[81]
22	1.2%Co/γ-Al ₂ O ₃	Imp	210	2	2	350 °C, 16 h, H ₂	45-55	C ₅₊	80	[82]
23	20%Co-0.15%Ru/Al-Si	IWI	230	2	2	420 °C, 4 h, 10% H ₂ in He + 420 °C, 4 h, H ₂	20	NA	NA	[83]
24	20%Co/Al-Si	combustion	230	3	2.3	927 °C, 20 h, H ₂	40	C ₆₊	78	[84]
25	20%Co/Al-Si	Imp	230	3	2.3	927 °C, 20 h, H ₂	32	C ₆₊	75	[84]
26	20%Co/Al	combustion	230	3	2.3	927 °C, 20 h, H ₂	33	C ₆₊	89	[84]
27	20%Co/Al	Imp	230	3	2.3	927 °C, 20 h, H ₂	20	C ₆₊	80	[84]
28	13%Co-0.2%Ru-3%Zr/γ-Al ₂ O ₃	IWI	220	2.4	2	350 °C, 20 h, H ₂	54	C ₅₊	73.1	[85]
29	13%Co-0.2%Ru-3%Zr/5%SiO ₂ -γ-Al ₂ O ₃	IWI	220	2.4	2	350 °C, 20 h, H ₂	72	C ₅₊	70.3	[85]

(Continued)

Table 3. (Continued).

No	Catalyst	Preparation method	T (°C)	P (MPa)	H ₂ /CO	In-situ reduction	CO conv. %	Main product	Sel. %	Ref
30	13%Co-0.2%Ru-3%Zr/10%SiO ₂ -γ-Al ₂ O ₃	IWI	220	2.4	2	350 °C, 20 h, H ₂	78	C ₅ +	74.5	[85]
31	10%Co/γ-Al ₂ O ₃	IWI	220	2	2	350 °C, 17 h, 5% H ₂ in Ar	13.7	C ₅ +	93.1	[65]
32	10%Co/γ-Al ₂ O ₃	IWI	220	2	2	350 °C, 17 h, 5%CO in He	33	C ₅ +	60.9	[65]
33	15%Co/Al ₂ O ₃ (nanostructured)	IWI	210	1	2	450 °C, 10 h, H ₂	21.7	C ₅ +	75	[86]
34	20%Co/Al ₂ O ₃ (boehmite)	Imp	230	1	2	400 °C, 6 h, H ₂	61	C ₅ +	89	[87]
35	20%Co/Al ₂ O ₃ (gibbsite)	Imp	230	1	2	400 °C, 6 h, H ₂	22	C ₅ +	90	[87]
36	5%Au/10%Co/Al ₂ O ₃	deposition-coprecipitation	220	2	2	350 °C, 10 h, H ₂	16.4	C ₅ +	80.1	[88]
37	25%Co/Al ₂ O ₃	Imp	220	2.2	2.1	Ex-situ: 350 °C, 15 h, H ₂ ;He=1:3	50%	C ₅ +	83.4	[89]
38	15wt.%Co/Al ₂ O ₃	melt infiltration	230	2	1	400 °C, 6 h, H ₂	39	C ₅ +	88	[90]
								C ₅ -C ₉	15	
								C ₁₀ -C ₂₀	41	
								C ₂₁ +	33	

also increased due to the inhibited mobility of the cobalt particles on the surface of nanostructured alumina.

The absence of micropores in the organized mesoporous alumina leads to a better dispersion of transition metal oxide. It does not allow a portion of the oxide to be hidden in the micropores and not reachable for the substrate molecules.^[91] The stability of small metal particles could be improved at a higher concentration of basic sites through strong metal-support interaction, which causes a high activity in oxidation reactions. The interaction of active species with the surface of alumina support is affected by the different coordination of aluminum at the surface of channel walls. Different methods for synthesis of organized mesoporous alumina with different surface area, pore size, and pore volumes have been used, such as 1) surfactant routes using an anionic surfactant, a cationic surfactant, and nonionic surfactant methods; 2) non-surfactant method; and 3) nonocasting method. Further studies on the synthesis methods showed that the development of Al-O-Al bonds is not completed after the synthesis, and during the early stage of the calcination treatment, further condensation of these bonds proceeds. It is contrary to the synthesis of mesoporous silicates, whereas the condensation is almost completed during the synthesis, and unlike the organized mesoporous alumina, the final textural properties are not noticeably affected by the temperature of calcination treatment.^[91]

The effect of the crystalline phase and pore size of mesoporous alumina on the crystallite size of cobalt and catalytic performance in FT synthesis have been investigated.^[4,74–76,87] Unlike the incipient wetness impregnation method, the synthesized catalysts using the combustion method did not have a strong metal-support interaction. In addition, due to the high temperature of the combustion process, the concentration of the irreducible cobalt-alumina compounds decreased; thus, the catalytic activity increased.

Najafabadi et al.^[76] applied the atomic layer deposition (ALD) method for the preparation of Co/ γ -Al₂O₃ catalysts and their performance in FT reaction were compared with the catalysts prepared by impregnation method. The ALD catalysts revealed a narrower size distribution and higher dispersion of cubic cobalt nanoparticles compared with the spherical particles in catalyst prepared by the impregnation method. The impregnation method is based on the pore volume filling, while the ALD is a self-limited surface chemisorption method. More uniform cobalt particles were generated on the alumina using the ALD method. In contrast, in the impregnation method, the wide pore size distribution of the alumina caused a wide cobalt particle distribution. Thus a higher CO conversion and C₅₊ selectivity and a lower CH₄ selectivity obtained over the ALD catalysts.

The effect of different phases of Al₂O₃ supports including γ -, α -, θ - and δ -Al₂O₃ prepared from γ -Al₂O₃, with small, medium pore sizes, by heat treatment, on the product selectivity in FT reaction has been studied by Rane et al.^[77] The 12 wt.% Co/Al₂O₃ catalysts with almost uniform cobalt metal particle size of 8–10 nm were

prepared by incipient wetness impregnation method. The catalysts with the medium pore size were found to be reduced at lower temperatures than the catalysts with small pore size. The FT reaction at 210 °C, 20 bar, and $H_2/CO=2$ showed higher C_{5+} selectivity for the catalyst with medium pore size. Compared with γ - and θ - Al_2O_3 catalysts, the α - and δ - Al_2O_3 supported catalysts revealed higher selectivity to C_{5+} , and the highest selectivity was observed for the α - Al_2O_3 catalyst. It has been reported that the concentration of active CH_x surface intermediates has a direct relationship with C_{5+} selectivity, with respect to the alumina phase and pore size.^[77]

Different types of alumina as supports for cobalt-based catalysts in FT reaction has been investigated by Mohammadnasabomran et al.^[78] The high specific surface area ordered mesoporous solid (FSM16) synthesized by an organic template method, and then Al_2O_3 -FSM16 (ALFSM) prepared using the impregnation method. Synthesized mesoporous Al_2O_3 (ALSM) prepared using Tergitol as a nonionic surfactant. Afterward, prepared supports, as well as the conventional mesoporous Al_2O_3 (ALCM), impregnated with cobalt nitrate to obtain 15 wt.% of Co/support catalysts. The highest reducibility was observed for the ALFSM supported catalyst (ALFSM>ALCM>ALSM), which could be attributed to the small particle size and higher cobalt dispersion on the interior and the exterior surface of the channelized structure of the ALFSM supported catalyst, which enhances the hydrogen spillover. The narrow particle size distribution could increase catalytic activity and enhance the FT reaction rate. A Higher dispersion and reducibility of the cobalt particles, thus higher catalytic activity and stability during 240 h of FT reaction was observed for the ALFSM supported catalyst.^[78]

Water is usually produced during FT synthesis ($nCO + (2n+1)H_2 \rightarrow C_nH_{2n+2} + nH_2O$), and it has an obvious effect on the catalytic activity, selectivity, deactivation, and the state of the catalyst.^[79,92] Almost for all types of cobalt catalysts supported on alumina, water found to have a positive effect on C_{5+} selectivity by increasing the chain propagation α -value. At high water concentration, the large pore γ - Al_2O_3 is more efficient than the small pore. The addition of water could enhance the CO activation, and consequently, increase the CH_x formation that leads to higher chain growth probabilities. Simultaneously, the concentration of hydrogen on the surface of cobalt catalyst decrease in the presence of water and results in lower methane formation.^[79,93] The effect of water is not related to the source of water, and the formation of water during the reaction or addition of water to the feed gas has the same effect. It is assumed that the influence of water could be due to the pore condensation, and water enhances the promotion of CH_x monomers. It is worth mentioning that high partial pressure of water has a direct relation with the hydrogen partial pressure. The Co/ Al_2O_3 spinels, which are inactive for FT reaction and required a very high temperature to reduce, could be formed due to the presence of water during the FT synthesis.^[80,94]

Rytter and Holman^[92,95] proposed a mechanistic model for FT synthesis in the presence of water on Co catalysts supported on γ - Al_2O_3 , which contains three

steps. In the first step, CO activation is facilitated by hydrogen transfer from water or hydroxyl to a hydroxycarbene intermediate to generate CH^* surface species on cobalt as chain building blocks. It has been assumed that hydrogenation by H^* is to a carbon atom, while hydrogenation from OH^* or H_2O is to an oxygen atom, which is in good agreement with the higher electronegativity of oxygen and general hydrogen bonding experience. The scission of hydroxycarbene by hydrogen could produce methylene or methylidyne (Figure 3a,b).

The next step is the chain growth (Figure 4). Initiation is started by C-C coupling between methylidyne (CH^*) and methylidyne to create a vinyl starting point for chain growth. The formed vinyl is then hydrogenated to ethylidene to create the first alkyl fraction of the chain. Then propagation is carried out by the addition of methylidyne to generate vinylene. The last step

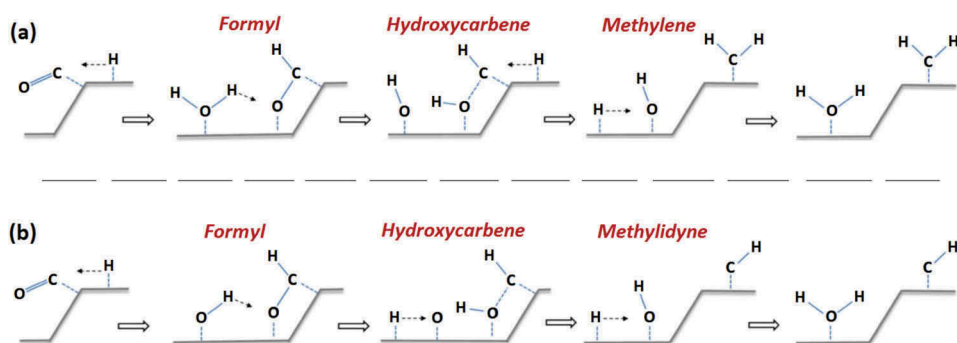


Figure 3. Hydrogen- and hydroxyl-assisted activation of CO to (a) methylene, (b) methylidyne.^[95]

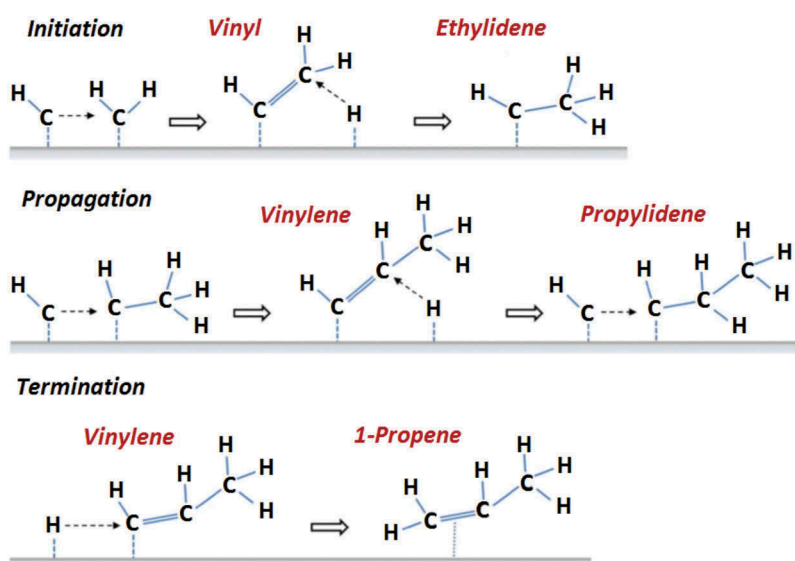


Figure 4. Proposed vinylene mechanism for initiation, propagation, and chain-growth during FT reaction on cobalt catalyst.^[95]

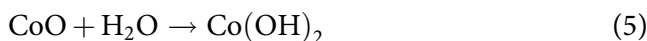
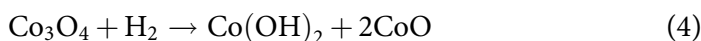
is the termination, by hydrogenation of the β - or α -carbon atoms of the formed vinylene. The hydrogenation of the α -carbon of vinylene terminates the chain to α -olefin. Chain growth probability only depends on the surface coverage of CH^* monomers.

The addition of a thin layer of SiO_2 could impede the formation of inactive $\text{Co}/\text{Al}_2\text{O}_3$ species and thus prevent the catalyst deactivation.^[81] The addition of silica to alumina leads to the formation of alumina support with improved porosity, higher surface area, optimal acid site concentration, and higher thermal and hydrothermal stabilities, which facilitate higher catalyst loadings and increase the catalyst activity and lifetime at higher reaction temperatures.^[83,96,97] Ali and Dasappa^[84] studied the effect of silica doping on Al_2O_3 (SDA, 40 wt.% SiO_2 , 60 wt.% Al_2O_3), and it was found that the high FT activity of Co catalyst obtained due to the decrease in the cobalt-support interaction for SDA supports. The modification of Al_2O_3 with SiO_2 led to the formation of strong Brønsted acid sites, through the formation of the bridge hydroxyl group, and also a higher Lewis acid sites created by isomorphous replacement of Si^{4+} ions by Al^{3+} ions at tetrahedral lattice sites.^[98] Compared with Al_2O_3 , the higher acidic sites on SDA suppress the wax formation, and selectivity to C_{10} - C_{24} hydrocarbons increased.^[84] The effect of silica modification on the $\text{Co}/\text{Al}_2\text{O}_3$ catalyst and its performance in the FT reaction also has been studied by Yaghoobpour et al..^[85] The addition of 10 wt. % silica inhibited the metal-support interaction and enhanced the catalyst reducibility, and therefore, catalytic performance considerably promoted over the silica promoted catalyst.

3.1.2. SiO_2

Silica is another commonly used support for FTS catalysts.^[64,99-102] Mesoporous silica has high surface area, narrow pore size distribution, ordered pore structure, which can enhance the metal dispersion, reducibility, catalytic activity, and thermal stability of the catalyst.^[2] There is plenty of hydroxyl silicon on the surface of SiO_2 , and their nature, concentration, and distribution significantly affect the distribution and reduction properties of the SiO_2 supported cobalt-based catalysts. Also, compared to the alumina support, silica has weaker metal-support interaction, which is beneficial for the reduction of cobalt, and enhances the cobalt dispersion and increases the number of active sites.^[103,104] The interaction of small unreduced CoO particles and silica leads to the formation of high surface area cobalt orthosilicate (Eq. 3), which are difficult to reduce to the active metal site at the FT reaction temperature. Cobalt hydroxide can also be generated by hydrogenolysis of Co_3O_4 (Eq. 4) or from the reaction of CoO with water (Eq. 5), and then cobalt hydroxide reacts with migrating silicic acid to produce cobalt silicate (eq. 6)^[105-107]:





The catalytic activity of different silica supported cobalt-based catalysts in the FT reaction are summarized in Table 4. Co/SiO₂ catalyst prepared by hydrogen dielectric barrier discharge (H₂-DBD) plasma treatment and the effect of H₂-DBD plasma treatment on the structure of the catalyst, reducibility, and cobalt dispersion was investigated by Fu et al.^[106] Results revealed that the H₂-DBD treatment could be used for decomposition of cobalt precursors, as well as a more efficient reduction of Co₃O₄ compared to the traditional calcination and reduction processes. However, the most important disadvantage of this treatment is the formation of more Co₂SiO₄ species during the treatment. Compared with the traditional preparation method, higher cobalt dispersion obtained, but due to the formation of more Co₂SiO₄ species, the catalytic activity decreased.

In another study, Co catalysts supported on Al₂O₃ and SiO₂ were prepared by deposition–precipitation, and their catalytic performance in FT reaction in a fixed bed reactor has been investigated.^[88] The temperature programmed reduction (TPR) analysis suggested that the cobalt species existed with different degrees of interaction with the SiO₂ support, or there were some cobalt species inside the inner pores of silica support, which required higher temperature for reduction. Reducibility of the cobalt species limited by the diffusion through pores by the water produced during the reduction. Compared with the Co/Al₂O₃, smaller Co particle size observed for the Co/SiO₂ catalyst with the higher surface area. Smaller Co particle size could lead to higher metal-support interaction and thus reduce the reduction extent. Compared with Co/Al₂O₃ catalyst, Co/SiO₂ catalyst showed higher selectivity to C₅₊ and lower selectivity to CH₄.

The source of cobalt as a precursor also could affect the activity and selectivity of the catalyst. Other parameters, such as preparation steps, including impregnation, drying, and calcination, are affecting the catalyst properties and performance. The cobalt precursor decomposition and calcination steps are playing a critical role in the cobalt dispersion.^[121] Compared with cobalt acetate (A), using a mixture of cobalt nitrate (N) and cobalt acetate (A) impregnated on SiO₂ resulted in a highly active FT catalyst.^[99] Due to the stronger metal-support interaction in cobalt acetate catalyst, it was difficult to be reduced. The reduction degree of 79% and 15% were observed for the cobalt nitrate and cobalt acetate, respectively. Cobalt crystallite size in 10wt.%Co/SiO₂ catalysts were changed as follows: 10N>5N/5A>5A/5N>5A+5N>>10A, and the reduction degree was also following the same trend. The smaller crystallite could make a more robust interaction

Table 4. The catalytic activity of different silica supported cobalt-based catalysts in the FT reaction.

No	Catalyst	Preparation method	T (°C)	P (MPa)	H ₂ /CO	In-situ reduction	CO conv. %	Main product	Sel. %	Ref
1	40%Co/SiO ₂	Imp	240	1	2	NA	56.9	C ₅₊	NA	[99]
2	20%Co/SiO ₂	IWI	240	1	2	100 °C, 1h+400 °C, 10 h, H ₂	89.9	C ₅₊	98.2	[100]
3	20%Co/SiO ₂	Imp	220	1.99	2	230 °C, 24 h, H ₂	63.1	C ₅₊	88.2	[102]
4	20%Co/SiC	IWI	250	2	2	550 °C, 2 h, H ₂	53.9	C ₅₊	90.8	[103]
5	20%Co/SiC	IWI	230	0.8	2	350 °C, 12 h, H ₂	78.1	C ₅₊	79.5	[105]
6	20%Co/SiO ₂	IWI + hydrogen dielectric-barrier discharge (H ₂ -DBD) plasma	230	2	2	400 °C, 10 h, H ₂	74	C ₅₊	80	[106]
7	20%Co/SiO ₂	IWI	230	2	2	400 °C, 10 h, H ₂	75	C ₅₊	82	[106]
8	5%Au/10%Co/SiO ₂	deposition-coprecipitation	220	2	2	350 °C, 10 h, H ₂	6.1	C ₅₊	65.2	[88]
9	15wt.%Co/SiO ₂	melt infiltration	230	2	1	400 °C, 6 h, H ₂	37	C ₅₊ C ₅ -C ₉	88	[90]
10	3.6%Co(nanocryst.)/SiO ₂	deposition precipitation	220	2	2	500 °C, 8 h, 25% H ₂ in He	25	C ₂₁₊ C ₅₊	28 76	[108]
11	20%Co/SiO ₂	IWI	220	0.1	10	350 °C, 10 h, H ₂	NA	CH ₄ C ₂ -C ₅	99	[109]
12	5%Co/SiO ₂	Imp	240	2	2	400 °C, 6 h, H ₂	21.4	C ₅₊	1	[110]
13	5%Co/(CH ₃) ₃ -SiO ₂	Imp	240	2	2	400 °C, 6 h, H ₂	34.3	C ₅₊	50	[110]
14	5%Co/COOH-SiO ₂	Imp	240	2	2	400 °C, 6 h, H ₂	7	C ₅₊	68.2	[110]
15	5%Co/NH ₂ -SiO ₂	Imp	240	2	2	400 °C, 6 h, H ₂	4.43	C ₅₊	42.1	[110]
16	10%Co/SiO ₂	vacuum Imp	235	1	2	400 °C, 4 h, H ₂	33	C ₅₊	31.1	[111]
17	10%Co/glucose-SiO ₂	vacuum Imp	235	1	2	400 °C, 4 h, H ₂	38	C ₅₊	77.6	[111]
18	15%Co/SBA	IWI	220	2	2	400 °C, 10 h, H ₂	65.5	C ₅₊	70.2	[112]
								C ₅ -12 C ₁₃ -18	84 30.2 42.4	
19	Co/meso-macro-silica monolith	IWI	225	2	2	400 °C, 6 h, H ₂	30.7	C ₁₈₊	11.4	[113]
20	Co/meso-macro-silica monolith (+Al ₂ O ₃ =0.8%)	IWI	225	2	2	400 °C, 6 h, H ₂	65.8	C ₅₊	80.0	[113]

(Continued)

Table 4. (Continued).

No	Catalyst	Preparation method	T (°C)	P (MPa)	H ₂ /CO	In-situ reduction	CO conv. %	Main product	Sel. %	Ref
21	Co/meso-macro-silica monolith (+Al ₂ O ₃ =10%)	IWI	225	2	2	400 °C, 6 h, H ₂	23.4	C ₅₊	67.0	[113]
22	20%Co ₃ O ₄ @ mesoporous-SiO ₂	solvothermal method using PVP as the capping agent	240	2	2	400 °C, 10 h, H ₂	56.8	C ₅ -C ₁₈	58.6	[114]
23	20%Co ₃ O ₄ @carbonized-mesoporous-SiO ₂	solvothermal method using PVP as the capping agent	240	2	2	400 °C, 10 h, H ₂	87.7	C ₅ -C ₁₈	70.6	[114]
24	20%Co-2%Al ₂ O ₃ /SiO ₂	IWI	219	2	2	400 °C, 4 h, H ₂	46	C ₅₊	74.2	[115]
25	10%Co/10%Al ₂ O ₃ -SiO ₂	IWI	240	1	2	Ex-situ: 400 °C, 10 h, H ₂	38.9	C ₅₊	NA	[116]
26	10%Co-10% Al ₂ O ₃ /SiO ₂	Imp	240	1	2	Ex-situ: 400 °C, 10 h, H ₂	64	C ₅₊	NA	[117]
27	10%Co/2%TiO ₂ -SiO ₂	IWI	240	1	2	Ex-situ: 400 °C, 10 h, H ₂	68.7	C ₅₊	(α=0.87)	[118]
28	10%Co2%TiO ₂ /SiO ₂	Imp	240	1	2	Ex-situ: 400 °C, 10 h, H ₂	63.6	C ₅₊	65.3	[118]
29	10%Co/SiO ₂	IWI	230	2	2	400 °C, 12 h, H ₂	17.7	C ₅₊	72.1	[119]
30	10%Co/TiO ₂ -SiO ₂	IWI	230	2	2	400 °C, 12 h, H ₂	37	C ₅₊	71.4	[119]
31	10%Co/MCM-41	IWI	230	2	2	400 °C, 12 h, H ₂	30.4	C ₅₊	80.4	[119]
32	10%Co/TiO ₂ -MCM-41	IWI	230	2	2	400 °C, 12 h, H ₂	75.3	C ₅₊	85.2	[119]
33	15%Co/SiO ₂	IWI	220	2	2	400 °C, 10 h, H ₂	35	C ₅₊	84	[120]
34	15%Co/C-SiO ₂	IWI	220	2	2	400 °C, 10 h, H ₂	71	C ₅₊	89	[120]

with the support, which suppresses the reduction of CoO_x clusters. The bridge-type adsorbed CO with higher activity the linear type, was observed mostly for the 5N/5A and 5A/5N catalysts. In term of 5N/5A catalyst, it is supposed that first cobalt nitrate decomposed on SiO_2 and create a layer to weaken the strong metal-support interaction between the cobalt acetate and silica, and the impregnated species facilitated the reduction of cobalt acetate. The better reducibility properties and more active bridge-type of CO adsorbed on the Co metal sites, leads to the higher catalytic activity.

Different strategies have been used to weaken the cobalt-support interaction to enhance the reduction properties of the catalyst. The addition of a small amount of noble metals such as Pt, Re, Ru, with the high ability for the dissociative activation of hydrogen, could improve the catalyst reducibility and cobalt dispersion.^[89,121] Deactivation or passivation of the chemically active oxygen groups on the surface of the support could also weaken the metal-support interaction through grafting inactive or less active groups. The surface of the SiO_2 contains abundant silanol (SiOH) groups which can interact with cobalt oxides.

Changing the properties of these silanols using different organic groups has a strong influence on the dispersion, reducibility, and the performance of the catalyst. Co catalyst supported on the $(\text{CH}_3)_3$ -modified SiO_2 support ($\text{Co}/(\text{CH}_3)_3\text{-SiO}_2$) revealed high activity and C_{5+} selectivity, which could be due to the formation of a very hydrophobic silica-like surface by $(\text{CH}_3)_3$ group modification of SiO_2 . However, modification of SiO_2 with other organic compounds such as $\text{NH}_2(\text{CH}_2)_2\text{NH}_2$ -, COOH -, and NH_2 - decreased the catalytic activity.^[110]

The carbonaceous materials with an inactive surface, such as graphite, carbon nanotubes, carbon nanofibers, and activated carbon, exhibit weak metal-support interaction, and they were also extensively used as support for FT catalysts. It needs to be considered that, however, the reducibility of cobalt oxides over carbon-supported catalysts is high, but due to the weak interaction of metal and support, aggregation of active metals could occur easily and decrease the metal dispersion. Therefore, introducing carbon into metal oxide or vice versa could change the strength of the metal-support interaction.^[51,111] The addition of carbon into the oxide support create new support with variable metal-support interaction. For example, the $\text{Co}_3\text{O}_4@\text{C}$ -mesoporous SiO_2 ($\text{Co}_3\text{O}_4@\text{C-m-SiO}_2$) catalyst was synthesized via a solvothermal method using polyvinyl pyrrolidone (PVP) as a carbon source.^[114] The degree of reduction was gradually improved by increasing the carbon content due to the coverage of the reactive oxygen groups of m- SiO_2 with inert carbon and formation of more weak Co-C interaction instead of the strong interaction of Co and m- SiO_2 in the catalyst. This carbon modified catalyst revealed a rigid porous framework to allow free access of syngas and prevent the collapse of the mesoporous channel during the FT reaction. This behavior resulted in higher activity and stability of the FT catalyst.

The addition of alumina to Co/SiO_2 also could enhance its catalytic performance. The addition of 1 wt.% Al_2O_3 led to the more narrow size distribution of

Co⁰ nanoparticles by preventing the aggregation of particles and increased the cobalt dispersion.^[115] It is noticeable that in addition to the structural properties, the electronic properties are also affecting the catalyst performance. The CO adsorption could be facilitated in the presence of alumina on the surface of the catalyst due to the electron-donating character of Al₂O₃, and π -acceptor character of carbon monoxide. Thus, alumina can be considered as both structural and electronic promoters, which are favorable for CO adsorption. Al₂O₃ also can inhibit the adsorption of H₂ and decreases the H/C ratio on the surface of the catalyst.^[122,123] As a result of higher possibilities for the CO hydrogenation at higher hydrogen accessibility, the methane selectivity could increase. A higher concentration of CO on the surface could enhance the carbon chain growth probability and formation of long-chain products. Therefore, higher CO chemisorption and lower H/C ratio results in an increase in the C₅₊ selectivity on alumina promoted Co/SiO₂ catalyst. Zhang et al.^[116,117] also studied the promotional effects of alumina modification of Co/SiO₂ catalysts for the FT reaction in the slurry-phase reactor. They found that the addition of alumina to the Co/SiO₂ catalysts increased the cobalt dispersion without considerably hindering the reducibility, resulting in a significant improvement of the catalyst activity. The metal-support interaction adjusted by the addition of Al₂O₃, which was affecting the metal dispersion, preserving the high reduction degree of the catalyst. The high catalytic activity could be due to the increased bridge-type CO adsorption, which was easily dissociated to oxygen and carbon, and increased the FT reaction rate.

The addition of a small amount of TiO₂ to the Co/SiO₂ catalyst also had a similar effect on catalytic properties and activity.^[118,119] Hinchiranan et al.^[118] found that the addition of 2–10 wt.% of TiO₂ to the Co(10wt.%)/SiO₂ catalyst significantly improved the catalytic activity (in the slurry-phase reaction) by increasing the cobalt dispersion on SiO₂ support. The interaction of cobalt and silica support also adjusted by the addition of TiO₂ and resulted in a relatively high degree of reduction, and consequently, higher catalytic activity in FT reaction.

3.1.3. TiO₂

Among different support materials, TiO₂ found to be a proper candidate due to its high thermal and chemical stability as well as outstanding corrosion resistance. The size, nature, and the interaction of metal nanoparticles with TiO₂ are important parameters affecting the catalytic activity and selectivity. Anatase TiO₂ with a high specific surface area and strong interaction with metal nanoparticles are commonly used as support for heterogeneous catalysts.^[124] It has been reported that the strength of the cobalt-TiO₂ interaction was in the middle of SiO₂ and Al₂O₃ (Al₂O₃ > TiO₂ > SiO₂), which leads to the high reducibility and dispersion of the Co particles on the surface of TiO₂.^[125] The activity of the catalyst significantly depended on the crystal phase of TiO₂.^[126] Compared with the Co/TiO₂ catalyst with only the anatase crystal phase, the CO conversion increased by four times for the Co/TiO₂ catalyst with 15% of rutile phase. The particle size of Co₃O₄ could be

affected by TiO_2 properties and crystal phases. The average Co_3O_4 particle sizes on TiO_2 (P25, 85% anatase, 15% rutile) in 10 wt.%Co/ TiO_2 catalyst, prepared by the impregnation method, was 33 nm, which was higher than those of TiO_2 with only anatase (17 nm) and only rutile (19 nm) phase.^[127] The reduction of CoO to Co^0 found to be more difficult in anatase and rutile supported catalysts than the P25- TiO_2 supported catalyst.

The Co/ TiO_2 catalyst preparation method has a notable impact on catalytic performance. Catalytic properties of different Co/ TiO_2 catalysts prepared by incipient wetness impregnation with subsequent static drying (IWI-S), incipient wetness impregnation with fluidized bed drying (IWI-F) and deposition precipitation by ammonia evaporation (DPA) method has been studied by Eschemann and De Jong.^[128] However, the initial dispersion of cobalt oxide was similar for different catalysts, but the metal nanoparticles dispersion found to be decreased in the order $\text{DPA} > \text{IWI-F} > \text{IWI-S}$. The initial catalytic activities for the FT reaction also followed the same order, and the DPA prepared catalysts showed the highest C_{5+} selectivity. It was also found that after 200 h of reaction and at low CO conversion (35%), the activity of all catalysts decreased by about 20%, which could be due to the loss in the active metal surface area. As a result of cobalt particle growth, a significantly faster catalyst deactivation was observed at higher CO conversion.

Khosravi-Nikou and A. Bahrami^[129] applied an ultrasound-microwave-assisted method for the preparation of high loading active metal sites on Degussa TiO_2 (P25) support. The prepared catalyst with this method showed a higher BET surface area than the conventionally prepared catalysts. Higher reducibility of the ultrasound-microwave-assisted prepared catalysts than conventionally prepared catalysts could be due to the prohibition of cobalt species migration to the surface of the support and homogeneously distribution of cobalt particles inside and outside of the supports pores. The agglomeration of Co particles on the surface and non-uniform distribution of particles was observed during the conventional drying process. Increasing the cobalt loading on the support increased the reduction temperature. The FT reaction results over these catalysts revealed that the highest CO conversion obtained over 15% Co/ TiO_2 with the highest C_{18+} selectivity. Further increase in Co loading led to lower CO conversion and C_{18+} selectivity, which could be due to the decreased BET surface area and active metal sites.

The physicochemical properties and catalytic performance of cobalt FT catalysts supported on titania nanotube prepared by impregnation and homogeneous precipitation methods have been studied by Li et al.^[130] Results showed that the catalytic activity and product selectivities significantly affected by the preparation method. The Co- TiO_2 interaction may alter the electronic state of the active metal, and the weak interactions lead to the formation of lower valence cobalt. Analysis proved the presence of more Co^{2+} components on the surface of the homogeneously precipitated Co/ TiO_2 catalysts, approving the weak Co- TiO_2 interaction, which resulted in better reducibility and lower reduction temperature. The strong

metal-support interaction in the catalyst prepared by the impregnation method resulted in lower reducibility, and subsequently, lower catalytic activity (31%) and C_{5+} selectivity (31.5%), with higher selectivity to CH_4 (38.2%) and C_2-C_4 (30.3%). The CO conversion, C_{5+} , CH_4 , and C_2-C_4 selectivities over the catalyst prepared by the homogenous precipitation method was 74%, 62.6%, 26.3%, and 11.1%, respectively.

It has been reported that using TiO_2+SiO_2 mixed oxide as support could enhance the catalytic activity for the CO hydrogenation reaction.^[109] Increasing the TiO_2 amount in $Co/(TiO_2+SiO_2)$ catalysts led to a significant decrease in the reaction rate. This reduced activity attributed to the lower number of reduced cobalt metal on the surface of the catalyst for catalyzing the reaction. The methane selectivity also followed the same trend and decreased by increasing the amount of TiO_2 in mixed oxide support, while the highest C_2-C_5 selectivity follows the reverse trend and the highest C_2-C_5 selectivity observed for the catalyst with higher TiO_2 content. It is known that the CO hydrogenation is a polymerization reaction, and $-CH_2-$ insertion occurs over the active sites. Therefore, the nature of active sites significantly affects the product selectivity, propagation, and termination rate. It has been concluded that the presence of TiO_2 and increasing its amount in the mixed oxide support inhibited the chain growth probability and subsequently led to the formation of shorter-chain hydrocarbons (C_2-C_5). The catalytic activity of different titania supported cobalt-based catalysts in the FT reaction are summarized in Table 5.

3.1.4. Zeolites

Zeolites have been used extensively in industrial processes as ion-exchange agents, molecular sieves, and heterogeneous catalysts. In catalytic applications, zeolites are mainly used in their acidic form. The rare-earth-exchanged zeolites, mainly X and Y of the Faujasite structure with a small amount of ZSM-5, are mostly used in fluidized catalytic cracking. ZSM-5 and Faujasites also have been applied in synfuel production, isomerization, and other critical industrial reactions.^[136] The zeolite supported catalysts have been used in FT synthesis for gasoline production and enhancing the octane ratings. The active metal of the FT catalyst is responsible for the primary chain growth of hydrocarbon, which then restructuring at the zeolite acid sites to produce more aromatics and branched hydrocarbons, with higher octane rating and limited chain length.^[117] Zeolite's pore structure provides shape selectivity and limits the chain growth length, and its acidity enhances the oligomerization, cracking, and aromatization reactions that are involving in the restructuring of the FT products. Zeolites also show excellent resistance to coking and high stability in FT reaction conditions. The secondary acid-catalyzed isomerization and cracking could be enhanced in the presence of catalysts with small zeolite crystals, and this restructuring would occur on the external acid sites.

Due to the importance of the acid sites' role in the bifunctional FT catalysts, cobalt catalysts supported on different types of zeolites with high acidity but different pore structures were evaluated for their performance in FT reaction.^[137] It was found that the acidity of the catalysts (both the total number of acid sites and strength of the strongest acid sites) decreased in the order ZSM-34>ZSM-5>ZSM-11>ZSM-12. The ZSM-12 has the largest channel size with 12 membered ring channels, followed by 10 membered ring ZSM-11 and ZSM-5, and ZSM-34 with 8 membered ring channel has the smallest channel system. The CO conversion of the zeolite supported catalysts found to be linked to the channel size of the zeolites, and it was in the order ZSM-34<ZSM-5<ZSM-11<ZSM-12. The formation of small cobalt crystals increased by increasing the dimensions of the zeolite channels. It was reported that a remarkable hydrocarbon chain growth was occurring on cobalt crystallites on the zeolite's surface. Afterward, the main produced hydrocarbons were restructured at the available acid sites of zeolite to produce lighter products with fewer n-alkanes. The lightest products formed over the ZSM-12 supported catalyst, followed by ZSM-5, ZSM-11, and the ZSM-34 supported catalyst, showed the lowest selectivity to light hydrocarbons ($< C_{12}$), and it was more favored for production of heavier products containing more n-alkanes. Results revealed that an increase in secondary cracking reactions occurred for the products from the ZSM-12, ZSM-5, ZSM-11, and ZSM-34 supported catalysts, respectively. Compared with the strength and concentration of the acid sites, the accessibility to the internal acid sites is playing a more critical role in affecting the degree of secondary acid-catalyzed restructuring reactions of the primary FT products. The catalytic activity of different zeolite supported cobalt-based catalysts in the FT reaction are summarized in [Table 6](#).

The shape-selective feature of zeolites enables them to limit the formation of products larger than their cavity diameters, and they can restrict the chain growth and lead to the formation of lighter hydrocarbons in FT synthesis. Additionally, as mentioned earlier, the acidity of the zeolites promotes the secondary cracking, branching, oligomerization, and aromatization reactions of the main FT products. These properties of the zeolites could shift the FT product distribution toward lighter hydrocarbon fuels such as gasoline. The relation between the hydrocracking, isomerization rates, and porosity and acidity of the zeolitic supported FT catalysts has been studied by Subramanian et al.^[138] They found that the selectivity to C_5 - C_{12} hydrocarbons is related to the number of strong Brønsted acidic sites that exist in the zeolite structure. However, increasing the average pore diameter could lead to the formation of long-chain isoalkanes. According to Wang et al.,^[94] due to the smaller waxes and coke formation, the deactivation rate of the active phase could be decreased in the presence of zeolite with a mesoporous structure. However, the formation of carbon deposits could enhance by increasing acidity.^[139,148]

Table 6. The catalytic activity of different zeolite supported cobalt-based catalysts in the FT reaction.

No	Catalyst	Preparation method	T (°C)	P (MPa)	H ₂ /CO	In-situ reduction	CO conv. %	Main product	Sel. %	Ref
1	10%Co-ZSM-5	Imp	240	2	2	350 °C, 10 h, H ₂	60	<C ₁₂	81.4	[137]
2	10%Co-ZSM-11	Imp	240	2	2	350 °C, 10 h, H ₂	61	<C ₁₂	61.9	[137]
3	10%Co-ZSM-12	Imp	240	2	2	350 °C, 10 h, H ₂	79	<C ₁₂	81.7	[137]
4	10%Co-ZSM-34	Imp	240	2	2	350 °C, 10 h, H ₂	45	<C ₁₂	57.7	[137]
5	20%Co-0.1%Pt/ZSM-5	IWI	250	2	2	400 °C, 10 h, H ₂	26.8	C ₁₂₊	52.2	[138]
6	20%Co-0.1%Pt/SiO ₂ +ZSM-5	IWI	250	2	2	400 °C, 10 h, H ₂	26.4	C ₁₂₊	60.5	[138]
7	20%Co-0.1%Pt/MOR	IWI	250	2	2	400 °C, 10 h, H ₂	40.1	C ₁₂₊	60.9	[138]
8	20%Co-0.1%Pt/SiO ₂ +MOR	IWI	250	2	2	400 °C, 10 h, H ₂	39.7	C ₁₂₊	60.2	[138]
9	20%Co-0.1%Pt/BEA	IWI	250	2	2	400 °C, 10 h, H ₂	17.5	C ₁₂₊	55.8	[138]
10	20%Co-0.1%Pt/SiO ₂ +BEA	IWI	250	2	2	400 °C, 10 h, H ₂	54.9	C ₁₂₊	65	[138]
11	15%Co/ZSM-5(using TEOS as silica source)	IWI	220	2	2	400 °C, 10 h, H ₂	28.2	C ₅₊	45.5	[112]
								C ₅₋₁₂	31.2	
								C ₁₃₋₁₈	10.6	
12	15%Co/ZSM-5(using CTAB/TEOS as silica source)	IWI	220	2	2	400 °C, 10 h, H ₂	34.4	C ₅₊	74.7	[112]
								C ₁₈₊	3.7	
								C ₅₋₁₂	37.8	
								C ₁₃₋₁₈	29.5	
13	15%Co/ZSM-5(using P123/CTAB/TEOS as silica source)	IWI	220	2	2	400 °C, 10 h, H ₂	38.2	C ₁₈₊	7.4	[112]
								C ₅₊	74	
								C ₅₋₁₂	36.8	
								C ₁₃₋₁₈	29.1	
								C ₁₈₊	8.2	
14	20%Co/Al-BEA (Si/Al=12.5)	Imp	260	3	2	500 °C, 1 h, 95% H ₂ in Ar	68	C ₂₊ (liq. HC)	57	[139]
15	10%Co/Al-BEA (Si/Al=12.5)	Imp	260	3	2	500 °C, 1 h, 95% H ₂ in Ar	7	C ₂₊ (liq. HC)	53	[139]
16	20%Co/Si-BEA (Si/Al=1300)	two-step post-synthesis	260	3	2	500 °C, 1 h, 95% H ₂ in Ar	97	C ₂₊ (liq. HC)	84	[139]
17	10%Co/Si-BEA (Si/Al=1300)	two-step post-synthesis	260	3	2	500 °C, 1 h, 95% H ₂ in Ar	92	C ₂₊ (liq. HC)	83	[139]
18	15%Co/H-zeolite Y	melt infiltration	230	2	1	400 °C, 6 h, H ₂	36	C ₅₊	75.1	[90]
								C _{5-C₉}	34	
								C _{10-C₂₀}	38	
								C ₂₁₊	3.1	

(Continued)



Table 6. (Continued).

No	Catalyst	Preparation method	T (°C)	P (MPa)	H ₂ /CO	In-situ reduction	CO conv. %	Main product	Sel. %	Ref
19	15%Co/Na-zeolite Y	melt infiltration	230	2	1	400 °C, 6 h, H ₂	35	C ₅₊	78.2	[90]
								C ₅ -C ₉	26	
								C ₁₀ -C ₂₀	46	
20	15%Co/H-meso-zeolite Y	melt infiltration	230	2	1	400 °C, 6 h, H ₂	42	C ₂₁₊	6.2	[90]
								C ₅₊	81.2	
								C ₅ -C ₉	32	
								C ₁₀ -C ₂₀	47	
21	15%Co/Na-meso-zeolite Y	melt infiltration	230	2	1	400 °C, 6 h, H ₂	40	C ₂₁₊	2.2	[90]
								C ₅₊	89	
								C ₅ -C ₉	17	
								C ₁₀ -C ₂₀	60	
22	5%Co/beta zeolite	Imp	250	2	2	350 °C, 1 h, 10% H ₂ in N ₂	2.3	C ₂₁₊	12	[140]
23	10%Co/beta zeolite	Imp	250	2	2	350 °C, 1 h, 10% H ₂ in N ₂	11.9	C ₆₊	55.6	[140]
24	5%Co/meso-beta zeolite	Imp	250	2	2	350 °C, 1 h, 10% H ₂ in N ₂	4.1	C ₆₊	40.9	[140]
25	5%Co/meso-beta zeolite	Imp	250	2	2	350 °C, 1 h, 10% H ₂ in N ₂	14.1	C ₆₊	57.8	[140]
26	20%Co/micro-Al-beta zeolite	Imp	260	3	2	400 °C, 1 h, 95% H ₂ in Ar	70.8	C ₆₊	44	[138]
27	20%Co/meso-Al-beta zeolite	Imp	260	3	2	400 °C, 1 h, 95% H ₂ in Ar	7.1	C ₅₊	81.7	[138]
28	20%Co/meso-AlSi-beta zeolite	Imp	260	3	2	400 °C, 1 h, 95% H ₂ in Ar	40.8	C ₅₊	68.3	[138]
29	20%Co/meso-AlSi-beta zeolite	Imp	260	3	2	400 °C, 1 h, 95% H ₂ in Ar	48.5	C ₅₊	82.9	[138]
30	20%Co/micro-Si-beta zeolite	Imp	260	3	2	400 °C, 1 h, 95% H ₂ in Ar	99.0	C ₅₊	87.6	[138]
31	20%Co/meso-Si-beta zeolite	Imp	260	3	2	400 °C, 1 h, 95% H ₂ in Ar	99.6	C ₅₊	81.4	[138]
32	Co/meso-macro-beta zeolite	IWI	225	2	2	400 °C, 6 h, H ₂	41	C ₅₊	81.7	[113]
33	Co/conventional-beta zeolite	IWI	225	2	2	400 °C, H ₂	54.3	C ₅₊	68.3	[113]
34	20%Co-0.1%Pt/ZSM-5	IWI	250	2	2	400 °C, 10 h, H ₂	27	C ₅₊	55.1	[141]
35	10%Co/meso-zeolite	Imp	260	1	2	NA	25.9	C ₁₂₊	70.7	[142]
36	15%Co/H-ZSM-5	Imp	220	2	2	400 °C, 10 h, H ₂	71.2	C ₅₊	67.3	[143]
								C ₅ -C ₁₂	33.8	
								C ₁₂ -C ₁₈	29.7	
								C ₁₈₊	3.8	

(Continued)

Evaluation of the mesostructuration of beta-zeolite and metal content on the properties of the cobalt catalysts for FT synthesis revealed that increasing the metal loading and the mesostructuration of the zeolite resulted in a decreased specific surface area. An increase in the cobalt particle size observed by increasing the metal loading, which is more reducible due to the lower cobalt-support interaction, and therefore they are more active in FT reaction.^[140] It has been reported that the microporous structure of the catalysts leads to higher selectivity to lighter products (C₂-C₅). Mesostructuration of beta-zeolite resulted in a slight increase in the CO conversion and selectivity to heavier hydrocarbons (C₆₊), while the methane selectivity decreased. On the other hand, by increasing the cobalt loading from 5% to 10%, the CO conversion and selectivity to C₂-C₅ increased, but the C₆₊ selectivity decreased. The lowest olefin/paraffin ratio and the highest CO conversion observed for the 10% cobalt loading and mesostructured zeolite beta.

The mesoporous and microporous Co-Beta zeolite catalysts and their performance in FT synthesis have been studied by Sadek et al.^[147] The dealumination and formation of the larger Co nanoparticles were the main parameters for improving the catalytic activity and selectivity to liquid products. Also, decreasing the acidity of the catalysts improved the resistance for carbon deposition and increased their stability in the FT reaction. The C₁₀-C₁₄ isoalkanes and n-alkanes were the main liquid product over both micro- and mesoporous catalysts, while the ratio of isoalkane/n-alkane for the microporous zeolites was higher than on mesoporous zeolite.^[149] The micro-meso-macroporous beta zeolite (HB) supported cobalt catalyst with rich acidic sites increased the isoparaffins selectivity, and the macroporous structure of zeolite decreased the internal diffusion limitations.^[113] The diffusion limitations in the zeolite micropores, in particular for carbon monoxide, would lead to higher methane formation.

Xing et al.^[142] reported that the encapsulation of cobalt clusters inside the H-ZSM-5 zeolite (Co/MZ, 10 wt.% Co) resulted in higher isoparaffins selectivity in FT reaction (T = 260 °C; P = 1.0 MPa; H₂/CO = 2). The lower CO conversion observed over the Co/MZ than that of Co/SBA-15, under the same reaction conditions, which attributed to the low reduction degree of the Co/MZ catalyst and also the coverage of the active sites originated from the strong cobalt-zeolite interaction. The low chain growth probability ($\alpha=0.68$) of this catalyst also resulted in higher methane selectivity. In addition, presence of microporous cavities and acidic properties of the prepared catalyst led to the more methane formation in FT reaction.

The alkali treatment could create hierarchical structured ZSM-5 and enhance cobalt-support interaction.^[143] After calcination of silica support in the presence of alkali metal (Na⁺) as a structural promoter, the amorphous phase of silica changed to α -SiO₂ phase, and alkali treatment did not collapse the framework. The increase of α -SiO₂ content led to the formation of stronger cobalt-support interaction, and the cobalt particle sizes decreased by increasing the Si/Al ratio. The mesoporosity increased by increasing the Si/Al ratio. The Si/Al ratio of 80

found to be the optimum ratio that resulted in a narrow bimodal pore size distribution as well as a moderate cobalt-support interaction, and it had higher diesel selectivity and lower methane selectivity. Cheng et al. [144] synthesized a series of cobalt-based catalysts supported on mordenite composite (MOR/ZSM-5) using a solvent-free synthesis method with different crystallization times. The Co@MOR/ZSM-5 with crystallization times of 24–72 h revealed both weak and strong acid sites at 110 °C–312 °C and 340 °C–500 °C, while the catalyst with lowest crystallization time of 12 h, had a very small peak at 110 °C–312 °C, which could be due to the poor crystal development. The composite zeolites containing ZSM-5 found to be very active for conversion of syngas into gasoline range (C₅–C₁₁) hydrocarbons (Table 7), 72.3% selectivity to gasoline at 33.4% CO conversion obtained over Co@MOR/ZSM-5 catalyst. The high gasoline production could be due to the perfect crystal structure of composite at long crystallization time. The WGS reaction, which usually occurred on the Si-OH groups of the zeolites as an active site for the WGS reaction, is the main reason for the formation of CO₂ in the final product. [145] It was also found that the inadequate framing of Co particles within the MOR/ZSM-5 crystal improved the CO₂ selectivity for the zeolite composite with lower crystallization times (12 and 24 h). Lower isoparaffin selectivity observed for the Co@MOR/ZSM-5 catalysts compared with Co/NaZSM-5 and Co/NaMOR. Generally, all zeolites occupied acidic sites for hydrocracking and isomerization leading to higher isoparaffin selectivity. It has been reported that the occupation of the cation exchange sites of the zeolite by Na⁺ ions is ideal for cobalt deposition during impregnation with cobalt nitrate. [146] The cobalt deposition on H-form BEA zeolite through impregnation resulted in the localization of cobalt on both the external surface and in the micropores of zeolite. This simultaneous deposition of cobalt resulted in higher methane selectivity. The presence of cobalt particles on the external surface and high concentration of Brönsted acid sites in the micropores of the zeolite led to lower methane selectivity and higher selectivity to long-chain hydrocarbons, and isomerized hydrocarbons.

He et al. [150] investigated the direct synthesis of middle isoparaffins using multiple-functional capsule FT catalysts. Capsule catalysts with core-shell

Table 7. The catalytic performance of synthesized catalyst in FT reaction (reaction conditions: 260 °C, H₂/CO=1, 20 ml/min, 1 MPa, W/F=6 g.mol/h). [144].

Catalysts	CO conv. %	Selectivity %					
		CO ₂	CH ₄	C ₂ –C ₄	C ₅ –C ₁₁	C ₁₂₊	C _{iso}
CO/SiO ₂	30.4	6.3	12.1	29.8	49.0	9.6	11.1
Co/NaZSM-5	21.5	32.7	8.0	21.8	67.7	2.5	25.4
Co/NaMOR	33.0	10.3	13.0	18.8	41.3	27.0	25.9
CO@MOR/ZSM-5(12h)	21.9	18.5	11.0	12.0	63.1	13.9	18.9
CO@MOR/ZSM-5(24h)	33.9	18.5	13.9	16.8	63.6	5.8	19.6
CO@MOR/ZSM-5(48h)	28.9	6.8	14.5	13.3	58.2	14.0	18.3
CO@MOR/ZSM-5(72h)	33.4	10.3	9.6	15.9	72.3	2.2	18.6

structure were synthesized by coating a H-ZSM-5 membrane onto the surface of the Co/SiO₂ pellet. However, compared with Co/SiO₂, the CO conversion over the capsule catalysts was slightly lower, but they had a higher selectivity to lighter hydrocarbons containing isoparaffins. The heavier hydrocarbons and waxes which remained on the surface of the catalysts were subjected to the secondary isomerization and hydrocracking reactions on the acidic sites of the zeolite and converted to lighter hydrocarbons. The product selectivity to long-chain paraffins suppressed due to the successive isomerization and hydrocracking reactions, thus enhanced the selectivity toward the light isoparaffins.

A series of ZSM-5/SBA-15 composites were prepared and used as support for cobalt-based FT catalysts by Wu et al.^[147] In comparison with single supported catalysts (Co/SBA-15 and Co/ZSM-5), an excellent catalytic activity was observed over the composite catalyst (20% ZSM-5, 80% SBA-15, 15% Co loading) in FT reaction (240 °C, 2 MPa, and H₂/CO=2). This high activity could be due to the large pore size and high cobalt dispersion, which led to an optimum reducibility and acid site density. By increasing the amount of ZSM-5, a volcanic shape was observed for the selectivity profiles of the C₁-C₄ and C₅-C₂₂, and in the composite containing 20%ZSM-5 the product distribution shifted to the range of middle distillate hydrocarbons, with minimum selectivity to C₁-C₄ and maximum selectivity to C₅-C₂₂.

3.1.5. Carbonaceous materials

Carbonaceous materials are widely used as support materials for different catalytic reactions due to their different physical properties. Carbon materials exhibit excellent resistance in acidic and basic media. Their porous structure could be adjusted for specific reactions. An enhanced metal dispersion and adsorption are also possible due to the presence of various oxygenated functional groups and the amphoteric character of the carbon materials. Also, they have superb stability at high temperatures (even above 700 °C); however, in the presence of oxygen at above 220 °C, and for hydrogenation reactions at above 420 °C, they lost their stability.^[151-153] Compared with other support materials such as alumina and silica, carbon materials are less expensive, and porous carbons can be prepared in different physical forms such as fibers, pellets, granules, extrudates, etc. The active metals of the catalysts can be recovered by burning the carbon.^[151]

Surface oxygen groups are considered to enhance the metal-carbon support interaction and allowing better metal dispersion. Carbonaceous materials are the most commonly applied support for the preparation of the noble metal catalysts, especially for Pt-based catalysts.^[154] In addition to its role as the catalyst support, carbon also sometimes contribute to catalytic activity (hydrogen spillover) and reacts with other catalysts during the catalytic process. The spillover effect is usually enhanced in the presence of oxygen

groups such as hydroxyl and carboxyl groups on the surface of carbonaceous materials.^[151] However, Alumina, silica, and titania are widely applied as support for commercial FT catalysts, but due to the strong metal-support interaction, there is a high probability for the formation of difficult to reduce compounds. Therefore, to overcome this problem, carbonaceous materials have been chosen to be used as neutral supports for FT catalysts.

Due to the intrinsic inertness of their surface to form a weak interaction between the metal and support, which is very important to achieve a high degree of reduction, carbon materials found to be potential support for FT catalysts. The performance of different carbon materials such as activated carbon (AC) with an amorphous structure, and crystalline carbon structures such as carbon nanotubes (CNTs), carbon nanofibers (CNFs) and carbon nanohorns (CNHs) as support for cobalt-based FT catalysts have been extensively studied.^[7,120,155–164] The catalytic activity of different carbonaceous supported cobalt-based catalysts in the FT reaction are summarized in [Table 8](#).

The functionalization of CNTs could enhance its hydrophobicity and interaction with metal species. Generally, acid treatment is used as a wet chemical oxidation method for introducing oxygen-containing groups on the CNTs' walls. Acid functionalization of CNTs is also crucial to remove the amorphous carbon and metal impurities, produce more open-end tubes and create some defects in CNTs' structure. The interaction between metals and carbon support facilitate by the presence of defects and functional groups on CNTs' walls and improve the exchange of cations between metal and CNTs. Thus, the metal dispersion could affect by the functionalization.^[179,180]

Vosoughi et al.^[7] studied the effect of nitric acid concentrations (35, 50, and 70 wt.%) on the physicochemical properties of the CNTs' walls, and the catalytic performance of 15%Co on these acid-treated supports in FT reaction evaluated. Acid treatment with a high concentration of HNO₃ (70 wt.%) resulted in the formation of more defects on the CNTs' walls, as well as more anchoring sites for the cobalt metals, and consequently higher metal dispersion and thus higher CO conversion. Higher acid concentration also resulted in a decrease in cobalt crystallite size. By increasing the acid concentration from 35 wt.% to 70 wt.%, the reduction temperature of the metal nanoparticles decreased, and reducibility slightly increased ([Figure 5](#)). The catalytic activity evaluated in a fixed-bed reactor at the following reaction conditions: H₂/CO=2, 220 °C, and 2 MPa. The CO conversion increased by increasing the acid concentration; however, by increasing the reaction time up to 50 h, all catalysts lost their activity, but this decrease was lower for acid-treated CNTs. The catalyst stability could be related to the number of functional groups, defects, and the strength of cobalt-support interaction. The catalyst deactivation could cause by one or more of these reasons: 1) formation of cobalt carbide, 2) oxidation of cobalt in the presence of water, 3) sintering


Table 8. The catalytic activity of different carbonaceous supported cobalt-based catalysts in the FT reaction.

No	Catalyst	Preparation method	T (°C)	P (MPa)	H ₂ /CO	In-situ reduction	CO conv. %	Main product	Sel. %	Ref
1	15%Co/GNT	IWI	220	2	2	350 °C, 16 h, H ₂	22.0	C ₅₊	90.2	[7]
2	15%Co/GNT(35%HNO ₃)	IWI	220	2	2	350 °C, 16 h, H ₂	25.2	C ₅₊	87.9	[7]
3	15%Co/GNT(50%HNO ₃)	IWI	220	2	2	350 °C, 16 h, H ₂	27.5	C ₅₊	85.7	[7]
4	15%Co/GNT(70%HNO ₃)	IWI	220	2	2	350 °C, 16 h, H ₂	30.1	C ₅₊	81.2	[7]
5	3%Co/Carbon nanospheres	IWI	220	2	2	400 °C, 10 h, H ₂	<10	C ₅₊	51.3	[155]
6	3%Co/N-Carbon nanospheres	IWI	220	2	2	400 °C, 10 H ₂	<10	C ₅₊	74.4	[155]
7	12%Co/(CNF/carbon-feit)	IWI	210	2	2	350 °C, 16 h, H ₂	56	C ₅₊	80	[156]
8	15%Co/AC	IWI	220	3	2	430 °C, 4 h, H ₂	30.2	C ₅₊	32.8	[157]
								C ₆ -C ₁₈ alcohols	39.3	
9	15%Co-6.3SiO ₂ /AC	IWI	220	3	2	430 °C, 4 h, H ₂	76.6	C ₅₊	65.9	[157]
								C ₆ -C ₁₈ alcohols	54.6	
10	10%Co/N-HCS(hollow carbon spheres)	homogeneous deposition precipitation	250	1	2	350 °C, 18 h, H ₂	48	C ₅₊	52.8	[160]
11	10%Co/N-HCS(hollow carbon spheres)	homogeneous deposition precipitation	220	1	2	350 °C, 18 h, H ₂	34	C ₅₊	75.8	[160]
12	25%Co/N-NGC(nitrogen functionalized graphene nanosheets)	Imp	220	1.8	2	400 °C, 20 h, H ₂	78.6	C ₅₊	86.5	[161]
13	25%Co-0.5%Ru/N-NGC(nitrogen functionalized graphene nanosheets)	Imp	220	1.8	2	400 °C, 20 h, H ₂	86.9	C ₅₊	91.2	[161]
14	15%Co/GNT	modified photo-Fenton process	200	1	2	350 °C, 4 h, H ₂	80	C ₅₊	70.2	[162]
15	15%Co/GNT	IWI	200	1	2	350 °C, 4 h, H ₂	65	C ₅₊	45	[162]
16	6.1%Co/carbon spheres	thermal decomposition	232	1	2	352 °C, 3 h, H ₂	21	C ₅₊	81.9	[163]
17	6.1%Co/carbon spheres	IWI	232	1	2	352 °C, 3 h, H ₂	4.8	C ₅₊	59.5	[163]
18	6.1%Co/carbon spheres	ultrasonic Imp	232	1	2	352 °C, 3 h, H ₂	3	C ₅₊	59.5	[163]
19	15%Co/AC	Imp	220	3	2	430 °C, 4 h, H ₂	28.9	C ₅₊	32	[164]
20	15%Co-3wt.%Cr/AC	Imp	220	3	2	430 °C, 4 h, H ₂	45.6	C ₅₊	42.5	[164]
21	15%Co/GNT	Imp	230	2	2	400 °C, 10 h, H ₂	48.3	C ₂ -C ₄	28.6	[165]
								C ₅ -C ₁₂	38.1	

(Continued)

Table 8. (Continued).

No	Catalyst	Preparation method	T (°C)	P (MPa)	H ₂ /CO	In-situ reduction	CO conv. %	Main product	Sel. %	Ref
22	15%Co/CNT-functionalizes by H ₂ O ₂	Imp	230	2	2	400 °C, 10 h, H ₂	53.8	C ₂ -C ₄	32.5	[165]
23	15%Co/CNT	Imp	220	2	2	400 °C, 12 h, H ₂	75	C ₅ -C ₁₂	36.1	[166]
24	15%Co/CNT	Imp + magnetized water	220	2	2	400 °C, 12 h, H ₂	84	C ₅ -C ₁₂	37.8	[166]
25	5%Co/CNT	Imp	220	0.1	2	400 °C, 4 h, H ₂	13	C ₅ +	36	[167]
26	15%Co/CNT	Imp	220	0.1	2	400 °C, 4 h, H ₂	30	C ₅ +	46	[167]
27	40%Co/CNT	Imp	220	0.1	2	400 °C, 4 h, H ₂	20	C ₅ +	27	[168]
28	7%Co/AC	Imp	240	2.4	2	400 °C, 16 h, H ₂	31.8(syngas conv.)	CH ₄	18	[168]
29	15%Co/AC	Imp	240	2.4	2	400 °C, 16 h, H ₂	58.4(syngas conv.)	CH ₄	11.7	[168]
30	20%Co/AC	Imp	240	2.4	2	400 °C, 16 h, H ₂	70.2(syngas conv.)	CH ₄	18.4	[168]
31	15%Co-2%Ce/AC	Imp	240	2.4	2	400 °C, 16 h, H ₂	80.9(syngas conv.)	CH ₄	23.8	[168]
32	30%Co/CNT	Imp	220	2	2	380 °C, 20 h, H ₂	86	C ₅ +	32.7	[169]
33	15%Co/CNT	Imp	220	2	2	380 °C, 20 h, H ₂	48	C ₅ +	77	[169]
34	15%Co-1%Ru/CNT	Imp	220	2	2	380 °C, 20 h, H ₂	71	C ₅ +	70	[169]
35	15%Co-1%Ru/CNT	Imp	220	2	2	380 °C, 20 h, H ₂	5	C ₅ +	77	[169]
36	15%Co/CNT	Imp	220	2.5	2	400 °C, 24 h, H ₂	45	C ₅ +	87	[170]
37	25%Co/CNT	IWI	220	2	2	500 °C, 5 h, H ₂	28	C ₅ +	87	[171]
38	15%Co/CNT	IWI	220	2	2	500 °C, 5 h, H ₂	26	C ₅ +	72	[171]
39	12%Co/GNF	IWI	210	2	2	350 °C, 16 h, H ₂	40	C ₅ +	68	[172]
40	12%Co/GNF	thermal decomposition	220	1	2	Ex situ: 350 °C, 3 h, H ₂	5.7	C ₅ +	81.6	[173]
41	20%Co/CMK-3 (ordered mesoporous carbon)	IWI	230	2	2	400 °C, 10 h, H ₂	40	C ₅ +	93.8	[174]
42	20%Co/CNT	IWI	230	2	2	400 °C, 10 h, H ₂	64	C ₅ +	82.2	[174]
43	20%Co/AC	IWI	230	2	2	400 °C, 10 h, H ₂	60	C ₅ +	87.3	[174]
44	15%Co/AC(steam pretreated)	Imp	230	2.5	2	350 °C, 19 h, H ₂	NA	C ₅ +	77.7	[175]

(Continued)

Table 8. (Continued).

No	Catalyst	Preparation method	T (°C)	P (MPa)	H ₂ /CO	In-situ reduction	CO conv. %	Main product	Sel. %	Ref
45	15%Co/AC(steam pretreated)	Imp	230	2.5	2	350 °C, 19 h, H ₂	NA	C ₅₊	73.2	[175]
46	15%Co/AC	Imp	220	0.1	2	400 °C, 12 h, H ₂	12.6	C ₅₊	17.9	[176]
47	15%Co/CNT	Imp	220	0.1	2	400 °C, 12 h, H ₂	18.8	C ₅₊	29.1	[176]
48	15%Co/CNT-MgO(CNTs grown on MgO)	Imp	220	0.1	2	400 °C, 12 h, H ₂	10.6	C ₅₊	49.9	[176]
49	15%Co/CNT-Al ₂ O ₃ (CNTs grown on MgO)	Imp	220	0.1	2	400 °C, 12 h, H ₂	12.2	C ₅₊	41.3	[176]
50	13.2%Co/CNF	Imp	220	2.8	2	NA	NA	C ₅₊	86	[177]
51	4.3%Co/CNT	Imp	225	0.8	2	400 °C, 20 h, H ₂	25.9	C ₅₊	62.1	[178]
52	15%Co/CNT	deposition precipitation	225	0.8	2	400 °C, 20 h, H ₂	9.9	C ₅₊	72.1	[178]
53	5.2%Co/CS	Imp	225	0.8	2	400 °C, 20 h, H ₂	2.6	C ₅₊	99.1	[178]
54	1.5%Co/CS	deposition precipitation	225	0.8	2	400 °C, 20 h, H ₂	3.7	C ₅₊	94.8	[178]

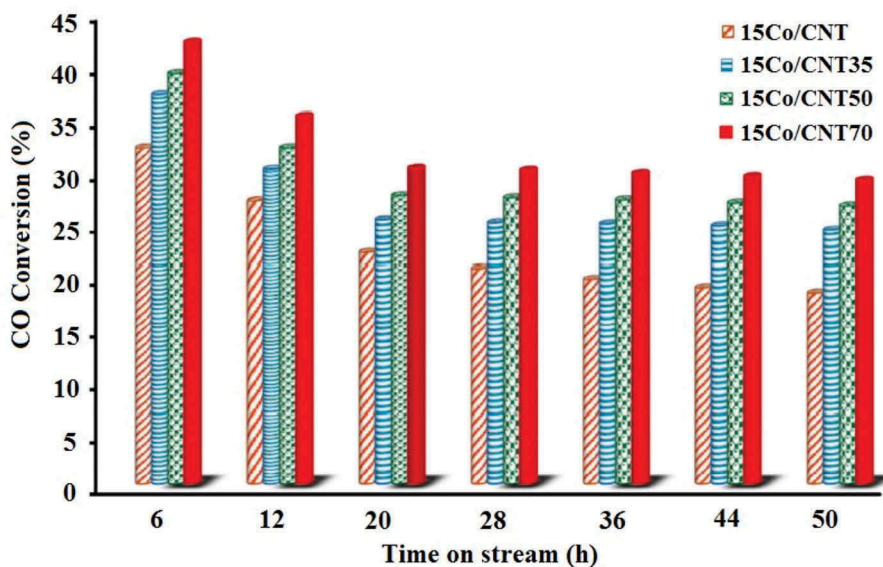


Figure 5. CO conversion for 15Co/CNT catalysts in FTS at 220 °C, 2 MPa, and 3000 cm³·g⁻¹·h⁻¹.^[7]

and migration of cobalt particles, 4) carburization and carbon deposition, 5) poisoning, 6) surface reconstruction, and 7) decrease in the adsorption/desorption rate of the reactant and products due to the formation of heavy hydrocarbons on the surface and inside the pores of the CNTs. On the other hand, the highest selectivity to C₅₊ and lowest CH₄ selectivity were observed for the untreated catalyst and the CNTs treated with lower acid concentration. Increasing the acid concentration improved the hydrogenation ability of CNT supports, thus increased the CH₄ selectivity.

Impregnation and precipitation are known as the most commonly used methods for the preparation of supported metal catalysts. However, only controlling the size and distribution of metal particles is possible using these two methods. Therefore, new synthesis methods such as atomic layer deposition, melt-infiltration, and colloidal synthesis are developed to improve the catalyst design. Among these different methods, colloidal synthesis of metal nanoparticles found to be suitable for the preparation of well-defined catalysts by controlling the size, shape, and composition of metal nanoparticles.^[181,182]

The functionalization of CNTs increased the reducibility of cobalt particles on the outer wall and inside the tubes due to the confinement and hydrogen spillover the functional groups. In the spillover process, the H₂ molecule dissociated into two atoms of hydrogen, which diffused on the supports surface, while some atoms attached to the metals. Thus, support of the catalyst acts as a reservoir for the hydrogen atoms.^[183,184] Increasing the cobalt particle sizes resulted in a decreased hydrogen concentration on the surface of the catalyst. On the other hand, increasing the hydrogen concentration on the surface of catalyst

led to a higher concentration of C_1 monomers with a higher degree of hydrogenation, thus, selectivity to lower hydrocarbons improved at smaller particle sizes. Other researchers^[162,166] also reported that the CO conversion and selectivity to C_{5+} increased by decreasing the cobalt particle size.

The dependency of catalytic properties of Co/CNT catalysts on the metal content from 1 to 40 wt.% has been investigated by Chernyak et al.^[167] It was observed that the cobalt particle sizes increased by increasing the metal content, while the reduction temperature of the catalysts was independent of their particle size, and it was only changed the intensities of the peaks belong to the reduction of cobalt oxides. The cobalt particle size in 1 wt.% Co/CNT was larger than other catalysts with higher cobalt content (5, 10, and 15 wt. %), and also the particle size distribution was wider for this catalyst. The larger cobalt particle size of 1 wt.%Co/CNT catalyst could be due to the tendency of the small metal particles for agglomeration. The 20 wt.%Co/CNT catalyst contained larger particles with broader size distribution. By increasing the cobalt concentration up to 20 wt.%, the CO conversion increased, and further increase in cobalt content (up to 40 wt.%) resulted in a sharp decrease in CO conversion, and the dependency of selectivities to the metal content found to be more complicated. The decrease in CO conversion by increasing the Co content above 20 wt.% was probably due to the poor stability of metal and agglomeration and formation of large particles, which significantly decreased the number of active sites on the surface. The capacity limitation for the uniform metal particle distribution at higher cobalt concentration led to the deposition of cobalt particles not only on the surface of CNTs but also on another metal particle to form agglomerates, thus decreased the effective metal surface area.^[167] Ma et al.^[168] also reported that increasing the cobalt content resulted in a lower C_{5+} selectivity and higher CH_4 selectivity, and they claimed that smaller particles are more active for the C_{5+} formation. However, in some other studies, it was found that the selectivity to C_{5+} increased by increasing the metal content of the catalyst.^[169-171]

Recently, the hollow carbon spheres functionalized by N-doping via a post-synthesis method have been used as support for cobalt-based FT catalysts.^[160] Hollow carbon spheres with a porous structure, high surface area, and low densities found to be promising support for the synthesis of highly dispersed catalysts, and metal nanoparticles could be placed inside the hollow carbon sphere and form a rattle of core-shell type catalyst.^[185,186] The post-synthesis N-doping method provided promising carbon support with more anchoring sites, high thermal stability, and immobilized the catalyst particles during the reaction, which minimized the particle agglomeration. The reduction temperature increased for the N-doped carbon spheres as a result of the stronger electronic interaction of cobalt oxide nanoparticles and the N-doped hollow carbon sphere. This interaction facilitated the electron transfer from the N-doped carbons to the Co oxide particles. The catalytic activity of the synthesized catalysts was evaluated in FT reaction at

220 °C and 250 °C, 1 MPa, and H₂/CO of 2, and the catalyst was reduced in-situ with pure H₂ at 350 °C.^[160] The N-doped catalyst showed higher activity than the un-doped one, which could be due to the smaller particle sizes of the cobalt oxides particles on N-doped support. The selectivity to C₅₊ decreased by introducing N and increasing the reaction temperature from 220 °C to 250 °C resulted in a significant decrease in C₅₊ selectivity, most probably due to the catalyst sintering at a higher temperature. A higher methane selectivity for N-doped catalysts also observed, which is in good agreement with the obtained results by Bezemer et al.^[46]

Carbon nanofibers (CNFs) also found to be promising graphitic support material for both cobalt- and iron-based FT catalysts. CNF comprises interwoven graphitic carbon with high purity, high chemical inertness, and high mechanical strength.^[153,164] Bezemer et al.^[177] studied the catalytic performance of Co/CNF catalysts in the FT reaction. Catalysts were prepared by wet impregnation method. The cobalt particle size of the catalysts changed from 3 to 13 nm by increasing the cobalt content from 5 to 12 wt.%, and metal particles were located on both the internal and external surfaces of the fibers. The catalysts with smaller particle sizes revealed a lower catalytic activity. A stable activity FT reaction after 400 h (220 °C, 2.8–4.2 MPa, and H₂:CO=2) with high C₅₊ selectivity of 86% was observed over this 12 wt.%Co/CNF catalyst.

The dependency of cobalt particle size with the catalytic activity and C₅₊ selectivity for different catalysts has been reported by several research groups.^[45,178,187,188] Borg et al.^[45] found that the maximum C₅₊ selectivity obtained at the cobalt particle size of 7–8 nm. In another research,^[179] it was reported that the turnover frequency (TOF) value for cobalt catalysts supported on carbonaceous materials significantly decreased for cobalt particles above 10 nm; and the C₅₊ selectivity increased by increasing of the cobalt particle size. The positive relationship in particle size and C₅₊ selectivity could be attributed to the easier formation of bridge-type adsorbed CO on large cobalt particles. Due to its weaker C–O bond, the bridge-type CO is much more active than the linear-type CO; therefore, it can be easily dissociated to carbon and oxygen. Gavrilović et al.^[41] also reported the same relationship between the cobalt particle size and catalytic activity and C₅₊ selectivity.

Activated carbon (AC) is one of the most commonly used amorphous carbons. Employing activated carbon as catalyst support could be mainly due to its low cost, abundance, high thermal stability in the oxygen-free atmosphere, high resistance to basic/acidic media, high micropores and mesopore volumes, high surface area, and flexibility for tuning of its textural properties and surface chemistry.^[189] Activated carbons have been widely used as support for cobalt-based FT catalysts.^[123,157,158,164,165–174,190] A series of cobalt-based catalysts supported on AC have been synthesized and characterized by Lahti et al..^[158] Different pre-treatments and metal loading techniques found to have a significant effect on the catalyst properties such as

specific surface area, pore distribution, ash value, and volume of mesopores. Acid treatment of AC could affect the catalytic activity by removing the impurities and inorganic compounds such as metals from carbon support. The analysis revealed that in all prepared catalysts, cobalt was successfully added onto carbon support. The highest metal dispersion was observed for the catalyst prepared by the ultrasonic-assisted impregnation method. The metals with smaller particle sizes were found to be difficult to reduce. TPR results also showed that compared with SiO₂ supported catalysts, the AC supported catalysts had lower reduction temperature in the second reduction step of cobalt oxide to metallic cobalt. In addition, the reduction temperature and degree of reduction positively affected by the HNO₃ pre-treatment. The formation of cobalt carbide (Co₂C) during the catalyst activation could reduce catalytic activity. Formation of Co₂C species could be inhibited by the addition of some promoters, such as Cr and Mn, as well as pre-treatment of AC, such as steam pre-treatment.^[175] Zhao et al.^[164] reported that introducing of Cr as a promoter (Co_xCr/AC catalyst) enhanced the CO hydrogenation and C–C coupling step by facilitating the H₂ adsorption, decreasing the formation of Co₂C species, and forming C-lean and H-rich surface chemicals environment. Catalytic performance of Co_xCr/AC catalysts in FT reaction at 220 °C, 3 MPa, and H₂:CO of 2 were also investigated. Compared with the un-promoted catalyst, a significant increase in the yield of transportation fuel observed by increasing the CO conversion.

A comparison between the catalytic properties and their activity in the FT reaction of the cobalt catalysts (20 wt.%) supported on ordered mesoporous carbon (CMK-3), CNTs, and AC have been made by Fu et al.^[174] It was found that the Co₃O₄ particles mostly distributed inside the tubes (or pores) of the CNT- and CMK-3 supported catalysts, but they were mainly outside the pores for AC supported catalyst. The particle sizes of Co₃O₄ depended on the support properties and structure. However, AC had the highest surface area, but after loading of Co on the support, the surface area significantly decreased from 1897 to 854 m²/g, because the entrance of the micropores could be blocked easier than mesopores. The cobalt particles were mainly located inside the CNTs tubes, and due to the spatial restriction effect, they will not aggregate under the reduction condition. The Co/AC catalyst showed the lowest selectivity to C₅₊ and the highest selectivity to methane. The Co/AC and Co/CMK-3 catalysts showed a very low or negligible activity for WGS reaction, and the selectivity for CO₂ over these catalysts was zero, while over the CNT supported catalysts the CO₂ selectivity was 0.34%. The electron transfer between the cobalt and CO molecules on Co/CNTs facilitated due to the good crystallized graphitic structure of CNTs, which resulted in a better catalytic activity than the other two catalysts.

3.2. Promoters

It is known that the active metal, loading amount, nature, and textural properties of the support, properties of additives, and the preparation method of the catalyst would have a significant effect on the physicochemical properties of the catalyst. The physicochemical properties of the cobalt catalyst comprise the cobalt particle size, dispersion, degree of reduction, number and nature of the active sites, electronic structure, and cobalt-support interaction. The cobalt-support interaction and the number of active sites directly affected by the supporting material and promoter, which is consequently affecting the FT catalytic performance. Promoters can be used as a structural, textural, electronic modifier, stabilizers, and catalyst-poison-resistant, which can improve the catalytic performance.^[191] Structural promoters are able to modify the surface properties by affecting the metal-support interaction, thus improving the metal dispersion and number of active metals. Electronic promoters can modify the electron density on the surface of the catalyst through addition or withdrawal of electron density near the Fermi level in the valence band of the metal.^[192,193] Different types of promoters, such as TiO₂, Al₂O₃, SiO₂, and CeO₂, are known as structural promoters.^[126,194–198] Addition of Ag, Pt, Re, and Ru as a promoter, resulted in the improved number of active sites, and it can enhance the reduction of CoO species by changing of the cobalt-support interaction, mainly by shifting the reduction of CoO to Co⁰ to the lower temperature.^[134,192,199,200] Moreover, electronic promoters can affect the dissociation of chemical bonds of the reactants and thus change the catalytic performance. Some promoters, such as noble metals, can act as both structural and electronic promoters, and sometimes it is difficult to define the exact function of the promoter due to the overlapping of the effects.^[201] The addition of Ru as promoter enhances the reducibility of cobalt catalyst by hydrogen spillover mechanism, and better reduction results in an improved catalyst activity.^[191] In this section, some highlights on noble metal, transition metal oxide, alkali and alkaline earth metal promoters for cobalt-based FT catalysts are discussed. The catalytic activity of cobalt-based catalysts modified with different types of promoters are summarized in Table 9.

3.2.1. Noble metals

Among different noble metals, platinum (Pt), ruthenium (Ru), and iridium (Ir) are the most patented promoters for FT cobalt-based catalysts.^[223] The effect of Ru and Pt as a promoter for the cobalt catalyst supported on CNTs has been studied by Zhang et al.^[203] Reduction temperature shifted to lower temperature by addition of 0.2 wt.% of the promoter and thus resulted in a considerable enhancement in the cobalt reduction. They also found that catalytic stability was enhanced by the addition of Pt to the Co/CNT catalyst. The strong metal-support interaction, for example, in Co/Al₂O₃ catalysts, resulted in a lower



Table 9. Catalytic activity of cobalt-based catalysts modified with different types of promoters in the FT reaction.

No	Catalyst	Preparation method	T (°C)	P (MPa)	H ₂ /CO	In-situ reduction	CO conv. %	Main product	Sel. %	Ref
Nobel metal promoters										
1	0.2%Ru8.2%Co/Silica (Cab-o-sil M-5)	Imp	190	0.1	2	400 °C, 5 h, H ₂	<10%	C ₅ +	72	[121]
2	12%Co/TiO ₂ (calcined)	IWI	220	2.07	2	Ex-situ:350 °C, 18 h, H ₂ ;He=1:3, then in-situ: 230 °C, 12 h, H ₂	29.8	C ₅ +	81.9	[134]
3	12%Co/TiO ₂ (un-calcined)	IWI	220	2.07	2	Ex-situ:350 °C, 18 h, H ₂ ;He=1:3, then in-situ: 230 °C, 12 h, H ₂	49	C ₅ +	85.1	[134]
4	0.5%Pt-12%Co/TiO ₂ (calcined)	IWI	220	2.07	2	Ex-situ:350 °C, 18 h, H ₂ ;He=1:3, then in-situ: 230 °C, 12 h, H ₂	45.3	C ₅ +	85.6	[134]
5	0.5%Pt-12%Co/TiO ₂ (un-calcined)	IWI	220	2.07	2	Ex-situ:350 °C, 18 h, H ₂ ;He=1:3, then in-situ: 230 °C, 12 h, H ₂	56.4	C ₅ +	84.4	[134]
6	9.3%Co/TiO ₂	Imp	220	2	2	350 °C, 8 h, H ₂ ;He=1:3	29.2	C ₅ +	85	[135]
7	0.12%Ag-9%Co/TiO ₂	Imp	220	2	2	350 °C, 8 h, H ₂ ;He=1:3	33.9	C ₅ +	89	[135]
8	0.11%Pt-8.9%Co/TiO ₂	Imp	220	2	2	350 °C, 8 h, H ₂ ;He=1:3	30.4	C ₅ +	83	[135]
9	0.18%Ru-7.3%Co/TiO ₂	Imp	220	2	2	350 °C, 8 h, H ₂ ;He=1:3	31.8	C ₅ +	88	[135]
10	0.25%Re-9.4%Co/TiO ₂	Imp	220	2	2	350 °C, 8 h, H ₂ ;He=1:3	33.1	C ₅ +	88	[135]
11	0.5%Pt-12%Co/TiO ₂	IWI	210	1	2	330 °C, 10 h, H ₂	28.6	C ₅ +	81.9	[202]
12	0.5%Pt-12%Co/TiO ₂ (treated by glow discharge plasma)	IWI	210	1	2	330 °C, 10 h, H ₂	66.3	C ₅ +	84.1	[202]
13	20%Co-0.1wt.%Pt/ZSM-5	IWI	250	2	2	400 °C, 10 h, H ₂	26.8	C ₁₂ +	52.2	[138]
14	20%Co-0.1%Pt/SiO ₂ +ZSM-5	IWI	250	2	2	400 °C, 10 h, H ₂	26.4	C ₁₂ +	60.5	[138]
15	20%Co-0.1%Pt/MOR	IWI	250	2	2	400 °C, 10 h, H ₂	40.1	C ₁₂ +	60.9	[138]
16	20%Co-0.1%Pt/SiO ₂ +MOR	IWI	250	2	2	400 °C, 10 h, H ₂	39.7	C ₁₂ +	60.2	[138]
17	20%Co-0.1%Pt/BEA	IWI	250	2	2	400 °C, 10 h, H ₂	17.5	C ₁₂ +	55.8	[138]
18	20%Co-0.1%Pt/SiO ₂ +BEA	IWI	250	2	2	400 °C, 10 h, H ₂	54.9	C ₁₂ +	65	[138]
19	20%Co-0.1%Pt/ZSM-5	IWI	250	2	2	400 °C, 10 h, H ₂	27	C ₁₂ +	52.0	[141]
20	20%Co-0.1%Pt/ZSM-5-HPW	IWI	250	2	2	400 °C, 10 h, H ₂	14	C ₁₂ +	21.0	[141]
21	20%Co-0.1%Pt/MOR	IWI	250	2	2	400 °C, 10 h, H ₂	40	C ₁₂ +	62.0	[141]
22	20%Co-0.1%Pt/MOR-HPW	IWI	250	2	2	400 °C, 10 h, H ₂	18	C ₁₂ +	32.0	[141]
23	20%Co-0.1%Pt/BEA	IWI	250	2	2	400 °C, 10 h, H ₂	18	C ₁₂ +	56.0	[141]
24	20%Co-0.1%Pt/BEA-HPW	IWI	250	2	2	400 °C, 10 h, H ₂	22	C ₁₂ +	21.0	[141]
25	15%Co/γ-Al ₂ O ₃	Imp	210	2.4	2	380 °C, 12 h, H ₂	39.6	C ₅ +	56	[191]

(Continued)

Table 9. (Continued).

No	Catalyst	Preparation method	T (°C)	P (MPa)	H ₂ /CO	In-situ reduction	CO conv. %	Main product	Sel. %	Ref
26	0.1%Ru-15%Co/γ-Al ₂ O ₃	Imp	210	2.4	2	380 °C, 12 h, H ₂	94.7	C ₅ +	71	[191]
27	0.1%Ru-1%Gd/15%Co/γ-Al ₂ O ₃	Imp	210	2.4	2	380 °C, 12 h, H ₂	84.1	C ₅ +	76	[191]
28	16%Co/γ-Al ₂ O ₃	IWI	220	2.5	2	400 °C, 5 h, H ₂	60.7	C ₅ +	81.8	[192]
29	0.1%Ag-16%Co/γ-Al ₂ O ₃	IWI	220	2.5	2	400 °C, 5 h, H ₂	71.3	C ₅ +	83.6	[192]
30	20%Co/γ-Al ₂ O ₃	Imp	220	2	2	350 °C, 12 h, H ₂	9.5	C ₅ +	65	[199]
31	0.5%Pt-20%Co/γ-Al ₂ O ₃	Imp	220	2	2	350 °C, 12 h, H ₂	19	C ₅ +	57	[199]
32	0.5%Pt-20%Co/γ-Al ₂ O ₃	physical mixing of 20% Pt/Al ₂ O ₃ and Co/Al ₂ O ₃	220	2	2	350 °C, 12 h, H ₂	13	C ₅ +	63	[199]
33	10%Co/CNT	Imp	220	2	2	350 °C, 5 h, H ₂	30.3	C ₅ +	73.6	[203]
34	0.5%Ru-10%Co/CNT	Imp	220	2	2	350 °C, 5 h, H ₂	31.4	C ₅ +	82.5	[203]
35	0.5%Pt-10%Co/CNT	Imp	220	2	2	350 °C, 5 h, H ₂	37.1	C ₅ +	79.3	[203]
36	25%Co/γ-Al ₂ O ₃	slurry Imp	220	2.2	2.1	Ex-situ: 350 °C, 15 h, H ₂ ; He=1:3	23.7	C ₅ +	85.3	[89]
37	0.26%Pd-25%Co/γ-Al ₂ O ₃	slurry Imp	220	2.2	2.1	Ex-situ: 350 °C, 15 h, H ₂ ; He=1:3	22.3	C ₅ +	74.4	[89]
38	0.5%Pt-25%Co/γ-Al ₂ O ₃	slurry Imp	220	2.2	2.1	Ex-situ: 350 °C, 15 h, H ₂ ; He=1:3	25.9	C ₅ +	82.3	[89]
39	0.27%Ru-25%Co/γ-Al ₂ O ₃	slurry Imp	220	2.2	2.1	Ex-situ: 350 °C, 15 h, H ₂ ; He=1:3	33.4	C ₅ +	85.2	[89]
40	10%Co/TiO ₂	Imp	230	2.35	2	Ex-situ: 300 °C, 16 h, H ₂	50.2	C ₅ +	64.5	[204]
41	0.2%Ru-10%Co/TiO ₂	Imp	230	2.35	2	Ex-situ: 300 °C, 16 h, H ₂	68.4	C ₅ +	74.5	[204]
42	12%Co/SiO ₂ (un-calcined)	IWI	220	2	2	Ex-situ: 350 °C, 18 h, H ₂ ; He=1:3	35.2	C ₅ +	84.2	[205]
43	0.5%Pt-12%Co/SiO ₂ (un-calcined)	IWI	220	2	2	Ex-situ: 350 °C, 18 h, H ₂ ; He=1:3	47.8	C ₅ +	81.1	[205]
44	0.276%Ag-12%Co/SiO ₂ (un-calcined)	IWI	220	2	2	Ex-situ: 350 °C, 18 h, H ₂ ; He=1:3	37.6	C ₅ +	78.1	[205]
45	15%Co/Al ₂ O ₃	IWI	190	0.1	2	400 °C, 5 h, H ₂	2.2	C ₅ +	84.2	[206]
46	0.1%Pt-20%Co/γ-Al ₂ O ₃	Imp	190	0.1	2	400 °C, 5 h, H ₂	18.4	C ₅ +	79.4	[206]
Transition metal promoters										
47	0.2%Re7%Co/Silica (Cab-o-sil M-5)	Imp	190	0.1	2	400 °C, 5 h, H ₂	<10	C ₅ +	69	[121]
48	12%Co/γ-Al ₂ O ₃	Imp	210	2	2	350 °C, 16 h, H ₂	45–55	C ₅ +	80	[82]
49	0.5%Re-12%Co/γ-Al ₂ O ₃	Imp	210	2	2	350 °C, 16 h, H ₂	45–55	C ₅ +	83.2	[82]
50	0.5%Re-12%Co/5%Mg-γ-Al ₂ O ₃	Imp	210	2	2	350 °C, 16 h, H ₂	45–55	C ₅ +	81.8	[82]
51	0.5%Re-12%Co/5%Zn-γ-Al ₂ O ₃	Imp	210	2	2	350 °C, 16 h, H ₂	45–55	C ₅ +	82.5	[82]
52	12%Co/γ-Al ₂ O ₃	IWI	210	2	2.1	350 °C, 16 h, H ₂	35	C ₅ +	82.2	[198]
53	20%Zr-12%Co/γ-Al ₂ O ₃	IWI	210	2	2.1	350 °C, 16 h, H ₂	35	C ₅ +	82.9	[198]

(Continued)



Table 9. (Continued).

No	Catalyst	Preparation method	T (°C)	P (MPa)	H ₂ /CO	In-situ reduction	CO conv. %	Main product	Sel. %	Ref
54	20%(10CeZr)-12%Co/γ-Al ₂ O ₃	IWI	210	2	2.1	350 °C, 16 h, H ₂	35	C ₅ +	81.7	[198]
55	20%Ce-12%Co/γ-Al ₂ O ₃	IWI	210	2	2.1	350 °C, 16 h, H ₂	35	C ₅ +	78.2	[198]
56	0.5%Re-20%Co/γ-Al ₂ O ₃	IWI	210	2	2.1	350 °C, 16 h, H ₂	50	C ₅ +	84.3	[207]
57	0.25%Re-12%Co/SiO ₂ (un-calcined)	IWI	220	2	2	Ex-situ: 350 °C, 18 h, H ₂ , He=1:3 Ex-situ: 350 °C, 15 h, H ₂ , He=1:3	35.6	C ₅ +	81.5	[205]
58	0.48%Re-25%Co/γ-Al ₂ O ₃	slurry Imp	220	2.2	2.1	Ex-situ: 350 °C, 15 h, H ₂ , He=1:3	35.8	C ₅ +	85.5	[89]
59	20%Co/θ-Al ₂ O ₃	Imp	230	1	2	400 °C, 6 h, H ₂	48	C ₅ +	82	[201]
60	1%Y-20%Co/θ-Al ₂ O ₃	Imp	230	1	2	400 °C, 6 h, H ₂	46	C ₅ +	79	[201]
61	1%La-20%Co/θ-Al ₂ O ₃	Imp	230	1	2	400 °C, 6 h, H ₂	50	C ₅ +	83	[201]
62	1%Ce-20%Co/θ-Al ₂ O ₃	Imp	230	1	2	400 °C, 6 h, H ₂	55	C ₅ +	82	[201]
63	1%Ti-20%Co/θ-Al ₂ O ₃	Imp	230	1	2	400 °C, 6 h, H ₂	38	C ₅ +	85	[201]
64	1%V-20%Co/θ-Al ₂ O ₃	Imp	230	1	2	400 °C, 6 h, H ₂	37	C ₅ +	86	[201]
65	1%Mn-20%Co/θ-Al ₂ O ₃	Imp	230	1	2	400 °C, 6 h, H ₂	48	C ₅ +	81	[201]
66	1%Zn-20%Co/θ-Al ₂ O ₃	Imp	230	1	2	400 °C, 6 h, H ₂	43	C ₅ +	78	[201]
67	1%Zr-20%Co/θ-Al ₂ O ₃	Imp	230	1	2	400 °C, 6 h, H ₂	49	C ₅ +	83	[201]
68	1%Mn-20%Co/θ-Al ₂ O ₃	Imp	230	1	2	400 °C, 6 h, H ₂	35	C ₅ +	81	[201]
69	2%La-0.5%V-20%Co/θ-Al ₂ O ₃	Imp	230	1	2	400 °C, 6 h, H ₂	77	C ₅ +	81	[201]
70	10%Co/TiO ₂	Imp	230	2.35	2	Ex-situ: 300 °C, 16 h, H ₂	50.2	C ₅ +	64.5	[204]
71	0.34%Re-10%Co/TiO ₂	Imp	230	2.35	2	Ex-situ: 300 °C, 16 h, H ₂	73.4	C ₅ +	80.8	[204]
72	10%Co/SiO ₂	Imp	230	2	2	400 °C, 12 h, H ₂	41.7	C ₅ +	82.5	[208]
73	10%Co/TiO ₂ -SiO ₂	Imp	230	2	2	400 °C, 12 h, H ₂	85.9	C ₅ +	85.6	[208]
74	10%Co/TiO ₂ -ZrO ₂ -SiO ₂	Imp	230	2	2	400 °C, 12 h, H ₂	80.3	C ₅ +	75.4	[208]
75	Co/SiO ₂	IWI	220	1	2	450 °C, 2 h, H ₂	NA	C ₅ +	72	[209]
76	Zr-Co/SiO ₂ (atomic ratio Zr:Co=1)	IWI	220	1	2	450 °C, 2 h, H ₂	NA	C ₅ +	82.0	[218]
77	Mn-Co/SiO ₂ (atomic ratio Mn:Co=0.1)	IWI	220	1	2	450 °C, 2 h, H ₂	NA	C ₅ +	78	[209]
78	20%Co/SBA	Imp	220	2	2	400 °C, 10 h, H ₂	23.1	C ₅ +	64.7	[210]
79	2%Mn-20%Co/SBA	Imp	220	2	2	400 °C, 10 h, H ₂	13.2	C ₅ +	44.2	[210]
80	1%Re-20%Co/SBA	Imp	220	2	2	400 °C, 10 h, H ₂	43.0	C ₅ +	74.2	[210]
81	15%Co/Al ₂ O ₃	IWI	240	0.5	2.1	350 °C, 16 h, H ₂ , He=1:1	48	C ₅ +	60.0	[211]
82	Mn-15% Co/Al ₂ O ₃ (Mn:CO=1:4)	Imp	240	0.5	2.1	350 °C, 16 h, H ₂ , He=1:1	50	C ₅ +	72	[211]
83	Mn/15% Co/Al ₂ O ₃ (Mn:CO=1:4)	Sequential Imp	240	0.5	2.1	350 °C, 16 h, H ₂ , He=1:1	49	C ₅ +	72	[211]
84	15% Co/Mn/Al ₂ O ₃ (Mn:CO=1:4)	Sequential Imp	240	0.5	2.1	350 °C, 16 h, H ₂ , He=1:1	48	C ₅ +	72	[211]

(Continued)

Table 9. (Continued).

No	Catalyst	Preparation method	T (°C)	P (MPa)	H ₂ /CO	In-situ reduction	CO conv. %	Main product	Sel. %	Ref
85	12%Co/SiO ₂	IWI	220	1	2	400 °C, 2 h, H ₂	45	C ₅ +	80	[212]
86	Mn-12%Co/SiO ₂ (Mn:Co=0.125)	IWI	220	1	2	400 °C, 2 h, H ₂	44	C ₅ +	85	[212]
87	20%Co/CNT	Imp	260	2	2	500 °C, 5 h, H ₂	95	C ₅ +	65.1	[213]
88	0.5%Ni-20%Co/CNT	Imp	260	2	2	500 °C, 5 h, H ₂	95.5	C ₅ +	67.4	[213]
89	15%Co/SiC	Imp	240	2	2	450 °C, 6 h, H ₂	71	C ₅ +	80	[214]
90	5%Zr-15%Co/SiC	Imp	240	2	2	450 °C, 6 h, H ₂	82	C ₅ +	81	[214]
91	5%Mn-15%Co/SiC	Imp	240	2	2	450 °C, 6 h, H ₂	81	C ₅ +	82	[214]
Alkali and alkaline metal promoters										
91	20%Co/θ-Al ₂ O ₃	Imp	230	1	2	400 °C, 6 h, H ₂	48	C ₅ +	82	[201]
92	1%Mg-20%Co/θ-Al ₂ O ₃	Imp	230	1	2	400 °C, 6 h, H ₂	33	C ₅ +	84	[201]
93	1%Ca-20%Co/θ-Al ₂ O ₃	Imp	230	1	2	400 °C, 6 h, H ₂	40	C ₅ +	81	[201]
94	1%Sr-20%Co/θ-Al ₂ O ₃	Imp	230	1	2	400 °C, 6 h, H ₂	44	C ₅ +	82	[201]
95	1%Ba-20%Co/θ-Al ₂ O ₃	Imp	230	1	2	400 °C, 6 h, H ₂	46	C ₅ +	79	[201]
96	15%Co/SiC	Imp	240	2	2	450 °C, 6 h, H ₂	71	C ₅ +	80	[214]
97	5%Ca-15%Co/SiC	Imp	240	2	2	450 °C, 6 h, H ₂	13	C ₅ +	5	[214]
98	CoCu/TiO ₂	deposition-precipitation (DP)	250	5	3	350 °C, 8 h, H ₂	23.1	C ₅ +	4.9	[215]
99	2.5%Li-30%(CoCu)/TiO ₂	DP	250	5	3	350 °C, 8 h, H ₂	38.2	C ₅ +	2.7	[215]
100	2.5%Na-30%(CoCu)/TiO ₂	DP	250	5	3	350 °C, 8 h, H ₂	18.4	C ₅ +	42.1	[215]
101	2.5%K-30%(CoCu)/TiO ₂	DP	250	5	3	350 °C, 8 h, H ₂	10.1	C ₅ +	20.3	[215]
102	2.5%Rb-30%(CoCu)/TiO ₂	DP	250	5	3	350 °C, 8 h, H ₂	8.4	C ₅ +	16.8	[215]
103	2.5%Cs-30%(CoCu)/TiO ₂	DP	250	5	3	350 °C, 8 h, H ₂	13.4	C ₅ +	9.5	[215]
104	20%Co/Al ₂ O ₃	Imp	200	0.1	2	450 °C, 1 h, H ₂	94	C ₅ +	41	[216]
105	Li-20%Co/Al ₂ O ₃ (Li:Co=0.01)	Imp	200	0.1	2	450 °C, 1 h, H ₂	82	C ₅ +	71	[216]
106	Na-20%Co/Al ₂ O ₃ (Li:Co=0.01)	Imp	200	0.1	2	450 °C, 1 h, H ₂	76	C ₅ +	88	[216]
107	Rb-20%Co/Al ₂ O ₃ (Li:Co=0.01)	Imp	200	0.1	2	450 °C, 1 h, H ₂	86	C ₅ +	80	[216]
108	Cs-20%Co/Al ₂ O ₃ (Li:Co=0.01)	Imp	200	0.1	2	450 °C, 1 h, H ₂	68	C ₅ +	83	[216]
109	K-20%Co/Al ₂ O ₃ (Li:Co=0.02)	Imp	200	0.1	2	450 °C, 1 h, H ₂	83	C ₅ +	84	[216]
110	20%Co/SiO ₂	IWI	250	2	2	400 °C, 5 h, H ₂	94.4	C ₅ +	73.3	[217]
111	0.1%Na-20%Co/SiO ₂	IWI	250	2	2	400 °C, 5 h, H ₂	39.6	C ₅ +	60.7	[217]
112	10%Co/Al ₂ O ₃	Imp	190	0.1	2	450 °C, 1 h, H ₂	47	C ₅ +	74	[218]

(Continued)

Table 9. (Continued).

No	Catalyst	Preparation method	T (°C)	P (MPa)	H ₂ /CO	In-situ reduction	CO conv. %	Main product	Sel. %	Ref
113	1%Mg-10%Co/Al ₂ O ₃	Imp	190	0.1	2	450 °C, 1 h, H ₂	45	C ₅ +	75	[218]
114	1%Ca-10%Co/Al ₂ O ₃	Imp	190	0.1	2	450 °C, 1 h, H ₂	45	C ₅ +	89	[218]
115	1%Ba-10%Co/Al ₂ O ₃	Imp	190	0.1	2	450 °C, 1 h, H ₂	67	C ₅ +	82	[218]
116	15%Co/Al ₂ O ₃	IWI	230	1	2	450 °C, 12 h, H ₂	31.7	C ₅ +	79.8	[219]
117	2%BaO-15%Co/Al ₂ O ₃	IWI	230	1	2	450 °C, 12 h, H ₂	36.0	C ₅ +	83.3	[219]
118	15%Co/Al ₂ O ₃	IWI	230	1	2	450 °C, 12 h, H ₂	32.1	C ₅ +	77.7	[220]
119	0.5%Mg-15%Co/Al ₂ O ₃	IWI	230	1	2	450 °C, 12 h, H ₂	35.6	C ₅ +	75.2	[220]
120	15%Co/Al ₂ O ₃	IWI	230	1	2	280 °C, 14 h, H ₂	35.3	C ₅ +	77.8	[221]
121	1%CaO-15%Co/Al ₂ O ₃	IWI	230	1	2	280 °C, 14 h, H ₂	39.7	C ₅ +	83.5	[221]
122	20%Co/Al ₂ O ₃	IWI	250	2	2	400 °C, 6 h, H ₂	58.4	C ₅ +	67.6	[222]
123	1%Ba-20%Co/Al ₂ O ₃	IWI	250	2	2	400 °C, 6 h, H ₂	58.3	C ₅ +	76.8	[222]
124	20%Co/SiC	IWI	250	2	2	550 °C, 2 h, H ₂	53.9	C ₅ +	90.8	[103]
125	12.5%Co-2%Ca/SiC	IWI	250	2	2	550 °C, 2 h, H ₂	59.3	C ₅ +	98.5	[103]
126	20%Co-2%Ca/SiC	IWI	250	2	2	550 °C, 2 h, H ₂	50.9	C ₅ +	98.2	[103]

reduction of metal oxides, a lower number of active metals, and subsequently a lower catalyst activity. Addition of small amounts of noble metals (Pt, Ru, Pd, Ir, Au, Ag, etc.) as a promoter, facilitate the Co reduction, and increase the number of active metal sites, most probably by hydrogen dissociation and spillover from the surface of the promoter.^[89,201,207,224]

Generally, a very low amount of noble metals (~0.1–0.5 wt.%) are used as a promoter, not only due to their high cost, but also because it is known that the higher amounts may lead to the blocking of the cobalt active sites. However, noble metals were extensively studied and used as catalyst promoters, but owing to their high cost, their industrial application significantly increase the cost of the catalysts. Ru, as a catalyst promoter, has been extensively studied, and it showed both structural and electrical promotion effect.^[89,126,134,161,193,204,225–227] It was reported that Ru, as a structural promoter, facilitates the cobalt reduction through a hydrogen spillover from Ru to Co, and causing an increase in the number of Co⁰ sites, leading to an increase in the rate of CO hydrogenation. This behavior does not depend on the support material, and for all cobalt catalyst with different supports such as Al₂O₃, SiO₂, and TiO₂, the reduction temperature (reduction of CoO_x to Co⁰) decreases and leads to an improved cobalt dispersion. Moreover, the electronic enhancement effect of Ru has been widely investigated, and it is worth mentioning that the Ru promoted cobalt-catalysts revealed high C₅₊ selectivity as well as high turnover frequency rates.^[228]

In another study,^[135] investigation of noble metals effect on the catalytic activity of the Co/TiO₂ catalysts revealed that promoted catalysts had lower reduction temperature of cobalt oxide to metallic cobalt, and this effect was more evident for Pt and Ru compared with Re and Ag. This effect was noticeable at the higher loading of promoters. The Pt-promoted catalysts showed higher CO conversion, but lower C₅₊ selectivity, while other promoted catalysts showed higher C₅₊ selectivities and high cobalt time yield. When low surface area materials such as TiO₂ are used as support, it is not easy to prepare highly dispersed metals on the surface of the support, and strong metal-support interaction also resulted in the formation of unreduced compounds. As mentioned before, the addition of promoters such as Pt can overcome these problems and enhance the reducibility.^[202] Iglesia et al.^[37,229] reported that compared with Co/TiO₂ catalyst, the turnover rate and C₅₊ selectivity increased over Ru promoted Co/TiO₂ catalyst, without apparent changes in cobalt dispersion, reaction kinetics, and activation energies. However, the addition of Ru resulted in a higher density of Co⁰ sites. Moreover, the presence of Ru inhibits the catalyst deactivation by preventing the deposition of carbon on the Co particles. These promotion behaviors need intimate contact between Ru and Co atoms, a state that forms during the oxidation of the bimetallic precursors by calcination at high temperatures

(>300 °C). Rapid deactivation of the catalysts at high temperature is a known problem of the ruthenium supported cobalt-based catalysts.^[230]

Pt and Re as structural promoters have been widely investigated in cobalt-based FT catalysis.^[134,205,225–227,231] Mehrbod et al.^[134] reported that the Pt promoted cobalt catalysts (0.5%Pt-12%Co/TiO₂) showed higher CO conversion compared with Au, Re, and Ag promoted catalysts. They also found that the uncalcined catalysts have higher CO conversion than the corresponding calcined catalyst, and also promotion with Re and Ag did not significantly affect the CO conversion. Their stability was similar to the stability of un-promoted Co/TiO₂. However, for the SiO₂ supported cobalt catalysts (12%Co/SiO₂), it was observed that the stability of the un-calcined promoted catalysts (Ru, Pt, Ag) was slightly lower than the calcined catalysts, while the stability of the Re promoted catalyst remained almost constant. There was no visible deactivation, and 0.477%Re-12%Co/SiO₂ revealed the highest catalytic activity compared to the other promoted catalysts.^[205] The catalytic activity of cobalt-based catalysts modified with different noble metal promoters can be found in [Table 9](#).

Nabaho et al.^[199] studied the properties and catalytic performance of the Pt promoted Co/Al₂O₃ FT catalyst. The catalysts prepared by a sequential impregnation (Pt-Co/Al₂O₃) and also by physical mixing of Pt/Al₂O₃ and Co/Al₂O₃ (hybrid). The addition of Pt in Co/Al₂O₃ (Pt-Co/Al₂O₃) resulted in enhanced reducibility, and reduction peaks shifted to a lower temperature, while for the hybrid Pt-Co/Al₂O₃, the reduction peaks did not change and they were close to the peaks belong to the Co/Al₂O₃ catalyst. The poor reducibility of the hybrid catalyst might be related to the longer distances between Co and Pt on the separate supports, as well as the poor intimate contact between the large support particles that contributed to the surface discontinuity, which plays a vital role in the successful migration of spillover hydrogen. It was observed that the high-temperature peak (at 840 °C), belongs to the non-stoichiometric cobalt alumina complexes and/or CoAl₂O₄ (for the non-promoted catalyst), disappeared in both promoted catalysts prepared by hybrid and sequential impregnation method. Since the peak of the non-stoichiometric cobalt aluminate was disappeared in both promoted catalysts, it can be concluded that direct Pt-Co interaction was not required to prevent the formation of mixed oxides. Formation of mixed support oxides could be prohibited by the addition of promoters via intimate (chemical and/or physical) interaction with cobalt or by depositing as a layer between the support and cobalt crystallites.

Precursor decomposition can be affected by the presence of promoters. It has been reported that the kinetic of the precursor decomposing could be affected by the formation of the ruthenium nitrosyl nitrate in the cobalt-silica supported catalyst and compared with the un-promoted catalyst, the Ru-promoted catalyst decomposed at a lower temperature.^[232] Moreover, the crystallite size of cobalt oxide decreased in Ru-promoted catalysts. The higher

cobalt dispersion in the noble metal promoted catalysts could be due to the higher concentration of cobalt oxide nucleation and crystallization sites. Crystallization of cobalt oxide can occur on the sites related to the noble metals, and the higher concentration of the crystallization sites resulted in a higher number of cobalt particles and thus a higher dispersion of cobalt in the catalyst.^[233]

The adsorption of CO molecules and desorption of the products could be enhanced by the addition of Ru and Re to the Co/Al₂O₃ catalyst, while the addition of Pd and Pt resulted in a decreased CO adsorption and hydrogenation reaction enhanced probably by providing a source for dissociated hydrogen.^[64] Similar behavior was observed for the titania supported cobalt catalyst.^[204] The addition of 0.2 wt.% of Ru to the Co/TiO₂ catalyst enhanced the reducibility, and all peaks shifted to the lower temperatures. Furthermore, the average cobalt particle size in the promoted catalyst (8–8.5 nm) was slightly smaller than the un-promoted catalyst (11 nm). The CO conversion and C₅₊ selectivity also increased over both Re and Ru promoted catalysts. The Co/SiO₂ catalyst promoted by Ru revealed a significant enhancement in reducibility, but did not have a remarkable effect on the dispersion. The cobalt metal dispersion was significantly affected by the addition of Pt and Pd, with little changes in cobalt reduction. The addition of Ru to Co/SiO₂ increased the CO conversion, but the methane selectivity remained constant, while Pt and Pd resulted in higher methane selectivity.^[234]

3.2.2. Transition metals

The incorporation of the promoter can adjust the metal-support interaction. Promoters can also positively affect the reducibility of the cobalt oxides by decreasing the formation of non-reducible species, thus, enhancing the catalyst activity.^[125,208] The addition of ZrO₂ to the Pt/TiO₂ catalyst partially inhibits the TiO_x migration on the Pt/ZrO₂/TiO₂ catalyst calcined at a lower temperature, which is highly useful for the formation of Pt–TiO_x active sites. However, calcination of catalysts at higher temperatures resulted in a higher migration of TiO_x onto the metal surface due to the formation of an oxidized platinum phase with smaller particle sizes.^[235]

Johnson and Bell^[209] have studied catalytic performance for FT synthesis using the Co/SiO₂ catalysts promoted by different metals oxides, including Zr, Mn, La, Gd, and Ce. It was observed that for all promoted catalysts the selectivity to CH₄ decreased, and the C₅₊ selectivity increased by increasing the promoter/Co ratio up to certain level and following this order: Zr>Gd>Mn,Ce>La; and the selectivities were insensitive to further increase of the promoter loading. This behavior could be due to the formation of a metal–metal-oxide interface between the Co and the promoter. The coverage of the cobalt nanoparticle surface by the promoter at a higher ratio of Co/promoter increased the product selectivity. The catalytic performance of the promoted catalysts could be affected

by both the active sites and the interface with the promoter oxide. The addition of Zr improved the reducibility and cobalt dispersion and consequently improved the catalytic activity. Incorporation of ZrO_2 caused an increase in H_2 chemisorption and suppressed the CO adsorption, increase the H/C ratio on the catalyst surface, and enhance the hydrogenation of surface carbon species. Therefore, selectivity to heavy hydrocarbons was decreased, while methane selectivity was increased. Furthermore, the electron transfer from support to cobalt through the Zr–O–Si structure resulted in an improved electron density of cobalt species. The promotional effect of Zr also reported for the cobalt-based catalysts supported on $\gamma\text{-Al}_2\text{O}_3$.^[198] The obtained results for promoting the Co/ Al_2O_3 catalyst with Zr and combination of Zr and Ce showed that the Zr-rich catalyst has the highest degree of reducibility. It was suggested that the H_2 -spillover has a more prominent role in the reducibility of the catalyst than the presence of a reducible phase.^[198] Jacobs et al.^[125] reported that increasing the cobalt loading in Co/ Al_2O_3 and Co/ TiO_2 catalysts resulted in an increased cobalt cluster size, decreased the metal-support interaction, thus, improved reducibility. The addition of zirconia as a promoter to Co/ Al_2O_3 and Co/ TiO_2 catalysts caused a considerable decrease in the cobalt cluster size, increased the metal-support interactions, and consequently decreased the reducibility of the catalysts. However, incorporation of Co/ Al_2O_3 and Co/ SiO_2 with Zr enhanced the dispersion of cobalt species.

Mn promoted Co/ $\gamma\text{-Al}_2\text{O}_3$ catalyst for the FT synthesis has been studied by Pedersen et al.^[211] These catalysts exhibited a higher activity, selectivity to C_{5+} , and olefins, while the lower CH_4 selectivity was observed. It was found that Mn promoted catalysts, not only did not enhanced the reducibility, but also caused an increase in reduction temperature. However, the reducibility of catalysts found to be related to the preparation method of the catalysts and the catalyst prepared by sequential impregnation (first Mn, then Co) showed a very similar pattern to Co/ $\gamma\text{-Al}_2\text{O}_3$ catalyst; while in the co-impregnated catalyst the reduction peaks significantly shifted to a higher temperature, which could be due to the strong CO–Mn interaction. Co–Mn catalysts could create a $\text{Co}_{3-x}\text{Mn}_x\text{O}_4$ mixed oxide, which remains in the oxidic state during the operation and reduction of this oxidic phase probably increased the reduction temperature. All Mn-promoted catalysts show the lower dispersion than the un-promoted catalyst. It has been suggested that the facilitated CO dissociation (due to the increase of binding energy for all species on Co in the presence of Mn) resulted in the higher intrinsic activity. Product selectivity distribution could be associated to the inhibited hydrogenation activity. The addition of Mn to cobalt-based catalyst supported on SiO_2 and porous silica also had the same behavior and caused an increase in C_{5+} selectivity and decrease the selectivity to $\text{C}_1\text{-C}_4$.^[212,236]

An enhanced alcohol formation over Zn promoted Co/ SiO_2 catalyst reported by Singh et al.^[237] The addition of Fe to the Co/AC catalyst also resulted in increased alcohol ($\text{C}_1\text{-C}_{16}$) formation, which ascribed to the formation of CO_2C species and

Co-Fe alloy [238]; the catalytic activity improved due to the enhanced the metal dispersion and CO uptake after incorporation of Fe. Addition of different types of metals such as alkaline earth metals and transition metals (Mg, Ca, Sr, Ba, Y, La, Ce, Ti, V, Mn, Zn, Zr, and Mo) as a promoter to the Co/Al₂O₃ catalysts for FT synthesis have been investigated by Shimura et al. [201] Reducibility and surface area of the catalyst decreased in the presence of V, Mo, and Mn, while the TOFs of these catalysts were much higher than the un-promoted catalyst. The addition of other promoters (other than V, Mo, and Mn) to the Co/Al₂O₃ catalyst caused some changes in the reducibility and surface area of the catalyst, though the TOFs did not affect by the type of the promoter. The catalysts promoted with the rare earth elements (Ce and La) revealed the highest overall activity of FT synthesis. It was observed that catalytic activity increased by the simultaneous loading of both La and V, and the catalytic activity of the Co/[La(2%)+V(0.5%)]/Al₂O₃ catalyst was 1.6 times higher than the Co/Al₂O₃ catalyst, and also higher surface area and TOF was observed over this catalyst.

Nickel is another transition metal that has been used as a promoter for the Co/ γ -Al₂O₃ FT catalyst. [239,240] By the addition of Ni, the reduction temperature of the Co₃O₄→CoO shifted to the lower temperature, while the second peak belongs to CoO→Co⁰ did not change. Ni promoter also increases the dispersion and inhibits the sintering of the Co particles at elevated temperature and during the reduction of CoO to Co⁰. Promotion of the Co/CNT catalysts with Ni also resulted in the same behavior in reduction properties, and the incorporation of Ni also resulted in hydrocracking of heavier hydrocarbons to lighter ones. [213] Excessive hydrocracking leads to an increase in the formation of gaseous hydrocarbons; thus, an optimum amount of Ni is required to maximize the production of liquid hydrocarbons (C₅-C₂₀). Zr, Mn, and Ca (5 wt.%) promoted 15%Co/SiC catalysts prepared by stepwise impregnation method, and their catalytic performance for the FT synthesis have been investigated. [214] The crystallite size of Co₃O₄ increased, and dispersion of Co⁰ decreased after the addition of the promoter. The larger crystallite size and the outer surface location of Co₃O₄ species for the Co/Zr/SiC catalyst led to the lower interaction between Co and SiC support and consequently resulted in a facilitated reduction. The CO conversion increased by about 10% over Mn or Zr, while it was decreased by about 60% decrease for the Ca-promoted catalyst. The product distribution showed that the light hydrocarbons (CH₄ and C₂-C₄) were the main products over Co/Ca/SiC catalysts; however, the long-chain hydrocarbons (C₅-C₂₂) were the major products over the Zr, and Mn promoted catalysts for the FT synthesis. A summary of the catalytic activity cobalt-based catalysts promoted with several transition metal can be seen in Table 9.

3.2.3. Alkali and alkaline earth metals

Alkali metals as promoters have been widely used for many industrial catalytic processes. Alkalis are known to have strong basicity, and they can modify the

local electron density of the transition metal either directly or through the support.^[215,241–244] Electron donation from the alkalis to transition metal could result in the electron charge of the orbitals of the transition metal atoms, which consequently caused an increase in the degree of back-donating from these orbitals toward the antidonating orbitals of the chemisorbed H₂ and therefore suppress the H₂ adsorption, but enhancing CO chemisorption and dissociation.^[215,241–244] Alkali metals have been extensively used as promoters for iron-based FT catalysts to enhance catalytic activity and product selectivity. It has been reported that the wax formation and olefins yields increased over the K promoted Fe-catalysts (Fe₃C), while the methane formation decreased.^[245]

Generally, alkali metals are used as chemical promoters for FT catalysts to increase the activity and C₅₊ selectivity and reduce CH₄ production. Evaluation of the catalytic performance of the Co/Al₂O₃ catalysts promoted by alkali metals (Li, Na, K, Rb, and Cs) revealed the positive effect of promoters on the C₅₊ selectivity, while the CO conversion decreased in the following order: un-promoted > Rb > Li > Na > K ≈ Cs.^[216] The selectivity to olefin found to be inversely related to the electronegativity of the alkali promoter and the olefin/paraffin ratio increased in the following order: un-promoted < Li < Na < K; and the highest C₅₊ selectivity and lowest CH₄ selectivity obtained over K-promoted catalyst. The strong electropositive nature of K, and transferring the electron to the 3d orbital of cobalt, could be the reasons for the promoting effect of potassium, which leads to the increased CO adsorption. The effect of K on the catalytic performance of 20% Co/0.5%Re/γ-Al₂O₃ catalysts has been studied by Gavrilović et al.^[41] It was found that the addition of potassium decreased the catalytic activity, and increased the C₅₊ and CO₂ selectivities.

The addition of Na to Co–Re/γ-Al₂O₃ catalyst has been found to have a negative effect on the FT catalyst activity.^[246] The catalytic activity did not affect by addition of a small amount of Na (<1000 ppm) because the low amount of Na did not affect the chemisorption or heats of adsorption for CO or H₂. However, the addition of a higher amount of Na (10,000 or 20,000 ppm) caused a considerable decrease in the catalytic activity, which could be due to the rise in both geometric and electronic effects. The dramatic decrease of catalytic activity could be due to the stronger adsorption of reactants as well as the diffusion barrier caused by the site-blocking from Na atoms. The effect of Na on the catalytic performance and structure of Co/SiO₂ catalyst was studied by Dai et al.^[217] It was observed that the incorporation of Na, decreased the surface area and particle size, and increased the reduction temperature, and consequently, decreased the CO conversion. However, selectivity to oxygenates (mainly alcohol) increased. The addition of Na enhanced the formation of Co₂C with sphere-like morphology, and the metallic cobalt converted to cobalt carbide during the reaction process, which is acting as the active site for the production of oxygenate and olefin.

Unlike the alkali metals, which are mostly applied as a promoter for the Fe-based FT catalysts, alkaline earth metals are widely used for the promotion of cobalt-based FT catalysts. The catalytic performance affected by the incorporation of Mg, Ca, and Ba into the 10% Co/Al₂O₃ catalyst.^[218] As mentioned above, the positive effect of alkaline earth metals also related to their electron-donor properties, which increased in the order Mg<Ca<Ba. Increasing the electron density on the catalyst in the presence of alkaline earth metals leads to the stronger binding of CO with the metal surface and facilitates the hydrocarbon chain growth. Bao et al.^[219] reported that the reducibility of the 15Co/Al₂O₃ catalyst, especially the reduction of CoO to Co⁰, enhanced by the introduction of a small amount of Ba (≤2 wt.%), and CO conversion and C₅₊ selectivity increased. They also found that the catalytic activity decreased by increasing the Ba concentration to 5 wt.%. By increasing the Ba loading, the interaction between Ba and CaO resulted in a decreased reducibility and weakened CO adsorption ability; therefore, CO conversion decreased. The effect of MgO and CaO on the Co/Al₂O₃ catalyst for the FT reaction was studied by the same group.^[220,221] It was found that the addition of a certain amount of these alkaline earth metals could inhibit the interaction between the support and cobalt oxide, enhance the reducibility and consequently improve the catalyst performance. Recently, Guo et al.^[225] reported the same behavior for the Ba-promoted Co/Al₂O₃. The adsorption of CO and H₂ on the surface could be affected by the electron transfer from Ba to the cobalt surface, and the hydrogenation ability decreased; thus, selectivities to higher hydrocarbons and olefins increased, and formation of CH₄ decreased. Alkaline earth (Ca, Ba) and alkali metal (Na, K) have been used as a promoter for Co/CeO₂ catalyst for the high-temperature WGS reaction.^[247] A slightly higher CO conversion observed for all promoted catalysts at 450 °C; however, compared to alkaline earth metal promoted catalysts, alkali metal promoted catalysts were deactivated rapidly. The alkaline earth metal promoted catalysts revealed higher stability and enhanced sintering resistance. Compared with the alkali metal promoted catalysts, alkaline earth metal promoted catalysts found to have a relatively smaller crystallite size of Co⁰ after WGS reaction. The catalytic activity cobalt-based catalysts promoted with several alkali and alkaline earth metals can be seen in Table 9.

4. Fischer–Tropsch reactors

The conversion of syngas to fuels and higher hydrocarbons is a highly exothermic reaction, and in addition to the catalyst, the reactor must be designed appropriately to handle the heat of reaction. The reactor is a crucial part of catalytic reactions. The reactor design can be complicated due to the presence of three phases (i.e., gas, liquid, and solid). Different types of FT reactors are used in the commercial FT process, including fixed-bed, fluidized-bed, and slurry bubble columns^[73,248–250] (Figure 6). Slurry bubble column and multi-tubular fixed-bed

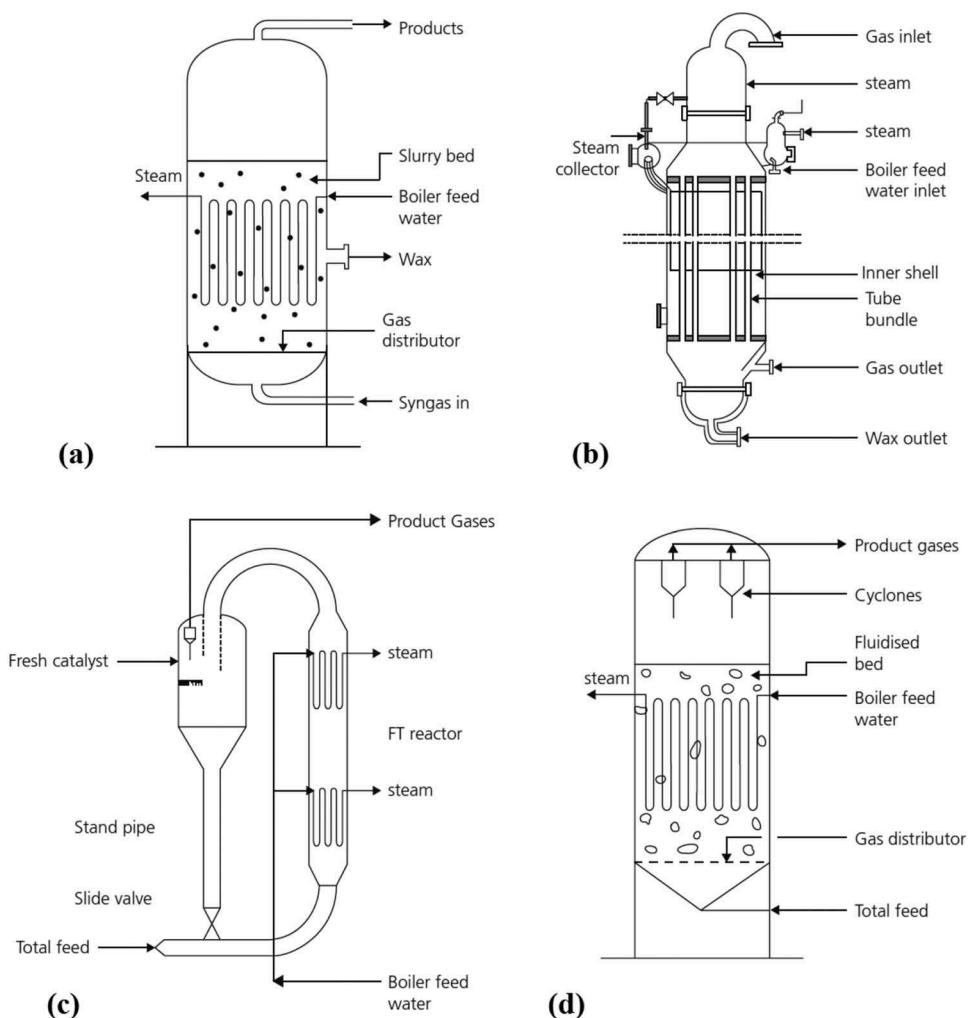


Figure 6. Possible reactors for Fischer–Tropsch synthesis. a) Slurry bubble column reactor, b) Multitubular trickle bed reactor, c) circulating fluidized-bed reactor, and d) fixed fluidized-bed reactor.^[248]

reactors are usually used for LTFT processes, while HTFT reactors include circulating and fixed fluidized-bed reactors. LTFT microchannel reactors are recently being used for small-scale applications.^[250]

4.1. Fluidized-bed reactors

Fluidized-bed reactors were developed mainly for the HTFT process because the FT reaction has to occur in the gas phase. This type of reactors have the following advantages: 1) excellent heat transfer and temperature control during the highly exothermic FT reaction; 2) the probability of using the smaller catalyst particles to avoid the intraparticle diffusion, which limits the pressure drop and

the reaction rate; 3) ease of catalyst replacement and loading fresh catalyst during the reaction; 4) better mixing of the catalyst particles and a higher solid-gas contact efficiency; 5) higher gas throughput which resulted in a higher production capacity.^[25,251] Circulating fluidized-bed reactors have been used at Sasol for many years. In this type of reactor, a fine catalyst (40–150 μm) is entrained by a high-velocity gas stream (1–2 m/s) through a riser reactor. Catalysts were separated from the effluent by cyclones and returned to the reactor inlet. The reaction heat could be removed by cooling tubes inside the reactor.^[252] Some disadvantages of this type of reactors are 1) the high operating temperature (320 °C–350 °C) to achieve adequate productivity with the low surface area catalysts which are required to be resistance against attrition, 2) low chain growth probability (α) operation and formation of only vapor-phase products, 3) the pressure drop through the catalyst bed, and 4) the energy required for circulation of the catalyst.^[248]

The catalyst strength is another critical parameter in the fluidized-bed reactor, while the stability is less important because the catalyst can be refreshed continuously.^[253] These reactors require special equipment (cyclones) for the separation of catalysts from gas products, which affect the cost-efficiency. Using small catalyst particles also may increase the possibility of attrition and deposition of heavy products on the catalyst, and therefore, agglomeration and blockage of the fluidization. There are some complexities in design, operation, and scaling up the reactor, and it is necessary to accurately predict the mass transfer between phases, gas holdup, and dense-phase back-mixing, to avoid errors in commercial design.^[25] The two-phase HTFT fluidized-bed reactors were designed based on the Hydrocl process, and the first GTL commercial plant was operating in Brownsville, Texas, in 1950s.^[251] In 1955, the circulating fluidized-bed reactors were developed by Sasol in South Africa Coal and Oil (Sasol 1) in Sasolburg for the production of petrol and wax using HTFT and LTFT technologies, respectively. Later, in 1993, the initially designed circulating fluidized-bed reactors were replaced by Sasol Advanced Synthol (SAS) reactors.^[25,27]

Development of the fixed fluidized-bed reactors helped to overcome many of these operational disadvantages,^[254] and Sasol replaced all of the circulating fluidized-bed reactors with the newly developed fixed fluidized-bed reactors. Fluidized-bed reactors are divided into 1) two-phase (gas-catalyst) HTFT reactors, and 2) three-phase (gas with catalyst suspended in a hydrocarbon liquid slurry) LTFT reactors, which is known as slurry reactor.^[73,249] When alkenes and/or straight run fuels are the main products, two-phase fluidized systems are used in the HTFT reactors. For the production of long-chain waxes, LTFT process is used in either multitubular fixed-bed or three-phase fluidized-bed slurry reactors. Due to the high reaction temperature in HTFT fluidized-bed reactors, the main products are lower hydrocarbons (especially C_2 – C_4 olefins) and gasoline, while the production of heavy waxes and middle distillates are much lower than in LTFT process.^[253]

4.2. Slurry bubble column reactor

During the last decades, slurry bubble column reactors attract more attention from both academic and industrial sections. Generally, slurry-phase reactors are commercially used for the production of middle distillates. Nowadays, different types of slurry bubble column reactors are available, including simple bubble column, multi-shaft bubble column, cascade bubble column with sieve trays, packed bubble column, and bubble column with static mixers. The simple bubble column reactor is the most commonly used reactor for the FT reaction. The multi-shaft bubble column reactor also has been applied for the FT reaction by Exxon.^[248] Two types of slurry bubble column reactors used by Sasol and Exxon are shown in Figure 7.

The reactor with the cooling coils inside (Sasol slurry bubble column reactor) is the most frequently used. The idea of the slurry reactor designed by Exxon has some similarities to the tubular fixed-bed ARGE reactors (Lurgi design) which have been used at Sasol, South Africa, and only the fixed catalyst bed has been replaced with the slurry catalyst.^[248,249,255] Slurry bubble column reactors in a unit with a capacity of 2500 bbl/day introduced by Sasol in 1993. In addition to Sasol,

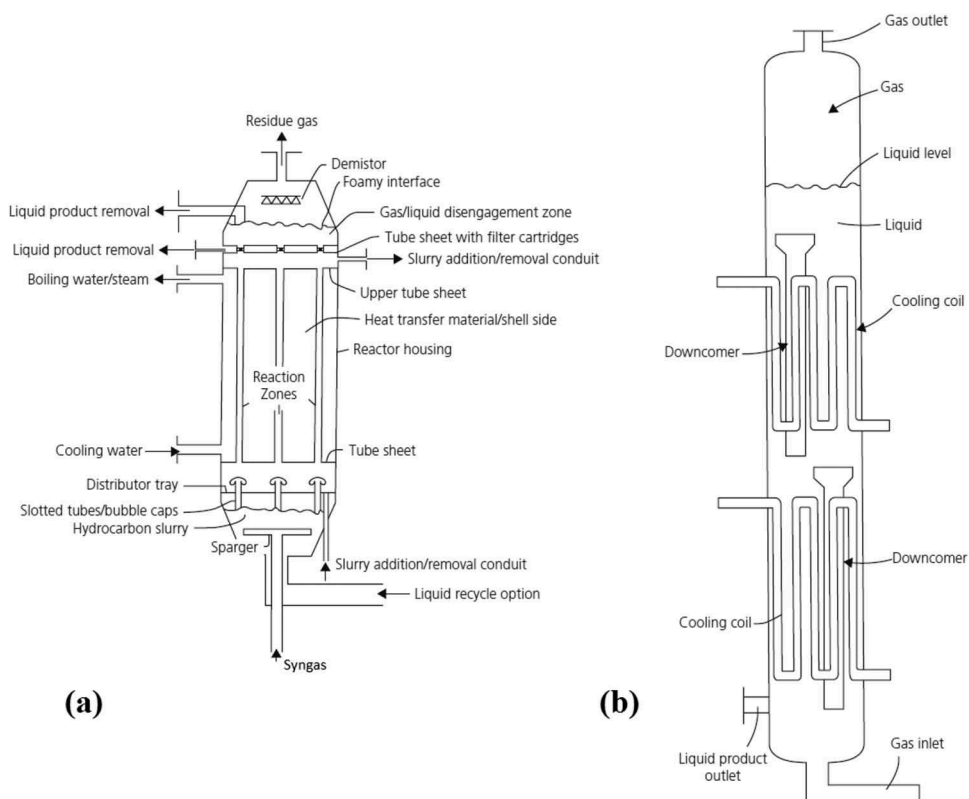


Figure 7. A) Schematic of an Exxon slurry reactor, b) Schematic of the Sasol slurry bubble column reactor.^[248]

other companies such as Exxon Mobil are also using this type of reactor on a commercial scale.^[253]

In slurry reactors, syngas is contacted (in a bubble column) with a slurry of fine catalyst suspended in heavy liquid products. Liquid products remove as a part of slurry, while the light hydrocarbons and unreacted syngas leave the reactor in the gas phase. Some advantages of this type of reactors are 1) excellent mixing of the phases which resulted in the superb heat and mass transfer rate, 2) high thermal stability because of the rather low radial and axial temperature gradient, 3) the possibility of continuously refreshing, addition and withdrawing of the catalyst during the process, and 4) lower maintenance and operation cost, due to the absence of mechanically moving parts. However, they also have some disadvantages, such as back mixing of the gas phase bubbling through the slurry, which resulted in a decreased gas-liquid mass transfer rate, and consequently lower conversion and selectivity. The whole catalyst also could be exposed to the sulfur poisoning due to continuous circulation, unlike the fixed-bed reactors in which the top section acts as a guard bed.^[25] In fix-bed reactors deactivation takes place in three regions of the reactor; firstly, in the top section, most of the catalyst particles are deactivated due to the presence of sulfur, then, in the middle region, they are less deactivated, and finally, in the bottom, almost no sulfur is found.

Moreover, separation of the solid catalysts from the liquid products and difficulties for the scale-up of these reactors are other challenges for their industrial application ^[253,256–258] Different hydrodynamic parameters such as turbulent parameters, liquid velocity, gas holdup, and bubble dynamics (including bubble chord length and bubble velocity), need to be considered for scaling up of these reactors. The gas-liquid interfacial area and the mixing intensity, and consequently, the heat and mass transfer rates and coefficients are affected by these parameters, and all these changes directly affect the conversion and selectivity of the reactor.^[257] The catalyst stability is a critical parameter, and new designs are based on more stable and active cobalt catalysts, and along with improvement in other aspects, new reactors can reach higher productivity. Different commercial plants are using slurry-bed reactors for FT synthesis, in both HTFT and LTFT processes, including Sasol-QP (Oryx) in Qatar, Escravos in Nigeria, and some plants in china such as Yitai CTL Plant, Shenhua Ningxia, and Synfuels (Table 2).^[22–26] The main products of FT synthesis using the slurry reactors (after refining, separation, and upgrading of the products) are gasoline, diesel oil, and wax.^[259] For example, in Sasol-QP (Oryx) plant based on LTFT technology, the main product is diesel and naphtha as a by-product, while this plant is using natural gas as feedstock and cobalt-based catalysts (Co-Al₂O₃).

4.3. Fixed-bed reactors

The fixed-bed reactors (Figure 8) are an appropriate type of reactors, due to the possibility of achieving the highest density of catalyst/reactor volume, and

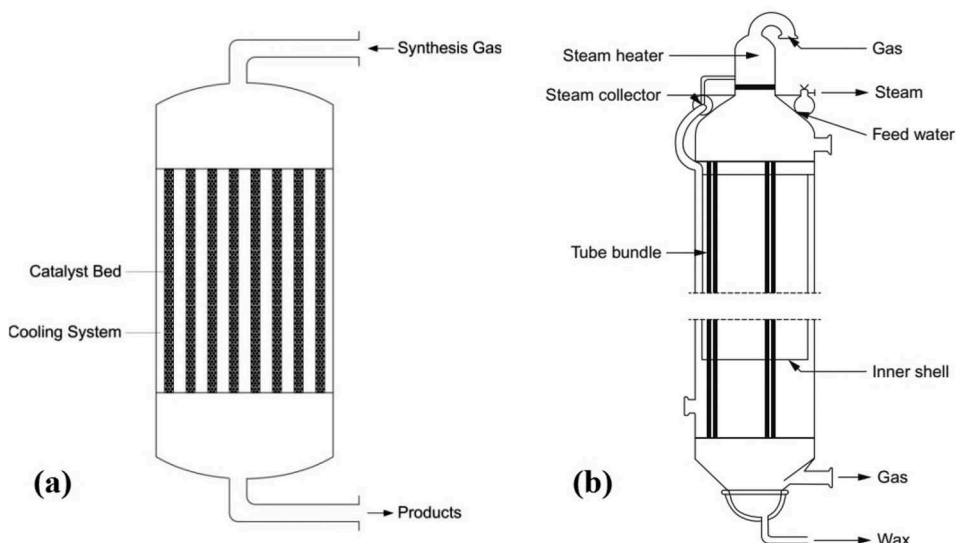


Figure 8. A) Multitubular fixed bed reactor ^[258]; b) The Arge reactor. ^[25]

also reaching the highest productivity/reactor volume with a uniform temperature. Fixed-bed reactors are used widely for the FT reactions. Different designs for fixed-bed reactors have been developed in the period before and during World War II, and later, after World War II, they were redesigned or modified to the reactors with higher potential for large-scale production of synthetic fuels. ^[25,252,258] Afterward, the multitubular fixed-bed reactors were designed by further development of the fixed-bed reactors. In 1955, this type of reactor was installed at the Sasol plant in South Africa (Arge reactor, **Figure 8b**). ^[25]

This reactor worked under the following operational conditions: 220 °C, 25 bar (for the reactor commissioned in 1955), and 45 bar (for the one commissioned in 1987). Later, in 1993, the FT plant Bintulu, Malaysia, was installed in a multitubular fixed-bed reactor in the SMDS process; LTFT technology and cobalt-based catalysts are used in this plant, and the main product (85-95%) is C₅₊. ^[25] SMDS process used in Las Raffan, Qatar, in the Pearl GTL facility (Shell (Pearl)), using cobalt-based catalysts and LTFT technology for production of mainly distillate and base oils with the capacity of 140,000 barrels a day (bpd) of GTL products. ^[29] Generally, during the FT reaction in a fixed-bed reactor, a complex mixture of hydrocarbons ranging from methane to wax is produced. The heat removal is a critical issue for these reactors, which leads to a lower productivity per reactor volume, and the reaction temperature strongly affects the product selectivity. ^[253] Other drawbacks of fixed-bed reactors are high-pressure drop, achieving low catalyst utilization, and limited diffusion. Usually, the catalyst particles with the size of few millimeters, which are contributing to the

intraparticle pore-diffusion limitation, are required to reduce the pressure drop and facilitate heat removal. Due to the diffusion limitation and capillary condensation, the catalyst pores are usually filled with produced heavy waxes.^[260] However, some advantages such as ease of catalyst loading and replacement, absence of the extra step for catalyst separation from the products, and simplicity of scale-up from a single tube to a pilot plant, fixed-bed reactors are the desired type of reactors.^[261] Fixed-bed reactors are usually operated in the concurrent mode, and both gas and liquid flow from the top to the bottom of the reactor. Due to the significant pressure drop across the bed, counter-current mode is not used in today's FT plants. By increasing the number of tubes in the fixed-bed reactor, the catalyst loading becomes more challenging, because each tube must have the same pressure drop to have the same flow of the reactants, and the same product distribution through each tube.^[248]

4.4. Recent developments in FT reactors

4.4.1. Microstructured reactors

Microstructured reactors are another type of reactor which is used for process intensification during FT synthesis, and the application of these reactors has been investigated over the last two decades.^[262] An excellent mass transfer characteristic obtained while using a large number of channels in these reactors. The small diameter of microchannels (ranging from 0.1 to 5 mm) causes an increase in the ratio of the surface area to the reactor volume, which significantly improves the heat transfer and enhances the temperature control.^[263] Heat removal from the catalyst and mass transfer from gas by the formed liquid phase to solid catalyst are also intensified within microstructures to reach the isothermal operation condition for the highly exothermic FT reaction.^[258,264] In microchannel reactors, each reactor module has thousands of process channels filled with the highly active FT catalyst interleaved with water-filled coolant channels (**Figure 9a**).^[265] The overall process is simplified due to the high conversion, which reduces or omits gas recycling. Because of the intensified mass transfer, a very high space-time yield, almost 100 times higher than the conventional slurry reactors, can be obtained. This compact, flexible, and the simplified system allows it to be a potential reactor for different reactions, either highly exothermic, such as FT synthesis, or highly endothermic, such as methane reforming. In these reactors, the highest catalytic activity and the most extended catalyst lifetime could be obtained due to the uniform temperature and efficient heat transfer across the reactor walls.

Different companies such as Velocys Inc. and Ineratec GmbH are driving the commercialization of microchannel FT technology.^[263] In 2010, Velocys demonstrated its first pilot plant in Austria; then after further pilot plant demonstration and manufacturing of commercial reactors and catalysts, they

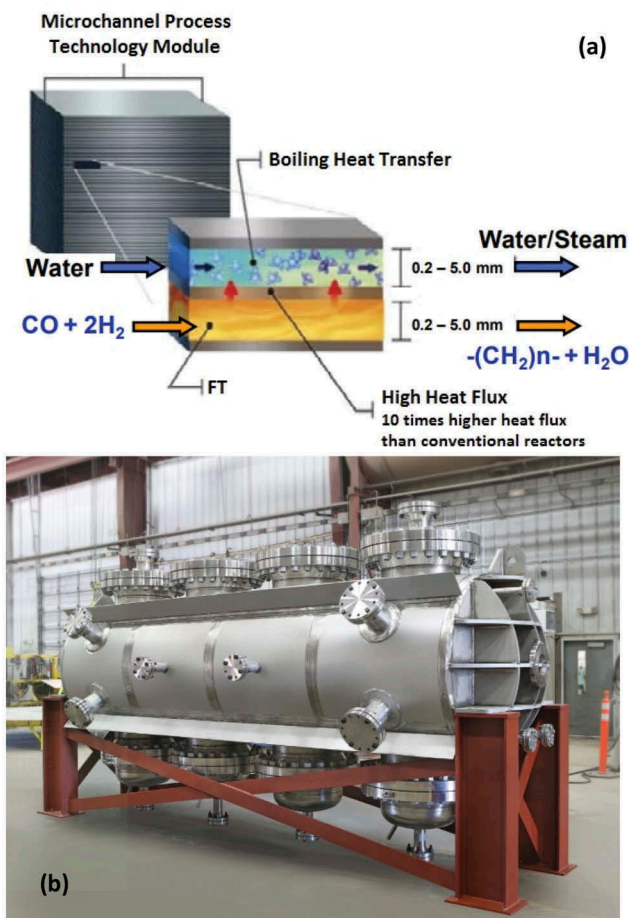


Figure 9. A) Microchannel FT reactor schematic ^[265]; b) Velocys' commercial microchannel FT reactor. ^[266]

established the first commercial plant in Oklahoma, USA, in 2016, and other demonstrations have tested this technology at pilot scale in North and South America, Europe and Australia. ^[266] The Velocys' commercial microchannel FT reactor can be seen in Figure 9b. In these reactors, process intensification occurs via a reduced specific reactor volume (volume per production capacity), speeding up the process by 10 to 1000 times, and increasing the catalyst productivity (quantity of the formed product per hour per catalyst volume). The system volume can be more than 10 times smaller compared with the conventional systems (which can be as large as 9 m in diameter and stand 60 m tall). ^[240] Because of the enhanced volumetric and catalytic productivity, the capital and operational cost decrease in microchannel FT reactors, compared to the conventional FT reactors, such as fixed-bed and slurry-bed reactors. ^[264,265]

The scale-up of the microchannel reactor for FT reaction using the high cobalt loading catalyst provided by Oxford Catalysts, Ltd. has been investigated

by Deshmukh et al.^[267] The catalyst activity was evaluated in four different reactors with catalyst bed lengths ranging from 4 to 62 cm and 1 to 276 parallel process channels. It was observed that productivity increased by increasing the length and number of microchannels. Good thermal control of the reactors also obtained due to the enhanced transport process in microchannel reactors. Different syngas feeds with different compositions were tested and resulted in the CO conversion of above 60% and low methane selectivity (<15%). A comparison between the catalyst productivity in different types of reactors (fixed-bed, slurry-bed, and microchannel), confirmed that the productivity of the microchannel is significantly higher than others (Figure 10).^[265]

4.4.2. Monolithic reactors

Monolithic reactors (Figure 11) are also often categorized as structured reactors, which were applied for FT synthesis. These reactors have been usually used for the rapid reaction of gaseous reactants, while the external surface of catalyst participates in the reaction, and due to the high gas flow, a low-pressure drop is required. Though, these reactors can also be used for slower reactions, which are usually carried out in slurry- or fixed-bed reactors.^[269] The effect of mass transfer in FT synthesis is very crucial. However, the reactants are in gas-phase, but usually, the surface of catalysts and pores are filled with liquid products, such as wax and water. Monolithic catalysts consist of many parallel channels with ceramic structures made of catalyst supports such as silica or alumina, while based on the cell density of the monolith, the channel diameters can vary between less than a millimeter to few millimeters. The thickness of the walls also varied between 0.1 to 0.3 mm.^[253,268] Monolith loop catalytic membrane reactor has been studied as a potential reactor for FT synthesis, and it was observed that the obtained yield per unit per reactor volume

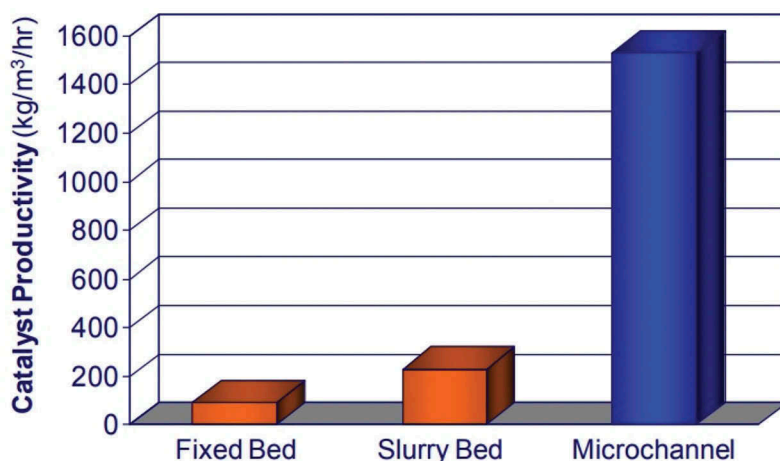


Figure 10. Microchannel FT achieves far higher catalyst productivity.^[265]

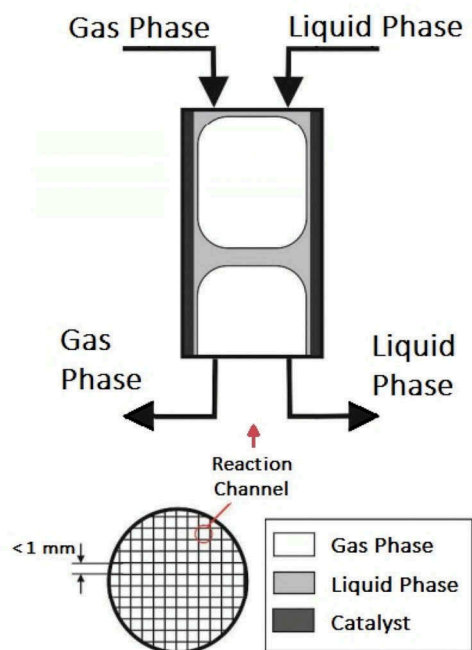


Figure 11. Schematic representation of the monolith microstructured catalyst reactor.^[268]

was lower than that for state-of-the-art slurry-bubble column and multi-tubular fixed-bed reactors.^[270]

Depending on the velocities of gas and liquid, different flow regimes are possible to occur in the channels. Syngas and liquid products flow co-currently, and they move along the channel in a Taylor flow or Slug flow regime. Monolithic reactors are operating in two-phase (gas-liquid) flow, and the mass transfer, particularly under Taylor flow conditions, is mainly in the thin film between the cylindrical bubbles and the channel walls containing the catalytic materials; and this mode of flow is possible in a wide range of gas and liquid superficial velocities.^[268,271] Compared with monolithic reactors, microchannel reactors have smaller channels, and they are more promising for achieving process intensification. A large number of the parallel small reaction volumes in microchannel reactors improved the mass and heat transfer within each volume.^[269] The monolithic reactor has the advantages of fixed-bed reactors, because it is not required to have the extra step for filtration and separation of catalysts from the products, and also due to the small particle size, the internal diffusion resistance is negligible. However, it still needs some improvement in the rate of heat transfer.

4.4.3. Multitubular reactors with structured packings

Structured packings are a good alternative to the currently existing slurry- and packed-bed reactors. They reveal more flexibility to the catalyst holdup, pressure drop, heat transfer properties, possible hydrodynamic regimes, and

flow rates.^[272] More enhanced heat transfer and thus an isothermal operation condition could be obtained over the microreactors with randomly packed catalyst beds. The smaller particle sizes are required for smaller channel sizes, which avoid diffusion limitations, and it also causes a significant pressure drop, thus limiting the potential reactor length.^[273,274] Due to the pressure drop, diffusion limitations, and thermal behavior, the optimum dimension of the tubes and catalyst pallets have to be considered for the conventional fixed-bed reactors. Micro-packed bed reactors are another option to attain higher heat transfer and lower pressure drop.^[275] These reactors show superb performance with the highly active catalysts, and depending on the particle size of catalyst, it can reduce the pressure drop or enhance the mass transfer.^[276,277] Different types of structured packings such as OCFS (open cross flow structures), CCFS (closed cross flow structures), aluminum foam, and knitted wire packing are shown in [Figure 12](#) Due to their highly porous structure and a much lower pressure drop, a higher liquid and gas throughputs obtain over the structured packings. As a result of the cross-flow in the inclined channels, OCFS has a superb radial mixing properties. CCFS also reveal a good radial heat transport, because the flow in this structure is

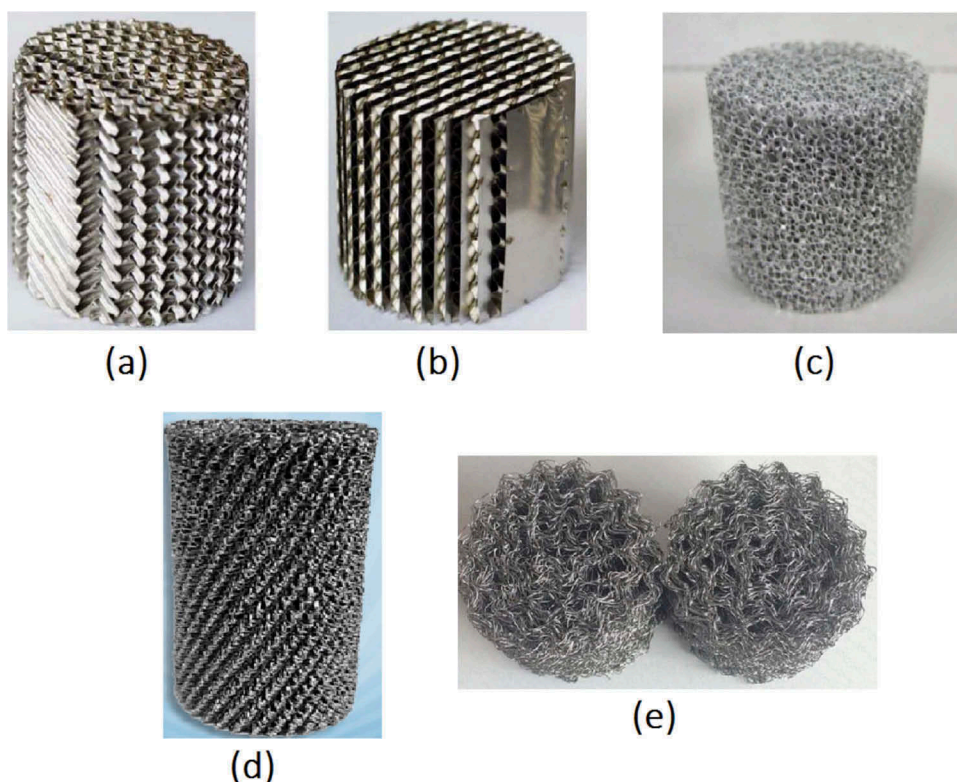


Figure 12. Structured packings, a) OCFS, b) CCFS, c) aluminum foam element, d) and e) knitted wire packing.^[278–280]

directed in a radial direction toward the wall. Foams are also found to be good structured packings due to their greater turbulence and improved convective heat transport. Knitted wire packings are also well-known because of their high mass transfer efficiency.^[278–280]

The limitation of the diffusion length resulted in some restrictions in catalyst size. The use of egg-shell catalysts, structured packings, and open foams as catalyst support was recommended to obtain a lower diffusion length, which results in a lower pressure drop and enhanced heat removal. The radial heat flux is enhanced by the higher radial convection of heat transfer, thus cause a lower temperature gradient and chain-growth probability. Compared with the conventional pellet packing in the tubular reactor, structured packings exhibited an enhanced thermal conductivity, by 19–60 times, depending on the composition of the gas-liquid phase of the fluid moving through the reactor.^[279] Other methods such as the use of bluff bodies as a passive method, and acoustics as an effective method, have been proposed for promoting mixing and improving the mass and heat transfer in the reformation reaction.^[281] It is worth noting that by using multitubular structured packing with a larger diameter of tubes, the capital cost of the reactor could be significantly decreased.^[262]

4.5. Comparison of different reactor types

The issues of reactor selection are investigated at three different strategy levels,^[253,282] namely, catalyst design (level I), injection and dispersion strategies (level II), and hydrodynamic flow regime (level III). Some of the advantages and disadvantages of different reactors are discussed, and a comparison of the reactors at different strategy levels is shown in Table 10. Different phenomena such as particle morphology (e.g., size, shape, and porous structure), diffusion characteristics, reaction kinetics, and reaction rates are considered at strategy level I. In the second level, the key issues are reactant and energy injection, selection of the optimum state of mixedness for concentration and temperature, separation of product or energy, and contact flow pattern. Level III is strongly dependent on the two other levels, and the desired hydrodynamic characteristics, such as heat and mass transfer behavior, catalyst stability, and reactor productivity can be combined with the requirements of the first two levels.^[253] The high surface-to-volume ratio in microtubular reactors results in the limitation of the radial heat transport distance and also decreases the thermal gradient within the reactor. The large thermal gradient in commercial-scale packed-bed FT reactors results in a wide range of product distributions and poor economics. Microtubular reactors with a high production rate and limited thermal gradient can improve selectivity to high valued FT process products. Slurry bubble column reactors with a uniform temperature profile produce a much narrower product selectivity. However, these reactors have a low production rate due to the reduced reactant concentration. Similar to packed-bed reactors, microtubular reactors as flow reactors show a high

Table 10. Comparison of different types of reactors.^[253]

	Requirements	Fluidized-bed	Slurry-bed	Multitubular fixed-bed	Monolithic
Level I	- High activity	~	~	~	~
	- Open morphology	~	~	~	~
	- Short diffusion lengths	+	+	-	+
Level II	- Concentration in plug flow	-	-	+	+
	- Temperature mixed	+	+	-	+
	- Staged feeding of reactants	-	-	-	+
	- Water vapor removal	-	-	-	+
	- Heat removal	+	+	-	+
	- Periodic operation	NA	NA	NA	NA
Level III	- High catalyst holdup	±	±	+	±
	- Good heat-transfer characteristics	+	+	-	+
	- Moderate to good mass-transfer characteristics	+	+	+	+
	- Catalyst attrition/separation	hours/d	hours/d	months/year	year
	- Minimal required catalyst stability	< 100 μm	< 100 μm	> 1 mm	< 50 μm*
	- Particle size		μm		

Note: +: sufficient/positive; -: negative; ±: moderate; ~: independent reactor type; NA: not available; hours/d: hours/days; *: tunable.

reaction rate but also operate with limited thermal gradients. These properties offer optimum conditions for exothermic reactions, such as the FT reaction to produce high valued products.^[252,253,282]

Monoliths are extruded metal structures, usually with a honeycomb shape of small-diameter channels. The small channels enhance the laminar flow, which promotes the mass transport properties. The wash-coating of thin catalyst layers is deposited onto the monolith walls. These structures are located inside a reactor tube, and the gap between the monolith and the reactor tube is the main limiting factor of this system. This gap is changed depending on the reactor condition, and the resistance to heat transport out of the system varies. This feature limits the size of the overall system due to the increasing resistance for thermal transport. Microtubular reactors have the catalytic structure chemically bonded to the tube wall, and there is no thermal resistance at the tube wall due to changing the gap length. Furthermore, the simplified production of gas and liquid phase processing all within the final reactor structure is beneficial over producing a metal structure, which must be fitted tightly within another tube. Microchannel reactors for FT reactions have exhibited high productivities at a single pass CO conversion of 90% and low CH₄ selectivity of 3.4%.^[283] The reactant gases (syngas) for the FT reaction can contact with the FT catalyst through a microchannel reactor to convert syngas to the products. Microchannel reactors use supported cobalt catalysts with the Co loading of at least 25 wt.%.^[284]

5. Concluding remarks

FTS is proven technology for converting syngas derived from natural gas, biomass and/or solid organic matter into valuable chemicals, such as liquid fuels. The

product selectivity and activity of catalysts can be optimized by changing their physicochemical properties through the variation of different parameters, such as support and promoters. Several studies have focused on the cobalt-based FT catalysts supported on traditional oxide supports. This paper presents a comprehensive literature review on the history of the FTS process and provides information about the effect of supports, promoters, and types of reactor on the catalytic performance of cobalt-based FT catalyst. Given the high ability of adsorption and dissociation of CO and H₂, different elements, mainly from groups 8–10, such as cobalt, iron, nickel, and ruthenium, were used as an active metal for FT catalysts. Cobalt-based catalysts with low WGS activity are suitable for the syngas with high H₂/CO ratio and production of heavy hydrocarbons, including diesel and wax. Cobalt catalysts also tend to have a longer lifetime than iron catalysts. An optimum number of cobalt particles should be well dispersed on the support to increase the catalytic activity and enhance the selectivity to liquid hydrocarbons. The optimization of product selectivity and catalytic activity is affected by the type of support and addition of promoters to the catalyst structure. The selection of a catalyst support is a crucial parameter as it can significantly affect the catalyst's performance. The support can improve the crystallization, metal dispersion, mass transfer of the reactant/products, and the mechanical and thermal stability of the catalyst. The metal–support interaction can be affected by the textural and physicochemical properties of the support. Thus, the selection of appropriate support materials with suitable properties, such as well-defined surface chemistry, high surface area, and proper pore size/volume, is crucial in designing an efficient catalyst.

Different materials, such as zeolite, Al₂O₃, TiO₂, SiO₂, and carbonaceous materials, have been widely used as support for the Co catalyst in FT synthesis. The presence of more Co⁰ active sites results in high catalytic activity and C₅₊ selectivity, and the catalyst's stability also increases because of the inhibited mobility of cobalt particles on the surface of nanostructured alumina. Modification of textural properties of alumina enhances the loading of active metals and increases the availability of active sites. Co/SiO₂ catalysts exhibit higher selectivity to C₅₊ and lower selectivity to CH₄ than Co/Al₂O₃ catalysts. Titanium oxide with high thermal and chemical stability and outstanding corrosion resistance is also used as a promising support material. The strength of the cobalt–TiO₂ interaction is between those of SiO₂ and Al₂O₃. Zeolites have also been extensively used in industrial processes; their shape-selective feature enables them to limit the formation of products larger than their pore diameters and formation of heavier hydrocarbons in FTS can be limited by restriction of the chain growth. Carbon materials show excellent resistance in both acidic and basic media, and their porous structure is adjustable for specific reactions. Given the intrinsic inertness surface of the carbon materials to form a weak interaction between the metal and the support, which is very important for achieving a high degree of reduction, these materials are suitable supports for FT catalysts.

Promoters can be used as a structural, textural, and electronic modifier, stabilizers, and catalyst-poison-resistant, which can improve the catalytic performance. Some promoters such as noble metals can act as both structural and electronic promoters. The exact function of the promoter is sometimes difficult to define due to the overlapping of effects. Different types of promoters, including noble metals (e.g., Pt, Pd, Ru, and Re), transition metal oxides (e.g., Zr, Mn, La, Gd, Cu, and Ni), alkali metals (e.g., Rb, K, Na, and Li), and alkaline earth metals (e.g., Mg, Ca, and Ba) and their effect on catalytic performance of cobalt-based FT catalysts have been studied.

FTS is a highly exothermic reaction, and the reactor must be designed properly to handle the heat of reaction. Different types of FT reactors are used in the commercial FT process, including slurry bubble column and fixed-bed reactors (for LTFT processes) and fluidized-bed reactors (for HTFT processes). In micro-channel reactors, which are recently being used for LTFT processes, a very high space-time yield can be achieved due to the intensified mass transfer. The uniform temperature and efficient heat transfer across the reactor walls significantly enhance the catalytic activity and lifetime.

Acknowledgments

This publication is a result of the project CATAMARAN, Reg. No. CZ.02.1.01/0.0/0.0/16_013/0001801, which has been co-financed by European Union from the European Regional Development Fund through the Operational Programme Research, Development and Education. This project has also been financially supported by the Ministry of Industry and Trade of the Czech Republic which has been providing institutional support for long-term conceptual development of research organization. The project CATAMARAN has been integrated into the National Sustainability Programme I of the Ministry of Education, Youth and Sports of the Czech Republic (MEYS) through the project Development of the UniCRE Centre (LO1606). The result was achieved using the infrastructure of the project Efficient Use of Energy Resources Using Catalytic Processes (LM2015039) which has been financially supported by MEYS within the targeted support of large infrastructures.

Highlights

- FTS is a promising method for the catalytic conversion of syngas into liquid fuels.
- Co catalysts are suitable for production of heavy hydrocarbons like diesel and wax.
- Physicochemical properties of catalyst affected by the support and promoter.
- Reactor must be selected properly to handle the heat of highly exothermic FT reaction.

ORCID

Zahra Gholami  <http://orcid.org/0000-0003-1762-2626>

References

- [1] Klass, D. L. *Biomass for Renewable Energy, Fuels, and Chemicals*; Academic Press, Elsevier Science, California, USA, 1998.
- [2] Gholami, Z.; Zabidi, N. A. M.; Gholami, F.; Ayodele, O. B.; Vakili, M. The Influence of Catalyst Factors for Sustainable Production of Hydrocarbons via Fischer-Tropsch Synthesis. *Rev. Chem. Eng.* 2017, 33(4), 337–358. DOI: 10.1515/revce-2016-0009.
- [3] Ail, S. S.; Dasappa, S. Biomass to Liquid Transportation Fuel via Fischer Tropsch Synthesis–Technology Review and Current Scenario. *Renew. Sustain. Energy Rev.* 2016, 58, 267–286. DOI: 10.1016/j.enconman.2016.02.075.
- [4] Vosoughi, V.; Badoga, S.; Dalai, A. K.; Abatzoglou, N. Modification of Mesoporous Alumina as a Support for Cobalt-Based Catalyst in Fischer-Tropsch Synthesis. *Fuel Process. Technol.* 2017, 162, 55–65. DOI: 10.1016/j.fuproc.2017.03.029.
- [5] Pratt, J. W. A Fischer-Tropsch Synthesis Reactor Model Framework for Liquid Biofuels Production. SANDIA Report: SAND2012-7848, 2012.
- [6] Okoye-Chine, C. G.; Moyo, M.; Liu, X.; Hildebrandt, D. A Critical Review of the Impact of Water on Cobalt-Based Catalysts in Fischer-Tropsch Synthesis. *Fuel Process. Technol.* 2019, 192, 105–129. DOI: 10.1016/j.fuproc.2019.04.006.
- [7] Vosoughi, V.; Badoga, S.; Dalai, A. K.; Abatzoglou, N. Effect of Pretreatment on Physicochemical Properties and Performance of Multiwalled Carbon Nanotube Supported Cobalt Catalyst for Fischer–Tropsch Synthesis. *Ind. Eng. Chem. Res.* 2016, 55(21), 6049–6059. DOI: 10.1021/acs.iecr.5b04381.
- [8] Odunsi, A. O.; O'Donovan, T. S.; Reay, D. A. Dynamic Modeling of Fixed-Bed Fischer-Tropsch Reactors with Phase Change Material Diluents. *Chem. Eng. Technol.* 2016, 39 (11), 2066–2076. DOI: 10.1002/ceat.201600196.
- [9] Van Santen, R.; Ciobică, I.; Van Steen, E.; Ghouri, M. Mechanistic issues in Fischer–Tropsch catalysis, *Advances in catalysis*; Elsevier, Burlington, USA, 2011; pp 127–187.
- [10] Van Santen, R.; Markvoort, A.; Filot, I.; Ghouri, M.; Hensen, E. Mechanism and Microkinetics of the Fischer–Tropsch Reaction. *Phys. Chem. Chem. Phys.* 2013, 15 (40), 17038–17063. DOI: 10.1039/c3cp52506f.
- [11] Van Der Laan, G. P.; Beenackers, A. A. C. M. Kinetics and Selectivity of the Fischer–Tropsch Synthesis: A Literature Review. *Catal. Rev.* 1999, 41(3–4), 255–318. DOI: 10.1081/CR-100101170.
- [12] Lesch, J. E. *The German Chemical Industry in the Twentieth Century*, 1sted.; Springer Science & Business Media, United states, 2000; 10.1007/978-94-015-9377-9
- [13] Stranges, A. N. A History of the Fischer-Tropsch Synthesis in Germany 1926–45. *Stud. Stud. Surf. Sci. Catal.* 2007, 163, 1–27. DOI: 10.1016/S0167-2991(07)80469-1.
- [14] Sabatier, P. New synthesis of Methane. *C. R.* 1902, 134, 514–516.
- [15] Storch, H. H. The Fischer-Tropsch and Related Processes for Synthesis of Hydrocarbons by Hydrogenation of Carbon Monoxide. *Adv. Catal.* 1948, 1, 115–156. DOI: 10.1016/S0360-0564(08)60674-4.
- [16] Davis, B. H.; Ocelli, M. L. *Fischer-Tropsch Synthesis, Catalysts and Catalysis: Advances and Applications*, 1st ed.; CRC Press, Amsterdam, The Netherlands, 2016.
- [17] Gordon, K. *Report on the petroleum and synthetic oil industry of Germany*; U.S. Department of Energy Office of Scientific and Technical Information, United

- States, 1947. <https://www.osti.gov/biblio/7178255-report-petroleum-synthetic-oil-industry-germany>
- [18] Storch, H. H.; Golumbic, N.; Anderson, R. A. *The Fischer-Tropsch and related Syntheses*; Wiley: New York, 1951.
- [19] Todd, E. Industry and Ideology: I. G. Farben in the Nazi Era. By Peter Hayes. New York: Cambridge University Press. *J. Econ. Hist.* 1988, 48(3), 752–753. DOI: 10.1017/S0022050700006112.
- [20] Becker, P. W.; Stokes, R. G.; The American Historical Review. *Divide and Prosper: The Heirs of I. G. Farben under Allied Authority, 1945–1951*; Berkeley and Los Angeles: University of California Press, 1988. DOI: 10.1086/ahr/95.5.1570.
- [21] Berghahn, V. R.; Gimbel, J. *Science, Technology, and Reparations: Exploitation and Plunder in Postwar Germany*; Stanford: Stanford University Press, 1990. DOI: 10.1086/ahr/96.4.1167.
- [22] Synfuels China. 2019. <http://www.synfuelschina.com.cn/en/about/>.
- [23] Minchener, A. J. Coal-to-Oil, Gas and Chemicals in China. Report CCC/181, IEA Clean Coal Centre, 2011. <https://www.usea.org/publication/coal-oil-gas-and-chemicals-china-ccc181>.
- [24] Moulijn, J. A.; Makkee, M.; van Diepen, A. E. *Chemical Process Technology*. John Wiley & Sons Ltd, United Kingdom, 2013.
- [25] Rauch, R.; Kiennemann, A.; Sauciu, A. Chapter 12 - Fischer-Tropsch Synthesis to Biofuels (BtL Process), in *The Role of Catalysis for the Sustainable Production of Biofuels and Bio-chemicals*; Elsevier: Amsterdam, 2013; pp 397–443.
- [26] Van de Loosdrecht, J.; Botes, F.; Ciobica, I.; Ferreira, A.; Gibson, P.; Moodley, D.; Saib, A.; Visagie, J.; Weststrate, C.; Niemantsverdriet, J. *Fischer-Tropsch Synthesis: Catalysts and Chemistry, Comprehensive Inorganic Chemistry II: from elements to applications*, 2n ed.; Amstrdam: Elsevier, 2013; pp 525–557.
- [27] Maitlis, P. M.; de Klerk, A. *Greener Fischer-Tropsch Processes: For Fuels and Feedstocks*; John Wiley & Sons: Weinheim, Germany, 2013.
- [28] Spivey, J. J.; Han, Y. F.; Dooley, K. M. *Catalysis: Volume 27*; UK: Royal Society of Chemistry, 2015. DOI: 10.1039/9781782622697.
- [29] Leckel, D. Diesel Production from Fischer–Tropsch: The Past, the Present, and New Concepts. *Energy Fuels.* 2009, 23(5), 2342–2358. DOI: 10.1021/ef900064c.
- [30] Ali, S.; Mohd Zabidi, N. A.; Subbarao, D. Correlation Between Fischer-Tropsch Catalytic Activity and Composition of Catalysts. *Chem. Cent. J.* 2011, 5, 68. DOI: 10.1186/1752-153X-5-68.
- [31] Liu, Y.; Fang, K.; Chen, J.; Sun, Y. Effect of Pore Size on the Performance of Mesoporous Zirconia-Supported Cobalt Fischer–Tropsch Catalysts. *Green Chem.* 2007, 9(6), 611–615. DOI: 10.1039/b614266d.
- [32] Srinivasan, N.; Espinoza, R. L.; Coy, K. L.; Jothimurugesan, K. US Patent, US6822008B2, 2004.
- [33] Espinoza, R. L.; Jin, Y.; Jothimurugesan, K.; Srinivasan, N. Patent, AU2003301247A1, 2006.
- [34] Choudhury, H. A.; Moholkar, V. S. Synthesis of Liquid Hydrocarbons by Fischer–Tropsch Process using Industrial Iron Catalyst. *Int. J. Innov. Res. Sci. Eng. Technol.* 2013, 2(8), 3493–3499.
- [35] Shafer, W. D.; Gnanamani, M. K.; Graham, U. M.; Yang, J.; Masuku, C. M.; Jacobs, G.; Davis, B. H. Fischer–Tropsch: Product Selectivity–The Fingerprint of Synthetic Fuels. *Catalysts.* 2019, 9(3), 259. DOI: 10.3390/catal9030259.
- [36] Dasgupta, D.; Wiltowski, T. Enhancing Gas Phase Fischer–Tropsch Synthesis Catalyst Design. *Fuel.* 2011, 90(1), 174–181. DOI: 10.1016/j.fuel.2010.07.037.

- [37] Iglesia, E.; Soled, S. L.; Fiato, R. A.; Via, G. H. Bimetallic synergy in cobalt ruthenium Fischer-Tropsch synthesis catalysts. *J. Catal.* **1993**, *143*(2), 345–368. DOI: [10.1006/jcat.1993.1281](https://doi.org/10.1006/jcat.1993.1281).
- [38] Iglesia, E. Design, synthesis, and use of Cobalt-Based Fischer-Tropsch Synthesis Catalysts. *Appl. Catal. A. Gen.* **1997**, *161*(1–2), 59–78. DOI: [10.1016/S0926-860X\(97\)00186-5](https://doi.org/10.1016/S0926-860X(97)00186-5).
- [39] Iglesia, E.; Soled, S. L.; Fiato, R. A. Fischer-Tropsch Synthesis on Cobalt and Ruthenium. Metal Dispersion and Support Effects on Reaction Rate and Selectivity. *J. Catal.* **1992**, *137*(1), 212–224. DOI: [10.1016/0021-9517\(92\)90150-G](https://doi.org/10.1016/0021-9517(92)90150-G).
- [40] Yang, J.; Frøseth, V.; Chen, D.; Holmen, A. Particle size effect for Cobalt Fischer-Tropsch Catalysts Based on In Situ CO Chemisorption. *Surf. Sci.* **2016**, *648*, 67–73. DOI: [10.1016/j.susc.2015.10.029](https://doi.org/10.1016/j.susc.2015.10.029).
- [41] Gavrilović, L.; Save, J.; Blekkan, E. A. The Effect of Potassium on Cobalt-Based Fischer-Tropsch Catalysts with Different Cobalt Particle Sizes. *Catalysts*. **2019**, *9*(4), 351. DOI: [10.3390/catal9040351](https://doi.org/10.3390/catal9040351).
- [42] Pendyala, V. R. R.; Jacobs, G.; Ma, W.; Klettlinger, J. L.; Yen, C. H.; Davis, B. H. Fischer-Tropsch Synthesis: Effect of Catalyst Particle (Sieve) Size Range on Activity, Selectivity, and Aging of a Pt Promoted Co/Al₂O₃ Catalyst. *Chem. Eng. J.* **2014**, *249*, 279–284. DOI: [10.1016/j.cej.2014.03.100](https://doi.org/10.1016/j.cej.2014.03.100).
- [43] Den Breejen, J.; Radstake, P.; Bezemer, G.; Bitter, J.; Frøseth, V.; Holmen, A.; De Jong, K. On the Origin of the Cobalt Particle Size Effects in Fischer-Tropsch Catalysis. *J. Am. Chem. Soc.* **2009**, *131*(20), 7197–7203. DOI: [10.1021/ja901006x](https://doi.org/10.1021/ja901006x).
- [44] de la Osa, A.; Romero, A.; Dorado, F.; Valverde, J.; Sánchez, P. Influence of Cobalt Precursor on Efficient Production of Commercial Fuels over FTS Co/SiC Catalyst. *Catalysts*. **2016**, *6*(7), 98. DOI: [10.3390/catal6070098](https://doi.org/10.3390/catal6070098).
- [45] Borg, Ø.; Dietzel, P. D.; Spjelkavik, A. I.; Tveten, E. Z.; Walmsley, J. C.; Diplas, S.; Eri, S.; Holmen, A.; Rytter, E. Fischer-Tropsch Synthesis: Cobalt Particle Size and Support Effects on Intrinsic Activity and Product Distribution. *J. Catal.* **2008**, *259*(2), 161–164. DOI: [10.1016/j.jcat.2008.08.017](https://doi.org/10.1016/j.jcat.2008.08.017).
- [46] Bezemer, G. L.; Bitter, J. H.; Kuipers, H. P.; Oosterbeek, H.; Holewijn, J. E.; Xu, X.; Kapteijn, F.; van Dillen, A. J.; de Jong, K. P. Cobalt Particle Size Effects in the Fischer-Tropsch Reaction Studied with Carbon Nanofiber Supported Catalysts. *J. Am. Chem. Soc.* **2006**, *128*(12), 3956–3964. DOI: [10.1021/ja058282w](https://doi.org/10.1021/ja058282w).
- [47] Sadek, R.; Chalupka, K. A.; Mierczynski, P.; Rynkowski, J.; Millot, Y.; Valentin, L.; Casale, S.; Dzwigaj, S. Fischer-Tropsch Reaction on Co-containing Microporous and Mesoporous Beta Zeolite Catalysts: The Effect of Pore Size and Acidity. *Catal. Today*. **2019**. DOI: [10.1016/j.cattod.2019.05.004](https://doi.org/10.1016/j.cattod.2019.05.004).
- [48] Bukur, D. B.; Lang, X.; Mukesh, D.; Zimmerman, W. H.; Rosynek, M. P.; Li, C. Binder/Support Effects on the Activity and Selectivity of Iron Catalysts in the Fischer-Tropsch Synthesis. *Ind. Eng. Chem. Res.* **1990**, *29*(8), 1588–1599. DOI: [10.1021/ie00104a003](https://doi.org/10.1021/ie00104a003).
- [49] Regalbuto, J. *Catalyst preparation: science and engineering*; CRC press, Taylor & Francis Group, New York, United States, **2016**.
- [50] Borg, Ø.; Eri, S.; Blekkan, E. A.; Storsæter, S.; Wigum, H.; Rytter, E.; Holmen, A. Fischer-Tropsch Synthesis over γ -Alumina-Supported Cobalt Catalysts: Effect of Support Variables. *J. Catal.* **2007**, *248*(1), 89–100. DOI: [10.1016/j.jcat.2007.03.008](https://doi.org/10.1016/j.jcat.2007.03.008).
- [51] Fu, T.; Li, Z. Review of Recent Development in Co-Based Catalysts Supported on Carbon Materials for Fischer-Tropsch Synthesis. *Chem. Eng. Sci.* **2015**, *135*, 3–20. DOI: [10.1016/j.ces.2015.03.007](https://doi.org/10.1016/j.ces.2015.03.007).
- [52] Khodakov, A. Y.; Griboval-Constant, A.; Bechara, R.; Zholobenko, V. L. Pore Size Effects in Fischer Tropsch Synthesis over Cobalt-Supported Mesoporous Silicas. *J. Catal.* **2002**, *206*(2), 230–241. DOI: [10.1006/jcat.2001.3496](https://doi.org/10.1006/jcat.2001.3496).

- [53] Wang, D.; Chen, C.; Wang, J.; Jia, L.; Hou, B.; Li, D. Silicon Carbide Supported Cobalt for Fischer–Tropsch Synthesis: Probing into the Cause of the Intrinsic Excellent Catalytic Performance. *RSC Adv.* **2015**, *5*(120), 98900–98903. DOI: [10.1039/C5RA22170F](https://doi.org/10.1039/C5RA22170F).
- [54] Wang, Y.-N.; Xu, -Y.-Y.; Xiang, H.-W.; Li, Y.-W.; Zhang, B.-J. Modeling of Catalyst Pellets for Fischer–Tropsch Synthesis. *Ind. Eng. Chem. Res.* **2001**, *40*(20), 4324–4335. DOI: [10.1021/ie010080v](https://doi.org/10.1021/ie010080v).
- [55] Qu, Z.; Huang, W.; Zhou, S.; Zheng, H.; Liu, X.; Cheng, M.; Bao, X. Enhancement of the Catalytic Performance of Supported-Metal Catalysts by Pretreatment of the Support. *J. Catal.* **2005**, *234*(1), 33–36. DOI: [10.1016/j.jcat.2005.05.021](https://doi.org/10.1016/j.jcat.2005.05.021).
- [56] Zamaniyan, A.; Mortazavi, Y.; Khodadadi, A. A.; Pour, A. N. Effect of Mass Transfer Limitations on Catalyst Performance During Reduction and Carburization of Iron Based Fischer-Tropsch Synthesis Catalysts. *J. Energy Chem.* **2013**, *22*(5), 795–803. DOI: [10.1016/S2095-4956\(13\)60106-0](https://doi.org/10.1016/S2095-4956(13)60106-0).
- [57] Merino, D.; Pérez-Miqueo, I.; Sanz, O.; Montes, M. On the Way to a More Open Porous Network of a Co–Re/Al₂O₃ Catalyst for Fischer–Tropsch Synthesis: Pore Size and Particle Size Effects on Its Performance. *Top. Catal.* **2016**, *59*(2–4), 207–218. DOI: [10.1007/s11244-015-0436-3](https://doi.org/10.1007/s11244-015-0436-3).
- [58] Li, H.; Wang, J.; Chen, C.; Jia, L.; Hou, B.; Li, D. Effects of Macropores on Reducing Internal Diffusion Limitations in Fischer–Tropsch Synthesis using A Hierarchical Cobalt Catalyst. *RSC Adv.* **2017**, *7*(16), 9436–9445. DOI: [10.1039/C6RA27166A](https://doi.org/10.1039/C6RA27166A).
- [59] Bartholomew, C. H.; Reuel, R. C. Cobalt-Support Interactions: Their Effects on Adsorption and Carbon Monoxide Hydrogenation Activity and Selectivity Properties. *Ind. Eng. Chem. Prod. Res. Dev.* **1985**, *24*(1), 56–61. DOI: [10.1021/i300017a011](https://doi.org/10.1021/i300017a011).
- [60] Gnanamani, M. K.; Ribeiro, M. C.; Ma, W.; Shafer, W. D.; Jacobs, G.; Graham, U. M.; Davis, B. H. Fischer–Tropsch synthesis: Metal–Support Interfacial Contact Governs Oxygenates Selectivity over CeO₂ Supported Pt–Co Catalysts. *Appl. Catal. A.* **2011**, *393* (1–2), 17–23. DOI: [10.1016/j.apcata.2010.11.019](https://doi.org/10.1016/j.apcata.2010.11.019).
- [61] Jung, J.-S.; Kim, S. W.; Moon, D. J. Fischer–Tropsch Synthesis over Cobalt Based Catalyst Supported on Different Mesoporous Silica. *Catal. Today.* **2012**, *185*(1), 168–174. DOI: [10.1016/j.cattod.2012.02.002](https://doi.org/10.1016/j.cattod.2012.02.002).
- [62] Marin, R. P.; Kondrat, S. A.; Davies, T. E.; Morgan, D. J.; Enache, D. I.; Combes, G. B.; Taylor, S. H.; Bartley, J. K.; Hutchings, G. J. Novel Cobalt Zinc Oxide Fischer–Tropsch Catalysts Synthesised using Supercritical Anti-Solvent Precipitation. *Catal. Sci. Technol.* **2014**, *4*(7), 1970–1978. DOI: [10.1039/c4cy00044g](https://doi.org/10.1039/c4cy00044g).
- [63] Pan, Z.; Bukur, D. B. Fischer–Tropsch Synthesis on Co/ZnO Catalyst—Effect of Pretreatment Procedure. *Appl. Catal. A. Gen.* **2011**, *404*(1–2), 74–80. DOI: [10.1016/j.apcata.2011.07.012](https://doi.org/10.1016/j.apcata.2011.07.012).
- [64] Ma, W.; Jacobs, G.; Sparks, D. E.; Gnanamani, M. K.; Pendyala, V. R. R.; Yen, C. H.; Klettlinger, J. L.; Tomsik, T. M.; Davis, B. H. Fischer–Tropsch Synthesis: Support and Cobalt Cluster Size Effects on Kinetics over Co/Al₂O₃ and Co/SiO₂ Catalysts. *Fuel.* **2011**, *90*(2), 756–765. DOI: [10.1016/j.fuel.2010.10.029](https://doi.org/10.1016/j.fuel.2010.10.029).
- [65] Khangale, P. R.; Meijboom, R.; Jalama, K. Fischer-Tropsch Synthesis over Unpromoted Co/γ-Al₂O₃ Catalyst: Effect of Activation with CO Compared to H₂ on Catalyst Performance. *Bull. Chem. React. Eng. Catal.* **2019**, *14*(1), 35–41. DOI: [10.9767/bcrec.14.1.2519.35-41](https://doi.org/10.9767/bcrec.14.1.2519.35-41).
- [66] Diehl, F.; Hugues, F.; Marion, M.-C.; Uzio, D. US Patent, US20100029792A1, **2011**.
- [67] Liu, C.; Hong, J.; Zhang, Y.; Zhao, Y.; Wang, L.; Wei, L.; Chen, S.; Wang, G.; Li, J. Synthesis of γ-Al₂O₃ Nanofibers Stabilized Co₃O₄ Nanoparticles as Highly Active and Stable Fischer–Tropsch Synthesis Catalysts. *Fuel.* **2016**, *180*, 777–784. DOI: [10.1016/j.fuel.2016.04.006](https://doi.org/10.1016/j.fuel.2016.04.006).

- [68] Iglesia, E.; Soled, S. L.; Baumgartner, J. E.; Reyes, S. C. Synthesis and Catalytic Properties of Eggshell Cobalt Catalysts for the Fischer-Tropsch Synthesis. *J. Catal.* **1995**, *153*(1), 108–122. DOI: [10.1006/jcat.1995.1113](https://doi.org/10.1006/jcat.1995.1113).
- [69] Jahangiri, H.; Bennett, J.; Mahjoubi, P.; Wilson, K.; Gu, S. A Review of Advanced Catalyst Development for Fischer-Tropsch Synthesis of Hydrocarbons from Biomass Derived Syn-Gas. *Catal. Sci. Technol.* **2014**, *4*(8), 2210–2229. DOI: [10.1039/c4cy00327f](https://doi.org/10.1039/c4cy00327f).
- [70] Luque, R.; de la Osa, A. R.; Campelo, J. M.; Romero, A. A.; Valverde, J. L.; Sanchez, P. Design and development of catalysts for Biomass-To-Liquid-Fischer-Tropsch (BTL-FT) processes for biofuels production. *Energy. Environ. Sci.* **2012**, *5*(1), 5186–5202. DOI: [10.1039/c1ee02238e](https://doi.org/10.1039/c1ee02238e).
- [71] van Steen, E.; Claeys, M. Fischer-Tropsch Catalysts for the Biomass-to-Liquid (BTL)-Process. *Chem. Eng. Technol.* **2008**, *31*(5), 655–666. DOI: [10.1002/ceat.200800067](https://doi.org/10.1002/ceat.200800067).
- [72] Khodakov, A. Y.; Chu, W.; Fongarland, P. Advances in the Development of Novel Cobalt Fischer-Tropsch Catalysts for Synthesis of Long-Chain Hydrocarbons and Clean Fuels. *Chem. Rev.* **2007**, *107*(5), 1692–1744. DOI: [10.1021/cr050972v](https://doi.org/10.1021/cr050972v).
- [73] Steynberg, A. Chapter 1 - Introduction to Fischer-Tropsch Technology. *Stud. Surf. Sci. Catal.* **2004**, *152*, 1–63. DOI: [10.1016/S0167-2991\(04\)80458-0](https://doi.org/10.1016/S0167-2991(04)80458-0).
- [74] Ail, S. S.; Benedetti, V.; Baratieri, M.; Dasappa, S. Fuel-Rich Combustion Synthesized Co/Al₂O₃ Catalysts for Wax and Liquid Fuel Production via Fischer-Tropsch Reaction. *Ind. Eng. Chem. Res.* **2018**, *57*(11), 3833–3843. DOI: [10.1021/acs.iecr.7b04174](https://doi.org/10.1021/acs.iecr.7b04174).
- [75] Fratallocchi, L.; Visconti, C. G.; Lietti, L.; Fischer, N.; Claeys, M. A Promising Preparation Method for Highly Active Cobalt Based Fischer-Tropsch Catalysts Supported on Stabilized Al₂O₃. *Appl. Catal. A: Gen.* **2018**, *556*, 92–103. DOI: [10.1016/j.apcata.2018.02.002](https://doi.org/10.1016/j.apcata.2018.02.002).
- [76] Taheri Najafabadi, A.; Khodadadi, A. A.; Parnian, M. J.; Mortazavi, Y. Atomic Layer Deposited Co/ γ -Al₂O₃ Catalyst with Enhanced Cobalt Dispersion and Fischer-Tropsch Synthesis Activity and Selectivity. *Appl. Catal. A: Gen.* **2016**, *511*, 31–46. DOI: [10.1016/j.apcata.2015.11.027](https://doi.org/10.1016/j.apcata.2015.11.027).
- [77] Rane, S.; Borg, Ø.; Yang, J.; Rytter, E.; Holmen, A. Effect of Alumina Phases on Hydrocarbon Selectivity in Fischer-Tropsch Synthesis. *Appl. Catal. A: Gen.* **2010**, *388*(1), 160–167. DOI: [10.1016/j.apcata.2010.08.038](https://doi.org/10.1016/j.apcata.2010.08.038).
- [78] Mohammadnasabomran, S.; Tavasoli, A.; Zamani, Y. The Impact of Different Alumina Supports on Cobalt-Catalyzed Fischer-Tropsch Synthesis and Investigation of Kinetic Model for the Catalyst with Optimum Performance. *React. Kinet. Mech. Catal.* **2019**, *128*(1), 217–234. DOI: [10.1007/s11144-019-01634-5](https://doi.org/10.1007/s11144-019-01634-5).
- [79] Rytter, E.; Borg, Ø.; Enger, B. C.; Holmen, A. α -Alumina as Catalyst Support in Co Fischer-Tropsch Synthesis and the Effect of Added Water; Encompassing Transient Effects. *J. Catal.* **2019**, *373*, 13–24. DOI: [10.1016/j.jcat.2019.03.013](https://doi.org/10.1016/j.jcat.2019.03.013).
- [80] Zhang, Y.; Koike, M.; Yang, R.; Hinchiranan, S.; Vitidsant, T.; Tsubaki, N. Multi-Functional Alumina-Silica Bimodal Pore Catalyst and its Application for Fischer-Tropsch Synthesis. *Appl. Catal. A: Gen.* **2005**, *292*, 252–258. DOI: [10.1016/j.apcata.2005.06.004](https://doi.org/10.1016/j.apcata.2005.06.004).
- [81] Rahmati, M.; Huang, B.; Schofield, L. M.; Fletcher, T. H.; Woodfield, B. F.; Hecker, W. C.; Bartholomew, C. H.; Argyle, M. D. Effects of Ag Promotion And Preparation Method on Cobalt Fischer-Tropsch Catalysts Supported on Silica-Modified Alumina. *J. Catal.* **2018**, *362*, 118–128. DOI: [10.1016/j.jcat.2018.03.027](https://doi.org/10.1016/j.jcat.2018.03.027).
- [82] Enger, B. C.; Fossan, Å.-L.; Borg, Ø.; Rytter, E.; Holmen, A. Modified Alumina as Catalyst Support for Cobalt in the Fischer-Tropsch Synthesis. *J. Catal.* **2011**, *284*(1), 9–22. DOI: [10.1016/j.jcat.2011.08.008](https://doi.org/10.1016/j.jcat.2011.08.008).

- [83] Rahmati, M.; Huang, B.; Mortensen, M. K.; Keyvanloo, K.; Fletcher, T. H.; Woodfield, B. F.; Hecker, W. C.; Argyle, M. D. Effect of Different Alumina Supports on Performance of Cobalt Fischer-Tropsch Catalysts. *J. Catal.* **2018**, *359*, 92–100. DOI: [10.1016/j.jcat.2017.12.022](https://doi.org/10.1016/j.jcat.2017.12.022).
- [84] Ail, S. S.; Dasappa, S. Investigations into Enhanced Wax Production with Combustion Synthesized Fischer-Tropsch Catalysts. *Energy Convers. Manage.* **2016**, *116*, 80–90. DOI: [10.1016/j.enconman.2016.02.075](https://doi.org/10.1016/j.enconman.2016.02.075).
- [85] Yaghoobpour, E.; Zamani, Y.; Zarrinpashne, S.; Zamaniyan, A. Fischer-Tropsch Synthesis: Effect of Silica on Hydrocarbon Production over Cobalt-Based Catalysts. *Chem. Papers.* **2019**, *73*(1), 205–214. DOI: [10.1007/s11696-018-0565-9](https://doi.org/10.1007/s11696-018-0565-9).
- [86] Liu, C.; Li, J.; Zhang, Y.; Chen, S.; Zhu, J.; Liew, K. Fischer-Tropsch Synthesis over Cobalt Catalysts Supported on Nanostructured Alumina with Various Morphologies. *J. Mol. Catal. A: Chem.* **2012**, *363-364*, 335–342. DOI: [10.1016/j.molcata.2012.07.009](https://doi.org/10.1016/j.molcata.2012.07.009).
- [87] Shimura, K.; Miyazawa, T.; Hanaoka, T.; Hirata, S. Fischer-Tropsch Synthesis over Alumina Supported Cobalt Catalyst: Effect of Crystal Phase and Pore Structure of Alumina Support. *J. Mol. Catal. A: Chem.* **2014**, *394*, 22–32. DOI: [10.1016/j.molcata.2014.06.034](https://doi.org/10.1016/j.molcata.2014.06.034).
- [88] Jalama, K.; Coville, N. J.; Xiong, H.; Hildebrandt, D.; Glasser, D.; Taylor, S.; Carley, A.; Anderson, J. A.; Hutchings, G. J. A Comparison of Au/Co/Al₂O₃ and Au/Co/SiO₂ Catalysts in the Fischer-Tropsch Reaction. *Appl. Catal. A: Gen.* **2011**, *395*(1), 1–9. DOI: [10.1016/j.apcata.2011.01.002](https://doi.org/10.1016/j.apcata.2011.01.002).
- [89] Ma, W.; Jacobs, G.; Keogh, R. A.; Bukur, D. B.; Davis, B. H. Fischer-Tropsch Synthesis: Effect of Pd, Pt, Re, and Ru Noble Metal Promoters on the Activity and Selectivity of a 25%Co/Al₂O₃ Catalyst. *Appl. Catal. A: Gen.* **2012**, *437-438*, 1–9. DOI: [10.1016/j.apcata.2012.05.037](https://doi.org/10.1016/j.apcata.2012.05.037).
- [90] Peng, X.; Cheng, K.; Kang, J.; Gu, B.; Yu, X.; Zhang, Q.; Wang, Y. Impact of Hydrogenolysis on the Selectivity of the Fischer-Tropsch Synthesis: Diesel Fuel Production over Mesoporous Zeolite-Y-Supported Cobalt Nanoparticles. *Angew. Chem. Int. Ed.* **2015**, *54*(15), 4553–4556. DOI: [10.1002/anie.201411708](https://doi.org/10.1002/anie.201411708).
- [91] Márquez-Alvarez, C.; Žilková, N.; Pérez-Pariente, J.; Čejka, J. Synthesis, Characterization and Catalytic Applications of Organized Mesoporous Aluminas. *Catal. Rev.* **2008**, *50*(2), 222–286. DOI: [10.1080/01614940701804042](https://doi.org/10.1080/01614940701804042).
- [92] Rytter, E.; Holmen, A. Perspectives on the Effect of Water in Cobalt Fischer-Tropsch Synthesis. *ACS Catal.* **2017**, *7*(8), 5321–5328. DOI: [10.1021/acscatal.7b01525](https://doi.org/10.1021/acscatal.7b01525).
- [93] Ma, W.; Jacobs, G.; Sparks, D. E.; Spicer, R. L.; Davis, B. H.; Klettlinger, J. L. S.; Yen, C. H. Fischer-Tropsch synthesis: Kinetics and Water Effect Study over 25%Co/Al₂O₃ Catalysts. *Catal. Today.* **2014**, *228*, 158–166. DOI: [10.1016/j.cattod.2013.10.014](https://doi.org/10.1016/j.cattod.2013.10.014).
- [94] Sirijaruphan, A.; Horváth, A.; Goodwin, J. G.; Oukaci, R. Cobalt Aluminate Formation in Alumina-Supported Cobalt Catalysts: Effects of Cobalt Reduction State and Water Vapor. *Catal. Lett.* **2003**, *91*(1–2), 89–94. DOI: [10.1023/B:CATL.0000006322.80235.8f](https://doi.org/10.1023/B:CATL.0000006322.80235.8f).
- [95] Rytter, E.; Holmen, A. Consorted Vinylene Mechanism for Cobalt Fischer-Tropsch Synthesis Encompassing Water or Hydroxyl Assisted CO-Activation. *Top. Catal.* **2018**, *61*, 1024–1034. DOI: [10.1007/s11244-018-0932-3](https://doi.org/10.1007/s11244-018-0932-3).
- [96] Mardkhe, M. K.; Huang, B.; Bartholomew, C. H.; Alam, T. M.; Woodfield, B. F. Synthesis and Characterization of Silica Doped Alumina Catalyst Support with Superior Thermal Stability and Unique Pore Properties. *J. Porous Mater.* **2016**, *23*(2), 475–487. DOI: [10.1007/s10934-015-0101-z](https://doi.org/10.1007/s10934-015-0101-z).
- [97] Keyvanloo, K.; Mardkhe, M. K.; Alam, T. M.; Bartholomew, C. H.; Woodfield, B. F.; Hecker, W. C. Supported Iron Fischer-Tropsch Catalyst: Superior Activity and

- Stability Using a Thermally Stable Silica-Doped Alumina Support. *ACS Catal.* **2014**, *4* (4), 1071–1077. DOI: [10.1021/cs401242d](https://doi.org/10.1021/cs401242d).
- [98] Daniell, W.; Schubert, U.; Glöckler, R.; Meyer, A.; Noweck, K.; Knözinger, H. Enhanced Surface Acidity in Mixed Alumina–Silicas: A Low-Temperature FTIR Study. *Appl. Catal. A. Gen.* **2000**, *196*(2), 247–260. DOI: [10.1016/S0926-860X\(99\)00474-3](https://doi.org/10.1016/S0926-860X(99)00474-3).
- [99] Sun, S.; Tsubaki, N.; Fujimoto, K. The Reaction Performances and Characterization of Fischer–Tropsch Synthesis Co/SiO₂ Catalysts Prepared from Mixed Cobalt Salts. *Appl. Catal. A: Gen.* **2000**, *202*(1), 121–131. DOI: [10.1016/S0926-860X\(00\)00455-5](https://doi.org/10.1016/S0926-860X(00)00455-5).
- [100] Zhang, Y.; Liu, Y.; Yang, G.; Sun, S.; Tsubaki, N. Effects of Impregnation Solvent on Co/SiO₂ Catalyst for Fischer–Tropsch Synthesis: A Highly Active and Stable Catalyst with Bimodal Sized Cobalt Particles. *Appl. Catal. A: Gen.* **2007**, *321*(1), 79–85. DOI: [10.1016/j.apcata.2007.01.030](https://doi.org/10.1016/j.apcata.2007.01.030).
- [101] Yan, Z.; Wang, Z.; Bukur, D. B.; Goodman, D. W. Fischer–Tropsch Synthesis on a Model Co/SiO₂ Catalyst. *J. Catal.* **2009**, *268*(2), 196–200. DOI: [10.1016/j.jcat.2009.09.015](https://doi.org/10.1016/j.jcat.2009.09.015).
- [102] Gnanamani, M. K.; Jacobs, G.; Shafer, W. D.; Davis, B. H. Fischer–Tropsch Synthesis: Activity of Metallic Phases of Cobalt Supported on Silica. *Catal. Today.* **2013**, *215*, 13–17. DOI: [10.1016/j.cattod.2013.03.004](https://doi.org/10.1016/j.cattod.2013.03.004).
- [103] de la Osa, A. R.; de Lucas, A.; Sánchez-Silva, L.; Díaz-Maroto, J.; Valverde, J. L.; Sánchez, P. Performing the Best Composition of Supported Co/SiC Catalyst for Selective FTS Diesel Production. *Fuel.* **2012**, *95*, 587–598. DOI: [10.1016/j.fuel.2011.11.002](https://doi.org/10.1016/j.fuel.2011.11.002).
- [104] Han, F.; Zhang, Z.; Niu, N.; Li, J. Preparation and Characterization of SiO₂/Co and C/Co Nanocomposites as Fisher–Tropsch Catalysts for CO₂ Hydrogenation. *Chem. Res. Chinese Universities.* **2018**, *34*(4), 635–642. DOI: [10.1007/s40242-018-7381-1](https://doi.org/10.1007/s40242-018-7381-1).
- [105] Kababji, A. H.; Joseph, B.; Wolan, J. T. Silica-Supported Cobalt Catalysts for Fischer–Tropsch Synthesis: Effects of Calcination Temperature and Support Surface Area on Cobalt Silicate Formation. *Catal. Lett.* **2009**, *130*(1), 72–78. DOI: [10.1007/s10562-009-9903-4](https://doi.org/10.1007/s10562-009-9903-4).
- [106] Fu, T.; Huang, C.; Lv, J.; Li, Z. Fischer–Tropsch Performance of an SiO₂-Supported Co-Based Catalyst Prepared by Hydrogen Dielectric-Barrier Discharge Plasma. *Plasma Sci. Technol.* **2014**, *16*(3), 232–238. DOI: [10.1088/1009-0630/16/3/11](https://doi.org/10.1088/1009-0630/16/3/11).
- [107] Wolf, M.; Gibson, E. K.; Olivier, E. J.; Neethling, J. H.; Catlow, C. R. A.; Fischer, N.; Claeys, M. In-Depth Characterisation of Metal-Support Compounds in Spent Co/SiO₂ Fischer–Tropsch Model Catalysts. *Catal. Today.* **2019**. DOI: [10.1016/j.cattod.2019.01.065](https://doi.org/10.1016/j.cattod.2019.01.065).
- [108] van Deelen, T. W.; Nijhuis, J. J.; Krans, N. A.; Zečević, J.; de Jong, K. P. Preparation of Cobalt Nanocrystals Supported on Metal Oxides To Study Particle Growth in Fischer–Tropsch Catalysts. *ACS Catal.* **2018**, *8*(11), 10581–10589. DOI: [10.1021/acscatal.8b03094](https://doi.org/10.1021/acscatal.8b03094).
- [109] Jongsomjit, B.; Wongsalee, T.; Praserttham, P. Catalytic Behaviors of Mixed TiO₂-SiO₂-Supported Cobalt Fischer–Tropsch Catalysts for Carbon Monoxide Hydrogenation. *Mater. Chem. Phys.* **2006**, *97*(2), 343–350. DOI: [10.1016/j.matchemphys.2005.08.016](https://doi.org/10.1016/j.matchemphys.2005.08.016).
- [110] Shi, L.; Li, D.; Hou, B.; Wang, Y.; Sun, Y. The Modification of SiO₂ by Various Organic Groups and its Influence on the Properties of Cobalt-Based Catalysts for Fischer–Tropsch Synthesis. *Fuel Process. Technol.* **2010**, *91*(4), 394–398. DOI: [10.1016/j.fuproc.2009.06.003](https://doi.org/10.1016/j.fuproc.2009.06.003).
- [111] Jiang, Z.-S.; Zhao, Y.-H.; Huang, C.-F.; Song, Y.-H.; Li, D.-P.; Liu, Z.-T.; Liu, Z.-W. Metal-Support Interactions Regulated via Carbon Coating – A Case Study of Co/SiO₂ for Fischer–Tropsch Synthesis. *Fuel.* **2018**, *226*, 213–220. DOI: [10.1016/j.fuel.2018.03.195](https://doi.org/10.1016/j.fuel.2018.03.195).
- [112] Wang, Y.; Jiang, Y.; Huang, J.; Liang, J.; Wang, H.; Li, Z.; Wu, J.; Li, M.; Zhao, Y.; Niu, J. Effect of Hierarchical Crystal Structures on the Properties of Cobalt Catalysts for Fischer–Tropsch Synthesis. *Fuel.* **2016**, *174*, 17–24. DOI: [10.1016/j.fuel.2016.01.045](https://doi.org/10.1016/j.fuel.2016.01.045).

- [113] Li, H.; Hou, B.; Wang, J.; Qin, C.; Zhong, M.; Huang, X.; Jia, L.; Li, D. Direct Conversion of Syngas to Isoparaffins over Hierarchical Beta Zeolite Supported Cobalt Catalyst for Fischer-Tropsch Synthesis. *Mol. Catal.* **2018**, *459*, 106–112. DOI: [10.1016/j.mcat.2018.08.002](https://doi.org/10.1016/j.mcat.2018.08.002).
- [114] Xie, R.; Wang, H.; Gao, P.; Xia, L.; Zhang, Z.; Zhao, T.; Sun, Y. Core@Shell Co_3O_4 @C-m- SiO_2 Catalysts with Inert C Modified Mesoporous Channel for Desired Middle Distillate. *Appl. Catal. A: Gen.* **2015**, *492*, 93–99. DOI: [10.1016/j.apcata.2014.12.023](https://doi.org/10.1016/j.apcata.2014.12.023).
- [115] Savost'yanov, A. P.; Yakovenko, R. E.; Sulima, S. I.; Bakun, V. G.; Narochnyi, G. B.; Chernyshev, V. M.; Mitchenko, S. A. The Impact of Al_2O_3 Promoter on an Efficiency of C_{5+} Hydrocarbons Formation over Co/SiO_2 Catalysts via Fischer-Tropsch Synthesis. *Catal. Today.* **2017**, *279*, 107–114. DOI: [10.1016/j.cattod.2016.02.037](https://doi.org/10.1016/j.cattod.2016.02.037).
- [116] Zhang, Y.; Koike, M.; Tsubaki, N. Preparation of Alumina-Silica Bimodal Pore Catalysts for Fischer-Tropsch Synthesis. *Catal. Lett.* **2005**, *99*(3), 193–198. DOI: [10.1007/s10562-005-2118-4](https://doi.org/10.1007/s10562-005-2118-4).
- [117] Zhang, Y.; Nagamori, S.; Hinchiranan, S.; Vitidsant, T.; Tsubaki, N. Promotional Effects of Al_2O_3 Addition to Co/SiO_2 Catalysts for Fischer-Tropsch Synthesis. *Energy. Fuels.* **2006**, *20*(2), 417–421. DOI: [10.1021/ef050218c](https://doi.org/10.1021/ef050218c).
- [118] Hinchiranan, S.; Zhang, Y.; Nagamori, S.; Vitidsant, T.; Tsubaki, N. TiO_2 Promoted Co/SiO_2 Catalysts for Fischer-Tropsch Synthesis. *Fuel Process. Technol.* **2008**, *89*(4), 455–459. DOI: [10.1016/j.fuproc.2007.11.007](https://doi.org/10.1016/j.fuproc.2007.11.007).
- [119] Wu, H.; Yang, Y.; Suo, H.; Qing, M.; Yan, L.; Wu, B.; Xu, J.; Xiang, H.; Li, Y. Effect of TiO_2 promotion on the structure and performance of silica-supported cobalt-based catalysts for Fischer-Tropsch synthesis. *J. Mol. Catal. A Chem.* **2014**, *390*, 52–62. DOI: [10.1016/j.molcata.2014.03.004](https://doi.org/10.1016/j.molcata.2014.03.004).
- [120] Cheng, K.; Subramanian, V.; Carvalho, A.; Ordonsky, V. V.; Wang, Y.; Khodakov, A. Y. The Role of Carbon Pre-Coating for the Synthesis of highly efficient Cobalt Catalysts for Fischer-Tropsch Synthesis. *J. Catal.* **2016**, *337*, 260–271. DOI: [10.1016/j.jcat.2016.02.019](https://doi.org/10.1016/j.jcat.2016.02.019).
- [121] Girardon, J. S.; Quinet, E.; Griboval-Constant, A.; Chernavskii, P. A.; Gengembre, L.; Khodakov, A. Y. Cobalt dispersion, reducibility, and surface sites in Promoted Silica-Supported Fischer-Tropsch Catalysts. *J. Catal.* **2007**, *248*(2), 143–157. DOI: [10.1016/j.jcat.2007.03.002](https://doi.org/10.1016/j.jcat.2007.03.002).
- [122] Fischer, N.; van Steen, E.; Claeys, M. Structure Sensitivity of the Fischer-Tropsch Activity and Selectivity on Alumina Supported Cobalt Catalysts. *J. Catal.* **2013**, *299*, 67–80. DOI: [10.1016/j.jcat.2012.11.013](https://doi.org/10.1016/j.jcat.2012.11.013).
- [123] Pei, Y.; Ding, Y.; Zhu, H.; Zang, J.; Song, X.; Dong, W.; Wang, T.; Lu, Y. Effect of Al_2O_3 Promoter on a Performance of C_1 – C_{14} α -Alcohols Direct Synthesis over Co/AC Catalysts via Fischer-Tropsch Synthesis. *Catal. Lett.* **2014**, *144*(8), 1433–1442. DOI: [10.1007/s10562-014-1283-8](https://doi.org/10.1007/s10562-014-1283-8).
- [124] Bagheri, S.; Muhd Julkapli, N.; Bee Abd Hamid, S. Titanium Dioxide as a Catalyst Support in Heterogeneous Catalysis. *Sci. World. J.* **2014**, *2014*. DOI: [10.1155/2014/727496](https://doi.org/10.1155/2014/727496).
- [125] Jacobs, G.; Das, T. K.; Zhang, Y.; Li, J.; Racoillet, G.; Davis, B. H. Fischer-Tropsch Synthesis: Support, Loading, and Promoter Effects on the Reducibility of Cobalt Catalysts. *Appl. Catal. A: Gen.* **2002**, *233*(1), 263–281. DOI: [10.1016/S0926-860X\(02\)00195-3](https://doi.org/10.1016/S0926-860X(02)00195-3).
- [126] Shimura, K.; Miyazawa, T.; Hanaoka, T.; Hirata, S. Fischer-Tropsch synthesis over TiO_2 Supported Cobalt Catalyst: Effect of TiO_2 Crystal Phase and Metal Ion Loading. *Appl. Catal. A: Gen.* **2013**, *460*–*461*, 8–14. DOI: [10.1016/j.apcata.2013.04.023](https://doi.org/10.1016/j.apcata.2013.04.023).
- [127] Xaba, B. M.; de Villiers, J. P. R. Sintering Behavior of TiO_2 -Supported Model Cobalt Fischer-Tropsch Catalysts under H_2 Reducing Conditions and Elevated Temperature. *Ind. Eng. Chem. Res.* **2016**, *55*(35), 9397–9407. DOI: [10.1021/acs.iecr.6b02311](https://doi.org/10.1021/acs.iecr.6b02311).

- [128] Eschemann, T. O.; de Jong, K. P. Deactivation Behavior of Co/TiO₂ Catalysts during Fischer–Tropsch Synthesis. *ACS Catal.* **2015**, *5*(6), 3181–3188. DOI: [10.1021/acscatal.5b00268](https://doi.org/10.1021/acscatal.5b00268).
- [129] Khosravi-Nikou, M.; Bahrami, A. A New Method for Synthesis of Cobalt-Based Nano-catalyst on Titania for Fischer-Tropsch Reaction. *Energy Sourc. A: Recovery Util. Environ. Effects.* **2015**, *37*(19), 2041–2046. DOI: [10.1080/15567036.2011.604372](https://doi.org/10.1080/15567036.2011.604372).
- [130] Li, J.; Wang, T.; Wu, L.; Li, X. Comparison of Titania Nanotube-Supported Cobalt Catalysts Prepared by Impregnation and Homogeneous Precipitation for Fischer–Tropsch Synthesis. *RSC Adv.* **2016**, *6*(92), 89770–89775. DOI: [10.1039/c6ra17130c](https://doi.org/10.1039/c6ra17130c).
- [131] Jalama, K.; Kabuba, J.; Xiong, H.; Jewell, L. L. Co/TiO₂ Fischer–Tropsch Catalyst Activation by Synthesis Gas. *Catal. Commun.* **2012**, *17*, 154–159. DOI: [10.1016/j.catcom.2011.10.029](https://doi.org/10.1016/j.catcom.2011.10.029).
- [132] Yu, S.; Ma, Y.; Zhi, Y.; Jing, H.; Su, H.-Q. Synthesis of Cobalt–Based Catalyst Supported on TiO₂ Nanotubes and its Fischer–Tropsch Reaction. *Integr. Ferroelectr.* **2013**, *147*(1), 59–66. DOI: [10.1080/10584587.2013.790737](https://doi.org/10.1080/10584587.2013.790737).
- [133] Delgado, J. A.; Claver, C.; Castellón, S.; Curulla-Ferré, D.; Ordonsky, V. V.; Godard, C. Fischer–Tropsch Synthesis Catalysed by Small TiO₂ Supported Cobalt Nanoparticles Prepared by Sodium Borohydride Reduction. *Appl. Catal. A: Gen.* **2016**, *513*, 39–46. DOI: [10.1016/j.apcata.2015.12.019](https://doi.org/10.1016/j.apcata.2015.12.019).
- [134] Mehrbod, M.; Martinelli, M.; Martino, A. G.; Cronauer, D. C.; Jeremy Kropf, A.; Marshall, C. L.; Jacobs, G. Fischer-Tropsch Synthesis: Direct Cobalt Nitrate Reduction of Promoted Co/TiO₂ Catalysts. *Fuel.* **2019**, *245*, 488–504. DOI: [10.1016/j.fuel.2019.02.083](https://doi.org/10.1016/j.fuel.2019.02.083).
- [135] Eschemann, T. O.; Oenema, J.; de Jong, K. P. Effects of Noble Metal Promotion for Co/TiO₂ Fischer–Tropsch Catalysts. *Catal. Today.* **2016**, *261*, 60–66. DOI: [10.1016/j.cattod.2015.06.016](https://doi.org/10.1016/j.cattod.2015.06.016).
- [136] Sachtler, W. M. H.; Zhang, Z. *Zeolite-Supported Transition Metal Catalysts*. In *Advances in Catalysis*; Eley, D. D., Pines, H., Weisz, P. B., Eds.; Academic Press, San Diego, United States, **1993**; pp 129–220.
- [137] Bessell, S. Investigation of Bifunctional Zeolite Supported Cobalt Fischer-Tropsch Catalysts. *Appl. Catal. A: Gen.* **1995**, *126*(2), 235–244. DOI: [10.1016/0926-860X\(95\)00040-2](https://doi.org/10.1016/0926-860X(95)00040-2).
- [138] Subramanian, V.; Zholobenko, V. L.; Cheng, K.; Lancelot, C.; Heyte, S.; Thuriot, J.; Paul, S.; Ordonsky, V. V.; Khodakov, A. Y. The Role of Steric Effects and Acidity in the Direct Synthesis of iso-Paraffins from Syngas on Cobalt Zeolite Catalysts. *ChemCatChem.* **2016**, *8*(2), 380–389. DOI: [10.1002/cctc.201500777](https://doi.org/10.1002/cctc.201500777).
- [139] Chalupka, K. A.; Casale, S.; Zurawicz, E.; Rynkowski, J.; Dzwigaj, S. The Remarkable Effect of the Preparation Procedure on the Catalytic Activity of CoBEA Zeolites in the Fischer–Tropsch Synthesis. *Micropor. Mesopor. Mater.* **2015**, *211*, 9–18. DOI: [10.1016/j.micromeso.2015.02.024](https://doi.org/10.1016/j.micromeso.2015.02.024).
- [140] Pereira, A. L. C.; González-Carballo, J. M.; Pérez-Alonso, F. J.; Rojas, S.; Fierro, J. L. G.; Rangel, M. D. C. Effect of the Mesos structuration of the Beta Zeolite Support on the Properties of Cobalt Catalysts for Fischer–Tropsch Synthesis. *Top. Catal.* **2011**, *54*(1), 179–189. DOI: [10.1007/s11244-011-9637-6](https://doi.org/10.1007/s11244-011-9637-6).
- [141] Carvalho, A.; Marinova, M.; Batalha, N.; Marcilio, N. R.; Khodakov, A. Y.; Ordonsky, V. V. Design of Nanocomposites with Cobalt Encapsulated in the Zeolite Micropores for Selective Synthesis of Isoparaffins in Fischer–Tropsch Reaction. *Catal. Sci. Technol.* **2017**, *7*(21), 5019–5027. DOI: [10.1039/c7cy01945a](https://doi.org/10.1039/c7cy01945a).
- [142] Xing, C.; Shen, W.; Yang, G.; Yang, R.; Lu, P.; Sun, J.; Yoneyama, Y.; Tsubaki, N. Completed Encapsulation of Cobalt Particles in Mesoporous H-ZSM-5 Zeolite Catalyst

- for Direct Synthesis of Middle Isoparaffin from Syngas. *Catal. Commun.* **2014**, *55*, 53–56. DOI: [10.1016/j.catcom.2014.06.018](https://doi.org/10.1016/j.catcom.2014.06.018).
- [143] Wang, Y.; Cao, X.; Jiang, Y.; Zhang, H.; Liang, J.; Wang, H.; Li, Z.; Wu, J. The Influence of Alkali Treatment for Synthesizing Hierarchical Zeolite on Behavior of Cobalt Fischer–Tropsch Synthesis Catalysts. *Catal. Surv. Asia.* **2017**, *21*(1), 28–36. DOI: [10.1007/s10563-016-9223-9](https://doi.org/10.1007/s10563-016-9223-9).
- [144] Cheng, S.; Mazonde, B.; Zhang, G.; Javed, M.; Dai, P.; Cao, Y.; Tu, S.; Wu, J.; Lu, C.; Xing, C.; et al. Co-Based MOR/ZSM-5 Composite Zeolites over a Solvent-Free Synthesis Strategy for Improving Gasoline Selectivity. *Fuel.* **2018**, *223*, 354–359. DOI: [10.1016/j.fuel.2018.03.042](https://doi.org/10.1016/j.fuel.2018.03.042).
- [145] Li, Y.; Wang, T.; Wu, C.; Lv, Y.; Tsubaki, N. Gasoline-Range Hydrocarbon Synthesis over Cobalt-Based Fischer–Tropsch Catalysts Supported on SiO₂/HZSM-5. *Energy Fuels.* **2008**, *22*(3), 1897–1901. DOI: [10.1021/ef700625z](https://doi.org/10.1021/ef700625z).
- [146] Flores, C.; Batalha, N.; Marcilio, N. R.; Ordonsky, V. V.; Khodakov, A. Y. Influence of Impregnation and Ion Exchange Sequence on Metal Localization, Acidity and Catalytic Performance of Cobalt BEA Zeolite Catalysts in Fischer-Tropsch Synthesis. *ChemCatChem.* **2019**, *11*(1), 568–574. DOI: [10.1002/cctc.201800728](https://doi.org/10.1002/cctc.201800728).
- [147] Wu, L.; Li, Z.; Han, D.; Wu, J.; Zhang, D. A Preliminary Evaluation of ZSM-5/SBA-15 Composite Supported Co Catalysts for Fischer–Tropsch Synthesis. *Fuel Process. Technol.* **2015**, *134*, 449–455. DOI: [10.1016/j.fuproc.2015.02.025](https://doi.org/10.1016/j.fuproc.2015.02.025).
- [148] Botes, F. G.; Böhringer, W. The addition of HZSM-5 to the Fischer–Tropsch Process for Improved Gasoline Production. *Appl. Catal. A.* **2004**, *267*(1–2), 217–225. DOI: [10.1016/j.apcata.2004.03.006](https://doi.org/10.1016/j.apcata.2004.03.006).
- [149] Sadek, R.; Chalupka, K. A.; Mierczynski, P.; Rynkowski, J.; Gurgul, J.; Dzwigaj, S. Cobalt Based Catalysts Supported on Two Kinds of Beta Zeolite for Application in Fischer-Tropsch Synthesis. *Catalysts.* **2019**, *9*, 497–519. DOI: [10.3390/catal9060497](https://doi.org/10.3390/catal9060497).
- [150] He, J.; Liu, Z.; Yoneyama, Y.; Nishiyama, N.; Tsubaki, N. Multiple-Functional Capsule Catalysts: A Tailor-Made Confined Reaction Environment for the Direct Synthesis of Middle Isoparaffins from Syngas. *Chem. Eur. J.* **2006**, *12*(32), 8296–8304. DOI: [10.1002/chem.200501295](https://doi.org/10.1002/chem.200501295).
- [151] Lam, E.; Luong, J. H. T. Carbon Materials as Catalyst Supports and Catalysts in the Transformation of Biomass to Fuels and Chemicals. *ACS Catal.* **2014**, *4*(10), 3393–3410. DOI: [10.1021/cs5008393](https://doi.org/10.1021/cs5008393).
- [152] Samandari-Masouleh, L.; Mostoufi, N.; Khodadadi, A. A.; Mortazavi, Y.; Maghrebi, M. Kinetic Modeling of Carbon Nanotube Production and Minimization of Amorphous Carbon Overlayer Deposition in Floating Catalyst Method. *Int. J. Chem. Reactor Eng.* **2012**, *10*(1), 1–23. DOI: [10.1515/1542-6580.2972](https://doi.org/10.1515/1542-6580.2972).
- [153] Samandari-Masouleh, L.; Mostoufi, N.; Khodadadi, A. A.; Mortazavi, Y.; Maghrebi, M. Modeling the Growth of Carbon Nanotubes in a Floating Catalyst Reactor. *Ind. Eng. Chem. Res.* **2012**, *51*(3), 1143–1149. DOI: [10.1021/ie201137j](https://doi.org/10.1021/ie201137j).
- [154] Sharma, S.; Pollet, B. G. Support materials for PEMFC and DMFC electrocatalysts—A review. *J. Power Sources.* **2012**, *208*, 96–119. DOI: [10.1016/j.jpowsour.2012.02.011](https://doi.org/10.1016/j.jpowsour.2012.02.011).
- [155] Cheng, Q.; Zhao, N.; Lyu, S.; Tian, Y.; Gao, F.; Dong, L.; Jiang, Z.; Zhang, J.; Tsubaki, N.; Li, X. Tuning Interaction between Cobalt Catalysts and Nitrogen Dopants in Carbon Nanospheres to Promote Fischer-Tropsch Synthesis. *Appl. Catal., B: Environ.* **2019**, *248*, 73–83. DOI: [10.1016/j.apcatb.2019.02.024](https://doi.org/10.1016/j.apcatb.2019.02.024).
- [156] Zarubova, S.; Rane, S.; Yang, J.; Yu, Y.; Zhu, Y.; Chen, D.; Holmen, A. Fischer–Tropsch Synthesis on Hierarchically Structured Cobalt Nanoparticle/Carbon Nanofiber/Carbon Felt Composites. *ChemSusChem.* **2011**, *4*(7), 935–942. DOI: [10.1002/cssc.201100046](https://doi.org/10.1002/cssc.201100046).
- [157] Pei, Y.; Ding, Y.; Zhu, H.; Du, H. One-Step Production of C1–C18 Alcohols via Fischer-Tropsch Reaction over Activated Carbon-Supported Cobalt Catalysts: Promotional Effect of

- Modification by SiO₂. *Chin. J. Catal.* **2015**, *36*(3), 355–361. DOI: [10.1016/S1872-2067\(14\)60252-7](https://doi.org/10.1016/S1872-2067(14)60252-7).
- [158] Lahti, R.; Bergna, D.; Romar, H.; Hu, T.; Comazzi, A.; Pirola, C.; Bianchi, C. L.; Lassi, U. Characterization of Cobalt Catalysts on Biomass-Derived Carbon Supports. *Top. Catal.* **2017**, *60*(17), 1415–1428. DOI: [10.1007/s11244-017-0823-z](https://doi.org/10.1007/s11244-017-0823-z).
- [159] Hatami, B.; Tavasoli, A.; Asghari, A.; Zamani, Y.; Zamaniyan, A. Kinetics Modeling of Fischer–Tropsch Synthesis on the Cobalt Catalyst Supported on Functionalized Carbon Nanotubes. *Kinet. Catal.* **2018**, *59*(6), 701–709. DOI: [10.1134/s0023158418060046](https://doi.org/10.1134/s0023158418060046).
- [160] Dlamini, M. W.; Phaahlamohlaka, T. N.; Kumi, D. O.; Forbes, R.; Jewell, L. L.; Coville, N. J. Post Doped Nitrogen-Decorated Hollow Carbon Spheres as a Support for Co Fischer–Tropsch Catalysts. *Catal. Today.* **2020**, *342*, 99–110. DOI: [10.1016/j.cattod.2019.01.070](https://doi.org/10.1016/j.cattod.2019.01.070).
- [161] Taghavi, S.; Tavasoli, A.; Asghari, A.; Signoretto, M. Loading and Promoter Effects on the Performance of Nitrogen Functionalized Graphene Nanosheets Supported Cobalt Fischer–Tropsch Synthesis Catalysts. *Int. J. Hydrogen Energy.* **2019**, *44*(21), 10604–10615. DOI: [10.1016/j.ijhydene.2019.03.015](https://doi.org/10.1016/j.ijhydene.2019.03.015).
- [162] Almkhelfe, H.; Li, X.; Thapa, P.; Hohn, K. L.; Amama, P. B. Carbon Nanotube-Supported Catalysts Prepared by a Modified Photo-Fenton Process for Fischer–Tropsch Synthesis. *J. Catal.* **2018**, *361*, 278–289. DOI: [10.1016/j.jcat.2018.02.009](https://doi.org/10.1016/j.jcat.2018.02.009).
- [163] Kuang, T.; Lyu, S.; Liu, S.; Zhang, Y.; Li, J.; Wang, G.; Wang, L. Controlled Synthesis of Cobalt Nanocrystals on the Carbon Spheres for Enhancing Fischer–Tropsch Synthesis Performance. *J. Energy Chem.* **2019**, *33*, 67–73. DOI: [10.1016/j.jechem.2018.08.012](https://doi.org/10.1016/j.jechem.2018.08.012).
- [164] Zhao, Z.; Lu, W.; Feng, C.; Chen, X.; Zhu, H.; Yang, R.; Dong, W.; Zhao, M.; Lyu, Y.; Liu, T.; et al. Increasing the Activity and Selectivity of Co-Based FTS Catalysts Supported by Carbon Materials for Direct Synthesis of Clean Fuels by the Addition of Chromium. *J. Catal.* **2019**, *370*, 251–264. DOI: [10.1016/j.jcat.2018.12.022](https://doi.org/10.1016/j.jcat.2018.12.022).
- [165] Nakhaei Pour, A.; Housaindokht, M. R.; Kamali Shahri, S. M. Fischer–Tropsch Synthesis over Cobalt/CNTs Catalysts: Functionalized Support and Catalyst Preparation Effect on Activity and Kinetic Parameters. *Ind. Eng. Chem. Res.* **2018**, *57*(41), 13639–13649. DOI: [10.1021/acs.iecr.8b02485](https://doi.org/10.1021/acs.iecr.8b02485).
- [166] Nakhaei Pour, A.; Karimi, J.; Taghipoor, S.; Gholizadeh, M.; Hashemian, M. Fischer–Tropsch Synthesis over CNT-Supported Cobalt Catalyst: Effect of Magnetic Field. *J. Iran. Chem. Soc.* **2017**, *14*(7), 1477–1488. DOI: [10.1007/s13738-017-1088-y](https://doi.org/10.1007/s13738-017-1088-y).
- [167] Chernyak, S. A.; Selyaev, G. E.; Suslova, E. V.; Egorov, A. V.; Maslakov, K. I.; Kharlanov, A. N.; Savilov, S. V.; Lunin, V. V. Effect of Cobalt Weight Content on the Structure and Catalytic Properties of Co/CNT Catalysts in the Fischer–Tropsch Synthesis. *Kinet. Catal.* **2016**, *57*(5), 640–646. DOI: [10.1134/s0023158416050062](https://doi.org/10.1134/s0023158416050062).
- [168] Ma, W.-P.; Ding, Y.-J.; Lin, L.-W. Fischer–Tropsch Synthesis over Activated-Carbon-Supported Cobalt Catalysts: Effect of Co Loading and Promoters on Catalyst Performance. *Ind. Eng. Chem. Res.* **2004**, *43*(10), 2391–2398. DOI: [10.1021/ie034116q](https://doi.org/10.1021/ie034116q).
- [169] Trépanier, M.; Tavasoli, A.; Dalai, A. K.; Abatzoglou, N. Co, Ru and K Loadings Effects on the Activity and Selectivity of Carbon Nanotubes Supported Cobalt Catalyst in Fischer–Tropsch Synthesis. *Appl. Catal. A. Gen.* **2009**, *353*(2), 193–202. DOI: [10.1016/j.apcata.2008.10.061](https://doi.org/10.1016/j.apcata.2008.10.061).
- [170] Tavasoli, A.; Abbaslou, R. M. M.; Trepanier, M.; Dalai, A. K. Fischer–Tropsch Synthesis over Cobalt Catalyst Supported on Carbon Nanotubes in a Slurry Reactor. *Appl. Catal. A. Gen.* **2008**, *345*(2), 134–142. DOI: [10.1016/j.apcata.2008.04.030](https://doi.org/10.1016/j.apcata.2008.04.030).
- [171] Lv, J.; Ma, X.; Bai, S.; Huang, C.; Li, Z.; Gong, J. Hydrogenation of Carbon Monoxide over Cobalt Nanoparticles Supported on Carbon Nanotubes. *Int. J. Hydrogen Energy.* **2011**, *36*(14), 8365–8372. DOI: [10.1016/j.ijhydene.2011.04.122](https://doi.org/10.1016/j.ijhydene.2011.04.122).

- [172] Yu, Z.; Borg, Ø.; Chen, D.; Enger, B. C.; Frøseth, V.; Rytter, E.; Wigum, H.; Holmen, A. Carbon Nanofiber Supported Cobalt Catalysts for Fischer–Tropsch Synthesis with High Activity and Selectivity. *Catal. Lett.* **2006**, *109*(1), 43–47. DOI: [10.1007/s10562-006-0054-6](https://doi.org/10.1007/s10562-006-0054-6).
- [173] Lyu, S.; Peng, B.; Kuang, T.; Rappé, K. G.; Zhang, Y.; Li, J.; Wang, L. Supported Cobalt Nanoparticles with a Single Active Phase for Fischer–Tropsch Synthesis. *ACS Appl. Nano Mater.* **2019**, *2*(4), 2266–2272. DOI: [10.1021/acsanm.9b00187](https://doi.org/10.1021/acsanm.9b00187).
- [174] Fu, T.; Jiang, Y.; Lv, J.; Li, Z. Effect of Carbon Support on Fischer–Tropsch Synthesis Activity and Product Distribution over Co-Based Catalysts. *Fuel Process. Technol.* **2013**, *110*, 141–149. DOI: [10.1016/j.fuproc.2012.12.006](https://doi.org/10.1016/j.fuproc.2012.12.006).
- [175] Xiong, J.; Ding, Y.; Wang, T.; Yan, L.; Chen, W.; Zhu, H.; Lu, Y. The Formation of CO₂ C Species in Activated Carbon Supported Cobalt-Based Catalysts and its Impact on Fischer–Tropsch Reaction. *Catal. Lett.* **2005**, *102*(3), 265–269. DOI: [10.1007/s10562-005-5867-1](https://doi.org/10.1007/s10562-005-5867-1).
- [176] Zaman, M.; Khodadi, A.; Mortazavi, Y. Fischer–Tropsch Synthesis over Cobalt Dispersed on Carbon Nanotubes-Based Supports and Activated Carbon. *Fuel Process. Technol.* **2009**, *90*(10), 1214–1219. DOI: [10.1016/j.fuproc.2009.05.026](https://doi.org/10.1016/j.fuproc.2009.05.026).
- [177] Bezemer, G. L.; van Laak, A.; van Dillen, A. J.; de Jong, K. P. Cobalt Supported on Carbon Nanofibers- A Promising Novel Fischer-Tropsch Catalyst. *Stud. Surf. Sci. Catal.* **2004**, *147*, 259–264. DOI: [10.1016/S0167-2991\(04\)80061-2](https://doi.org/10.1016/S0167-2991(04)80061-2).
- [178] Xiong, H.; Motchelaho, M. A. M.; Moyo, M.; Jewell, L. L.; Coville, N. J. Correlating the Preparation and Performance of Cobalt Catalysts Supported on Carbon Nanotubes and Carbon Spheres in the Fischer–Tropsch Synthesis. *J. Catal.* **2011**, *278*(1), 26–40. DOI: [10.1016/j.jcat.2010.11.010](https://doi.org/10.1016/j.jcat.2010.11.010).
- [179] Motchelaho, M. A. M.; Xiong, H.; Moyo, M.; Jewell, L. L.; Coville, N. J. Effect of Acid Treatment on the Surface of Multiwalled Carbon Nanotubes Prepared from Fe–Co Supported on CaCO₃: Correlation with Fischer–Tropsch Catalyst Activity. *J. Mol. Catal. A Chem.* **2011**, *335*(1), 189–198. DOI: [10.1016/j.molcata.2010.11.033](https://doi.org/10.1016/j.molcata.2010.11.033).
- [180] Karousis, N.; Tagmatarchis, N.; Tasis, D. Current Progress on the Chemical Modification of Carbon Nanotubes. *Chem. Rev.* **2010**, *110*(9), 5366–5397. DOI: [10.1021/cr100018g](https://doi.org/10.1021/cr100018g).
- [181] Munnik, P.; de Jongh, P. E.; de Jong, K. P. Recent Developments in the Synthesis of Supported Catalysts. *Chem. Rev.* **2015**, *115*(14), 6687–6718. DOI: [10.1021/cr500486u](https://doi.org/10.1021/cr500486u).
- [182] Zaera, F. Nanostructured Materials for Applications in Heterogeneous Catalysis. *Chem. Soc. Rev.* **2013**, *42*(7), 2746–2762. DOI: [10.1039/C2CS35261C](https://doi.org/10.1039/C2CS35261C).
- [183] Soleymanabadi, H.; Kakemam, J. A DFT Study of H₂ Adsorption on Functionalized Carbon Nanotubes. *Phys. E: Low-dimensional Syst. Nanostruct.* **2013**, *54*, 115–117. DOI: [10.1016/j.physe.2013.06.015](https://doi.org/10.1016/j.physe.2013.06.015).
- [184] Nakhaei Pour, A.; Keyvanloo, Z.; Izadyar, M.; Modaresi, S. M. Dissociative Hydrogen Adsorption on the Cubic Cobalt Surfaces: A DFT Study. *Int. J. Hydrogen Energy.* **2015**, *40*(22), 7064–7071. DOI: [10.1016/j.ijhydene.2015.04.028](https://doi.org/10.1016/j.ijhydene.2015.04.028).
- [185] Phaahlamohlaka, T. N.; Kumi, D. O.; Dlamini, M. W.; Jewell, L. L.; Coville, N. J. Ruthenium Nanoparticles Encapsulated inside Porous Hollow Carbon Spheres: A Novel Catalyst for Fischer–Tropsch Synthesis. *Catal. Today.* **2016**, *275*, 76–83. DOI: [10.1016/j.cattod.2015.11.034](https://doi.org/10.1016/j.cattod.2015.11.034).
- [186] Xu, H.; Yin, X.; Li, M.; Ye, F.; Han, M.; Hou, Z.; Li, X.; Zhang, L.; Cheng, L. Mesoporous Carbon Hollow Microspheres with Red Blood Cell Like Morphology for Efficient Microwave Absorption at Elevated Temperature. *Carbon.* **2018**, *132*, 343–351. DOI: [10.1016/j.carbon.2018.02.040](https://doi.org/10.1016/j.carbon.2018.02.040).
- [187] Liu, J.-X.; Wang, P.; Xu, W.; Hensen, E. J. M. Particle Size and Crystal Phase Effects in Fischer-Tropsch Catalysts. *Eng.* **2017**, *3*(4), 467–476. DOI: [10.1016/J.ENG.2017.04.012](https://doi.org/10.1016/J.ENG.2017.04.012).

- [188] Dai, Y.; Zhao, Y.; Lin, T.; Li, S.; Yu, F.; An, Y.; Wang, X.; Xiao, K.; Sun, F.,; Jiang, Z.; et al. Particle Size Effects of Cobalt Carbide for Fischer–Tropsch to Olefins. *ACS Catal.* **2019**, *9*(2), 798–809. DOI: [10.1021/acscatal.8b03631](https://doi.org/10.1021/acscatal.8b03631).
- [189] Yang, Y.; Chiang, K.; Burke, N. Porous Carbon-Supported Catalysts for Energy and Environmental Applications: A Short Review. *Catal. Today.* **2011**, *178*(1), 197–205. DOI: [10.1016/j.cattod.2011.08.028](https://doi.org/10.1016/j.cattod.2011.08.028).
- [190] Qian, W.; Zhang, H.; Ying, W.; Fang, D. The Comprehensive Kinetics of Fischer–Tropsch Synthesis over a Co/AC Catalyst on the Basis of CO Insertion Mechanism. *Chem. Eng. J.* **2013**, *228*, 526–534. DOI: [10.1016/j.cej.2013.05.039](https://doi.org/10.1016/j.cej.2013.05.039).
- [191] Bahadoran, F.; Moradian, A.; Shirazi, L.; Zamani, Y. Fischer–Tropsch Synthesis: Evaluation of Gd and Ru Promoters Effect on Co/ γ -Al₂O₃ Catalyst at Different Conditions. *Chem. Papers.* **2018**, *72*(2), 309–325. DOI: [10.1007/s11696-017-0281-x](https://doi.org/10.1007/s11696-017-0281-x).
- [192] Xu, R.; Hou, C.; Xia, G.; Sun, X.; Li, M.; Nie, H.; Li, D. Effects of Ag Promotion for Co/Al₂O₃ Catalyst in Fischer-Tropsch Synthesis. *Catal. Today.* **2020**, *342*, 111–114. DOI: [10.1016/j.cattod.2019.04.004](https://doi.org/10.1016/j.cattod.2019.04.004).
- [193] Morales, F.; Weckhuysen, B. M. Promotion Effects in Co-based Fischer-Tropsch Catalysis. *Catalysis.* **2006**, *19*(1), 1–40. DOI: [10.1002/chin.200702219](https://doi.org/10.1002/chin.200702219).
- [194] Liu, C.; He, Y.; Wei, L.; Zhao, Y.; Zhang, Y.; Zhao, F.; Lyu, S.; Chen, S.; Hong, J.; Li, J. Effect of TiO₂ Surface Engineering on the Performance of Cobalt-Based Catalysts for Fischer–Tropsch Synthesis. *Ind. Eng. Chem. Res.* **2018**, *58*(2), 1095–1104. DOI: [10.1021/acs.iecr.8b05069](https://doi.org/10.1021/acs.iecr.8b05069).
- [195] Munnik, P.; Krans, N. A.; de Jongh, P. E.; de Jong, K. P. Effects of Drying Conditions on the Synthesis of Co/SiO₂ and Co/Al₂O₃ Fischer–Tropsch Catalysts. *ACS Catal.* **2014**, *4*(9), 3219–3226. DOI: [10.1021/cs5006772](https://doi.org/10.1021/cs5006772).
- [196] Yu, S.-Y.; Huang, W.-L.; Ma, Y.; Cao, Z.; Su, H.-Q. Characterization of Cobalt-Based Catalyst Supported on CeO₂ Nanocubes for Fischer-Tropsch Synthesis. *Integr. Ferroelectr.* **2012**, *138*(1), 32–37. DOI: [10.1080/10584587.2012.688425](https://doi.org/10.1080/10584587.2012.688425).
- [197] Pan, Z.; Parvari, M.; Bukur, D. B. Fischer–Tropsch Synthesis on Co/Al₂O₃ Catalyst: Effect of Pretreatment Procedure. *Top. Catal.* **2014**, *57*(6), 470–478. DOI: [10.1007/s11244-013-0203-2](https://doi.org/10.1007/s11244-013-0203-2).
- [198] Garcilaso, V.; Barrientos, J.; Bobadilla, L.; Laguna, O.; Boutonnet, M.; Centeno, M.; Odriozola, J. Promoting Effect of CeO₂, ZrO₂ and Ce/Zr Mixed Oxides on Co/ γ -Al₂O₃ Catalyst for Fischer-Tropsch Synthesis. *Renew. Energy.* **2019**, *132*, 1141–1150. DOI: [10.1016/j.renene.2018.08.080](https://doi.org/10.1016/j.renene.2018.08.080).
- [199] Nabaho, D.; Niemantsverdriet, J. W.; Claeys, M.; van Steen, E. Hydrogen Spillover in the Fischer–Tropsch Synthesis: An Analysis of Platinum as a Promoter for Cobalt–Alumina Catalysts. *Catal. Today.* **2016**, *261*, 17–27. DOI: [10.1016/j.cattod.2015.08.050](https://doi.org/10.1016/j.cattod.2015.08.050).
- [200] Mandal, S.; Maity, S.; Gupta, P. K.; Mahato, A.; Bhanja, P.; Sahu, G. Synthesis of Middle Distillate Through Low Temperature Fischer-Tropsch (LTFT) Reaction over Mesoporous SDA Supported Cobalt Catalysts using Syngas Equivalent to Coal Gasification. *Appl. Catal. A. Gen.* **2018**, *557*, 55–63. DOI: [10.1016/j.apcata.2018.03.004](https://doi.org/10.1016/j.apcata.2018.03.004).
- [201] Shimura, K.; Miyazawa, T.; Hanaoka, T.; Hirata, S. Fischer–Tropsch Synthesis over Alumina Supported Cobalt Catalyst: Effect of Promoter Addition. *Appl. Catal. A. Gen.* **2015**, *494*, 1–11. DOI: [10.1016/j.apcata.2015.01.017](https://doi.org/10.1016/j.apcata.2015.01.017).
- [202] Hong, J.; Du, J.; Wang, B.; Zhang, Y.; Liu, C.; Xiong, H.; Sun, F.; Chen, S.; Li, J. Plasma-Assisted Preparation of Highly Dispersed Cobalt Catalysts for Enhanced Fischer–Tropsch Synthesis Performance. *ACS Catal.* **2018**, *8*(7), 6177–6185. DOI: [10.1021/acscatal.8b00960](https://doi.org/10.1021/acscatal.8b00960).
- [203] Zhang, H.; Chu, W.; Zou, C.; Huang, Z.; Ye, Z.; Zhu, L. Promotion Effects of Platinum and Ruthenium on Carbon Nanotube Supported Cobalt Catalysts for Fischer–Tropsch Synthesis. *Catal. Lett.* **2011**, *141*(3), 438–444. DOI: [10.1007/s10562-010-0536-4](https://doi.org/10.1007/s10562-010-0536-4).

- [204] Li, J.; Jacobs, G.; Zhang, Y.; Das, T.; Davis, B. H. Fischer–Tropsch Synthesis: Effect of Small Amounts of Boron, Ruthenium and Rhenium on Co/TiO₂ Catalysts. *Appl. Catal. A: Gen.* **2002**, 223(1), 195–203. DOI: [10.1016/S0926-860X\(01\)00752-9](https://doi.org/10.1016/S0926-860X(01)00752-9).
- [205] Martinelli, M.; Mehrbod, M.; Dawson, C.; Davis, B. H.; Lietti, L.; Cronauer, D. C.; Kropf, A. J.; Marshall, C. L.; Jacobs, G. Fischer-Tropsch Synthesis: Foregoing Calcination and Utilizing Reduction Promoters Leads to Improved Conversion and Selectivity with Co/Silica. *Appl. Catal. A. Gen.* **2018**, 559, 153–166. DOI: [10.1016/j.apcata.2018.04.013](https://doi.org/10.1016/j.apcata.2018.04.013).
- [206] Chu, W.; Chernavskii, P. A.; Gengembre, L.; Pankina, G. A.; Fongarland, P.; Khodakov, A. Y. Cobalt Species in Promoted Cobalt Alumina-Supported Fischer–Tropsch Catalysts. *J. Catal.* **2007**, 252(2), 215–230. DOI: [10.1016/j.jcat.2007.09.018](https://doi.org/10.1016/j.jcat.2007.09.018).
- [207] Rytter, E.; Borg, Ø.; Tsakoumis, N. E.; Holmen, A. Water as Key to Activity and Selectivity in Co Fischer-Tropsch Synthesis: γ -Alumina Based Structure-Performance Relationships. *J. Catal.* **2018**, 365, 334–343. DOI: [10.1016/j.jcat.2018.07.003](https://doi.org/10.1016/j.jcat.2018.07.003).
- [208] Wu, H.; Yang, Y.; Suo, H.; Qing, M.; Yan, L.; Wu, B.; Xu, J.; Xiang, H.; Li, Y. Effects of ZrO₂ Promoter on Physic-Chemical Properties and Activity of Co/TiO₂–SiO₂ Fischer–Tropsch Catalysts. *J. Mol. Catal. A Chem.* **2015**, 396, 108–119. DOI: [10.1016/j.molcata.2014.09.024](https://doi.org/10.1016/j.molcata.2014.09.024).
- [209] Johnson, G. R.; Bell, A. T. Effects of Lewis Acidity of Metal Oxide Promoters on the Activity and Selectivity of Co-Based Fischer–Tropsch Synthesis Catalysts. *J. Catal.* **2016**, 338, 250–264. DOI: [10.1016/j.jcat.2016.03.022](https://doi.org/10.1016/j.jcat.2016.03.022).
- [210] Martínez, A. N.; López, C.; Márquez, F.; Díaz, I. Fischer–Tropsch Synthesis of Hydrocarbons over Mesoporous Co/SBA-15 Catalysts: The Influence of Metal Loading, Cobalt Precursor, and Promoters. *J. Catal.* **2003**, 220(2), 486–499. DOI: [10.1016/S0021-9517\(03\)00289-6](https://doi.org/10.1016/S0021-9517(03)00289-6).
- [211] Pedersen, E. Ø.; Svenum, I.-H.; Blekkan, E. A. Mn Promoted Co Catalysts for Fischer-Tropsch Production of Light Olefins – An Experimental and Theoretical Study. *J. Catal.* **2018**, 361, 23–32. DOI: [10.1016/j.jcat.2018.02.011](https://doi.org/10.1016/j.jcat.2018.02.011).
- [212] Dinse, A.; Aigner, M.; Ulbrich, M.; Johnson, G. R.; Bell, A. T. Effects of Mn Promotion on the Activity and Selectivity of Co/SiO₂ for Fischer–Tropsch Synthesis. *J. Catal.* **2012**, 288, 104–114. DOI: [10.1016/j.jcat.2012.01.008](https://doi.org/10.1016/j.jcat.2012.01.008).
- [213] Wang, S.; Yin, Q.; Guo, J.; Zhu, L. Influence of Ni Promotion on Liquid Hydrocarbon Fuel Production over Co/CNT Catalysts. *Energy. Fuels.* **2013**, 27(7), 3961–3968. DOI: [10.1021/ef400726m](https://doi.org/10.1021/ef400726m).
- [214] Li, Z.; Wu, J.; Wu, L. Effect of Zr, Ca and Mn as promoters on the Co/SiC catalysts for the Fischer–Tropsch synthesis. *React. Kinet. Mech. Catal.* **2017**, 122(2), 887–900. DOI: [10.1007/s11144-017-1240-9](https://doi.org/10.1007/s11144-017-1240-9).
- [215] Shi, Z.; Yang, H.; Gao, P.; Chen, X.; Liu, H.; Zhong, L.; Wang, H.; Wei, W.; Sun, Y. Effect of Alkali Metals on the Performance of CoCu/TiO₂ Catalysts for CO₂ Hydrogenation to Long-Chain Hydrocarbons. *Chin. J. Catal.* **2018**, 39(8), 1294–1302. DOI: [10.1016/S1872-2067\(18\)63086-4](https://doi.org/10.1016/S1872-2067(18)63086-4).
- [216] Eliseev, O. L.; Tsapkina, M. V.; Dement'eva, O. S.; Davydov, P. E.; Kazakov, A. V.; Lapidus, A. L. Promotion of Cobalt Catalysts for the Fischer-Tropsch Synthesis with Alkali Metals. *Kinet. Catal.* **2013**, 54(2), 207–212. DOI: [10.1134/s0023158413020055](https://doi.org/10.1134/s0023158413020055).
- [217] Dai, Y.; Yu, F.; Li, Z.; An, Y.; Lin, T.; Yang, Y.; Zhong, L.; Wang, H.; Sun, Y. Effect of Sodium on the Structure-Performance Relationship of Co/SiO₂ for Fischer-Tropsch Synthesis. *Chin. J. Chem.* **2017**, 35(6), 918–926. DOI: [10.1002/cjoc.201600748](https://doi.org/10.1002/cjoc.201600748).
- [218] Eliseev, O. L.; Tsapkina, M. V.; Lapidus, A. L. Fischer–Tropsch synthesis on Cobalt Catalysts with Alkaline Earth Metal Additives. *Solid Fuel Chem.* **2016**, 50(5), 282–285. DOI: [10.3103/s0361521916050050](https://doi.org/10.3103/s0361521916050050).

- [219] Bao, A.; Li, J.; Zhang, Y. Effect of Barium on Reducibility and Activity for Cobalt-Based Fischer-Tropsch Synthesis Catalysts. *J. Natur. Gas Chem.* **2010**, *19*(6), 622–627. DOI: [10.1016/S1003-9953\(09\)60120-1](https://doi.org/10.1016/S1003-9953(09)60120-1).
- [220] Zhang, Y.; Xiong, H.; Liew, K.; Li, J. Effect of Magnesia on Alumina-Supported Cobalt Fischer-Tropsch Synthesis Catalysts. *J. Mol. Catal. A: Chem.* **2005**, *237*(1), 172–181. DOI: [10.1016/j.molcata.2005.04.057](https://doi.org/10.1016/j.molcata.2005.04.057).
- [221] Bao, A.; Liew, K.; Li, J. Fischer-Tropsch Synthesis on CaO-Promoted Co/Al₂O₃ Catalysts. *J. Mol. Catal. A Chem.* **2009**, *304*(1), 47–51. DOI: [10.1016/j.molcata.2009.01.022](https://doi.org/10.1016/j.molcata.2009.01.022).
- [222] Guo, S.; Wang, Q.; Wang, M.; Ma, Z.; Wang, J.; Hou, B.; Chen, C.; Xia, M.; Jia, L.; Li, D. A Comprehensive Insight into the Role of Barium in Catalytic Performance of Co/Al₂O₃ Catalyst for Fischer-Tropsch Synthesis. *Fuel.* **2019**, *256*, 115911. DOI: [10.1016/j.fuel.2019.115911](https://doi.org/10.1016/j.fuel.2019.115911).
- [223] Casci, J. L.; Lok, C. M.; Shannon, M. D. Fischer-Tropsch Catalysis: The Basis for an Emerging Industry with Origins in the Early 20th Century. *Catal. Today.* **2009**, *145*(1), 38–44. DOI: [10.1016/j.cattod.2008.08.032](https://doi.org/10.1016/j.cattod.2008.08.032).
- [224] Wang, L.; Guan, E.; Zhang, J.; Yang, J.; Zhu, Y.; Han, Y.; Yang, M.; Cen, C.; Fu, G.; Gates, B. C.; et al. Single-Site Catalyst Promoters Accelerate Metal-Catalyzed Nitroarene Hydrogenation. *Nat. Commun.* **2018**, *9*(1), 1362–1369. DOI: [10.1038/s41467-018-03810-y](https://doi.org/10.1038/s41467-018-03810-y).
- [225] Cook, K. M.; Perez, H. D.; Bartholomew, C. H.; Hecker, W. C. Effect of Promoter Deposition Order on Platinum-, Ruthenium-, or Rhenium-Promoted Cobalt Fischer-Tropsch Catalysts. *Appl. Catal. A Gen.* **2014**, *482*, 275–286. DOI: [10.1016/j.apcata.2014.05.013](https://doi.org/10.1016/j.apcata.2014.05.013).
- [226] Jermwongratanachai, T.; Jacobs, G.; Shafer, W. D.; Pendyala, V. R. R.; Ma, W.; Gnanamani, M. K.; Hopps, S.; Thomas, G. A.; Kitiyanan, B.; Khalid, S.; et al. Fischer-Tropsch Synthesis: TPR and XANES Analysis of the Impact of Simulated Regeneration Cycles on the Reducibility of Co/Alumina Catalysts with Different Promoters (Pt, Ru, Re, Ag, Au, Rh, Ir). *Catal. Today.* **2014**, *228*, 15–21. DOI: [10.1016/j.cattod.2013.10.057](https://doi.org/10.1016/j.cattod.2013.10.057).
- [227] Botha, J. M.; Visagie, J. L.; Cullen, A.; Taljaard, J. H.; Meyer, R. Patent, WO2016135577, **2018**.
- [228] Lapidus, A. L.; Krylova, A. Y.; Kapur, M. P.; Leongardt, E. V.; Fasman, A. B.; Mikhailenko, S. D. Synthesis of Hydrocarbons from CO and H₂ in the Presence of Co-Ru and Co-Pd Catalysts Containing Aluminum Oxide. *Bull. Russian. Acad. Sci. Division Chem. Sci.* **1992**, *41*(1), 45–48. DOI: [10.1007/bf00863910](https://doi.org/10.1007/bf00863910).
- [229] Iglesia, E.; Soled, S. L.; Fiato, R. A.; Via, G. H. Dispersion, support, and bimetallic effects in Fischer-Tropsch synthesis on cobalt catalysts *Stud. Surf. Sci. Catal.* **1994**, *81*, 433–442. DOI: [10.1016/S0167-2991\(08\)63908-7](https://doi.org/10.1016/S0167-2991(08)63908-7).
- [230] Combes, G. B.; Claridge, J. B.; Gallagher, J. R.; Rosseinsky, M. J.; Boldrin, P. Patent, WO2013054091A1, **2016**.
- [231] Rønning, M.; Tsakoumis, N. E.; Voronov, A.; Johnsen, R. E.; Norby, P.; van Beek, W.; Borg, Ø.; Rytter, E.; Holmen, A. Combined XRD and XANES Studies of a Re-Promoted Co/γ-Al₂O₃ Catalyst at Fischer-Tropsch Synthesis Conditions. *Catal. Today.* **2010**, *155* (3), 289–295. DOI: [10.1016/j.cattod.2009.10.010](https://doi.org/10.1016/j.cattod.2009.10.010).
- [232] Girardon, J.-S.; Constant-Griboval, A.; Gengembre, L.; Chernavskii, P.; Khodakov, A. Optimization of the Pretreatment Procedure in the Design of Cobalt Silica Supported Fischer-Tropsch Catalysts. *Catal. Today.* **2005**, *106*(1–4), 161–165. DOI: [10.1016/j.cattod.2005.07.119](https://doi.org/10.1016/j.cattod.2005.07.119).
- [233] Khodakov, A. Y. Enhancing Cobalt Dispersion in Supported Fischer-Tropsch Catalysts via Controlled Decomposition of Cobalt Precursors. *Braz. J. Phys.* **2009**, *39*(1A), 171–175. DOI: [10.1590/S0103-97332009000200008](https://doi.org/10.1590/S0103-97332009000200008).

- [234] Sun, S.; Fujimoto, K.; Yoneyama, Y.; Tsubaki, N. Fischer–Tropsch Synthesis using Co/SiO₂ Catalysts Prepared from Mixed Precursors and Addition Effect of Noble Metals. *Fuel*. 2002, 81(11–12), 1583–1591. DOI: [10.1016/S0016-2361\(02\)00090-X](https://doi.org/10.1016/S0016-2361(02)00090-X).
- [235] Ruppert, A. M.; Paryczak, T. Pt/ZrO₂/TiO₂ Catalysts for Selective Hydrogenation of Crotonaldehyde: Tuning the SMSI Effect for Optimum Performance. *Appl. Catal. A: Gen.* 2007, 320, 80–90. DOI: [10.1016/j.apcata.2006.12.019](https://doi.org/10.1016/j.apcata.2006.12.019).
- [236] Johnson, G. R.; Werner, S.; Bustillo, K. C.; Ercius, P.; Kisielowski, C.; Bell, A. T. Investigations of Element Spatial Correlation in Mn-Promoted Co-Based Fischer–Tropsch Synthesis Catalysts. *J. Catal.* 2015, 328, 111–122. DOI: [10.1016/j.jcat.2014.12.011](https://doi.org/10.1016/j.jcat.2014.12.011).
- [237] Singh, J. A.; Hoffman, A. S.; Schumann, J.; Boubnov, A.; Asundi, A. S.; Nathan, S. S.; Nørskov, J.; Bare, S. R.; Bent, S. F. Role of Co₂C in ZnO-promoted Co Catalysts for Alcohol Synthesis from Syngas. *ChemCatChem*. 2019, 11(2), 799–809. DOI: [10.1002/cctc.201801724](https://doi.org/10.1002/cctc.201801724).
- [238] Du, H.; Zhu, H.; Liu, T.; Zhao, Z.; Chen, X.; Dong, W.; Lu, W.; Luo, W.; Ding, Y. Higher Alcohols Synthesis via CO Hydrogenation on Fe-Promoted Co/AC Catalysts. *Catal. Today*. 2017, 281, 549–558. DOI: [10.1016/j.cattod.2016.05.023](https://doi.org/10.1016/j.cattod.2016.05.023).
- [239] Voss, G. J. B.; Fløystad, J. B.; Voronov, A.; Rønning, M. The State of Nickel as Promotor in Cobalt Fischer–Tropsch Synthesis Catalysts. *Top. Catal.* 2015, 58(14), 896–904. DOI: [10.1007/s11244-015-0456-z](https://doi.org/10.1007/s11244-015-0456-z).
- [240] Evenrud, V. *Nickel Promoted Cobalt Fischer-Tropsch Catalysts-Effect of Nickel on Reducibility and Cobalt Dispersion*; Norwegian University of Science and Technology (NTNU), Norway, 2012.
- [241] Li, J.; Cheng, X.; Zhang, C.; Yang, Y.; Li, Y. Effects of Alkali on Iron-Based Catalysts for Fischer–Tropsch Synthesis: CO Chemisorptions Study. *J. Mol. Catal. A: Chem.* 2015, 396, 174–180. DOI: [10.1016/j.molcata.2014.10.006](https://doi.org/10.1016/j.molcata.2014.10.006).
- [242] Jiang, F.; Zhang, M.; Liu, B.; Xu, Y.; Liu, X. Insights into the Influence of Support and Potassium or Sulfur Promoter on Iron-Based Fischer–Tropsch Synthesis: Understanding the Control of Catalytic Activity, Selectivity to Lower Olefins, and Catalyst Deactivation. *Catal. Sci. Technol.* 2017, 7(5), 1245–1265. DOI: [10.1039/c7cy00048k](https://doi.org/10.1039/c7cy00048k).
- [243] Xiong, H.; Motchelaho, M. A.; Moyo, M.; Jewell, L. L.; Coville, N. J. Effect of Group I Alkali Metal Promoters on Fe/CNT Catalysts in Fischer–Tropsch Synthesis. *Fuel*. 2015, 150, 687–696. DOI: [10.1016/j.fuel.2015.02.099](https://doi.org/10.1016/j.fuel.2015.02.099).
- [244] Abbaslou, R.; Dalai, A. Patent, CA2757012A1, 2019.
- [245] Tian, Z.; Wang, C.; Yue, J.; Zhang, X.; Ma, L. Effect of a Potassium Promoter on the Fischer–Tropsch Synthesis of Light Olefins over Iron Carbide Catalysts Encapsulated in Graphene-Like Carbon. *Catal. Sci. Technol.* 2019, 9(11), 2728–2741. DOI: [10.1039/c9cy00403c](https://doi.org/10.1039/c9cy00403c).
- [246] Patanou, E.; Lillebø, A. H.; Yang, J.; Chen, D.; Holmen, A.; Blekkan, E. A. Microcalorimetric Studies on Co–Re/γ-Al₂O₃ Catalysts with Na Impurities for Fischer–Tropsch Synthesis. *Ind. Eng. Chem. Res.* 2014, 53(5), 1787–1793. DOI: [10.1021/ie402465z](https://doi.org/10.1021/ie402465z).
- [247] Lee, Y.-L.; Jha, A.; Jang, W.-J.; Shim, J.-O.; Rode, C. V.; Jeon, B.-H.; Bae, J. W.; Roh, H.-S. Effect of Alkali and Alkaline Earth Metal on Co/CeO₂ Catalyst for the Water-Gas Shift Reaction of Waste Derived Synthesis Gas. *Appl. Catal. A: Gen.* 2018, 551, 63–70. DOI: [10.1016/j.apcata.2017.12.009](https://doi.org/10.1016/j.apcata.2017.12.009).
- [248] Jacobs, G.; Davis, B. H. *Reactor Approaches for Fischer–Tropsch Synthesis*. In *Multiphase Catalytic Reactors: Theory, Design, Manufacturing, and Applications*, Önsan, Z. I., Avci, A. K., Eds., John Wiley & Sons, Inc., United States, 2016; pp 269–294. DOI: [10.1002/9781119248491.ch12](https://doi.org/10.1002/9781119248491.ch12).
- [249] Steynberg, A. P.; Dry, M. E.; Davis, B. H.; Breman, B. B. Chapter 2 - Fischer-Tropsch Reactors. *Stud. Surf. Sci. Catal.* 2004, 152, 64–195. DOI: [10.1016/S0167-2991\(04\)80459-2](https://doi.org/10.1016/S0167-2991(04)80459-2).

- [250] Basha, O. M.; Sehabiague, L.; Abdel-Wahab, A.; Morsi, B. I. Fischer–Tropsch Synthesis in Slurry Bubble Column Reactors: Experimental Investigations and Modeling—A Review. *Int. J. Chem. React. Eng.* **2015**, *13*(3), 201–288. DOI: [10.1515/ijcre-2014-0146](https://doi.org/10.1515/ijcre-2014-0146).
- [251] Dancuart, L.; Steynberg, A. Fischer-Tropsch Based GTL Technology: A New Process? *Stud. Surf. Sci. Catal.* **2007**, *163*, 379–399. DOI: [10.1016/S0167-2991\(07\)80490-3](https://doi.org/10.1016/S0167-2991(07)80490-3).
- [252] Sie, S. T.; Krishna, R. Fundamentals and Selection of Advanced Fischer–Tropsch Reactors. *Appl. Catal. A. Gen.* **1999**, *186*(1), 55–70. DOI: [10.1016/S0926-860X\(99\)00164-7](https://doi.org/10.1016/S0926-860X(99)00164-7).
- [253] de Deugd, R. M.; Kapteijn, F.; Moulijn, J. A. Trends in Fischer–Tropsch Reactor Technology—Opportunities for Structured Reactors. *Top. Catal.* **2003**, *26*(1), 29–39. DOI: [10.1023/b:Toca.0000012985.60691.67](https://doi.org/10.1023/b:Toca.0000012985.60691.67).
- [254] Jager, B.; Dry, M. E.; Shingles, T.; Steynberg, A. P. Experience with a New Type of Reactor for Fischer-Tropsch Synthesis. *Catal. Lett.* **1990**, *7*(1), 293–301. DOI: [10.1007/bf00764510](https://doi.org/10.1007/bf00764510).
- [255] Mirzaei, A. A.; Arsalanfar, M.; Bozorgzadeh, H. R.; Samimi, A. A Review of Fischer-Tropsch Synthesis on the Cobalt Based Catalysts. *Phys. Chem. Res.* **2014**, *2*(2), 179–201. DOI: [10.22036/pcr.2014.5786](https://doi.org/10.22036/pcr.2014.5786).
- [256] Shaikh, A.; Al-Dahhan, M. Scale-up of Bubble Column Reactors: A Review of Current State-of-the-Art. *Ind. Eng. Chem. Res.* **2013**, *52*(24), 8091–8108. DOI: [10.1021/ie302080m](https://doi.org/10.1021/ie302080m).
- [257] Jasim, A. A.; Sultan, A. J.; Al-Dahhan, M. H. Influence of Heat-Exchanging Tubes Diameter on the Gas Holdup and Bubble Dynamics in a Bubble Column. *Fuel.* **2019**, *236*, 1191–1203. DOI: [10.1016/j.fuel.2018.09.049](https://doi.org/10.1016/j.fuel.2018.09.049).
- [258] Guettel, R.; Kunz, U.; Turek, T. Reactors for Fischer-Tropsch Synthesis. *Chem. Eng. Technol.* **2008**, *31*(5), 746–754. DOI: [10.1002/ceat.200800023](https://doi.org/10.1002/ceat.200800023).
- [259] Basu, S. Design-Development of Fischer-Tropsch Synthesis Reactor & Catalysts and their Interrelationship. *Bull. Catal. Soc. India.* **2007**, *6*, 1–21.
- [260] Wang, Y.-N.; Xu, -Y.-Y.; Li, Y.-W.; Zhao, Y.-L.; Zhang, B.-J. Heterogeneous Modeling for Fixed-Bed Fischer–Tropsch Synthesis: Reactor Model and its Applications. *Chem. Eng. Sci.* **2003**, *58*(3), 867–875. DOI: [10.1016/S0009-2509\(02\)00618-8](https://doi.org/10.1016/S0009-2509(02)00618-8).
- [261] Yang, J. H.; Kim, H.-J.; Chun, D. H.; Lee, H.-T.; Hong, J.-C.; Jung, H.; Yang, J.-I. Mass transfer limitations on Fixed-Bed Reactor for Fischer–Tropsch Synthesis. *Fuel Process. Technol.* **2010**, *91*(3), 285–289. DOI: [10.1016/j.fuproc.2009.10.010](https://doi.org/10.1016/j.fuproc.2009.10.010).
- [262] Vishwas Govind, P. *Design of Multiphase Reactors*; John Wiley & Sons, Inc., United States, **2015**; pp 47–86.
- [263] Schmidt, P.; Batteiger, V.; Roth, A.; Weindorf, W.; Raksha, T. Power-to-Liquids as Renewable Fuel Option for Aviation: A Review. *Chem. Ing. Tech.* **2018**, *90*(1–2), 127–140. DOI: [10.1002/cite.201700129](https://doi.org/10.1002/cite.201700129).
- [264] Loewert, M.; Hoffmann, J.; Piermartini, P.; Selinsek, M.; Dittmeyer, R.; Pfeifer, P. Microstructured Fischer-Tropsch Reactor Scale-up and Opportunities for Decentralized Application. *Chem. Eng. Technol.* **2019**. DOI: [10.1002/ceat.201900136](https://doi.org/10.1002/ceat.201900136).
- [265] LeViness, S.; Tonkovich, A.; Jarosch, K.; Fitzgerald, S.; Yang, B.; McDaniel, J. Improved Fischer-Tropsch Economics Enabled by Microchannel Technology. *White paper generated by Velocys.* **2011**, 1–7.
- [266] <http://www.velocys.com>.
- [267] Deshmukh, S. R.; Tonkovich, A. L. Y.; Jarosch, K. T.; Schrader, L.; Fitzgerald, S. P.; Kilanowski, D. R.; Lerou, J. J.; Mazanec, T. J. Scale-Up of Microchannel Reactors For Fischer–Tropsch Synthesis. *Ind. Eng. Chem. Res.* **2010**, *49*(21), 10883–10888. DOI: [10.1021/ie100518u](https://doi.org/10.1021/ie100518u).
- [268] Todić, B.; Ordonsky, V. V.; Nikačević, N. M.; Khodakov, A. Y.; Bukur, D. B. Opportunities for Intensification of Fischer–Tropsch Synthesis Through Reduced

- Formation of Methane over Cobalt Catalysts in Microreactors. *Catal. Sci. Technol.* **2015**, *5*(3), 1400–1411. DOI: [10.1039/C4CY01547A](https://doi.org/10.1039/C4CY01547A).
- [269] Holmen, A.; Venvik, H. J.; Myrstad, R.; Zhu, J.; Chen, D. Monolithic, Microchannel and Carbon Nanofibers/Carbon Felt Reactors for Syngas Conversion by Fischer-Tropsch Synthesis. *Catal. Today*. **2013**, *216*, 150–157. DOI: [10.1016/j.cattod.2013.06.006](https://doi.org/10.1016/j.cattod.2013.06.006).
- [270] Bradford, M. C. J.; Te, M.; Pollack, A. Monolith Loop Catalytic Membrane Reactor for Fischer-Tropsch Synthesis. *Appl. Catal. A. Gen.* **2005**, *283*(1), 39–46. DOI: [10.1016/j.apcata.2004.12.032](https://doi.org/10.1016/j.apcata.2004.12.032).
- [271] Schanke, D.; Bergene, E.; Holmen, A. US Patent, US6211255B1, **2001**.
- [272] Pangarkar, K.; Schildhauer, T. J.; van Ommen, J. R.; Nijenhuis, J.; Kapteijn, F.; Moulijn, J. A. Structured Packings for Multiphase Catalytic Reactors. *Ind. Eng. Chem. Res.* **2008**, *47*(10), 3720–3751. DOI: [10.1021/ie800067r](https://doi.org/10.1021/ie800067r).
- [273] Becker, H.; Güttel, R.; Turek, T. Performance of Diffusion-Optimised Fischer-Tropsch Catalyst Layers in Microchannel Reactors at Integral Operation. *Catal. Sci. Technol.* **2019**, *9*(9), 2180–2195. DOI: [10.1039/c9cy00457b](https://doi.org/10.1039/c9cy00457b).
- [274] Pangarkar, K.; Schildhauer, T. J.; van Ommen, J. R.; Nijenhuis, J.; Moulijn, J. A.; Kapteijn, F. Heat Transport in Structured Packings with Co-Current Downflow of Gas and Liquid. *Chem. Eng. Sci.* **2010**, *65*(1), 420–426. DOI: [10.1016/j.ces.2009.08.018](https://doi.org/10.1016/j.ces.2009.08.018).
- [275] Myrstad, R.; Eri, S.; Pfeifer, P.; Rytter, E.; Holmen, A. Fischer-Tropsch Synthesis in a Microstructured Reactor. *Catal. Today*. **2009**, *147*, S301–S304. DOI: [10.1016/j.cattod.2009.07.011](https://doi.org/10.1016/j.cattod.2009.07.011).
- [276] Knobloch, C.; Güttel, R.; Turek, T. Holdup and Pressure Drop in Micro Packed-Bed Reactors for Fischer-Tropsch Synthesis. *Chem. Ing. Tech.* **2013**, *85*(4), 455–460. DOI: [10.1002/cite.201200202](https://doi.org/10.1002/cite.201200202).
- [277] Knochen, J.; Güttel, R.; Knobloch, C.; Turek, T. Fischer-Tropsch Synthesis in Milli-Structured Fixed-Bed Reactors: Experimental Study and Scale-up Considerations. *Chem. Eng. Process. Process. Intens.* **2010**, *49*(9), 958–964. DOI: [10.1016/j.cep.2010.04.013](https://doi.org/10.1016/j.cep.2010.04.013).
- [278] Schildhauer, T. J.; Pangarkar, K.; van Ommen, J. R.; Nijenhuis, J.; Moulijn, J. A.; Kapteijn, F. Heat Transport in Structured Packings with Two-Phase Co-current Downflow. *Chem. Eng. J.* **2012**, *185–186*, 250–266. DOI: [10.1016/j.cej.2011.11.054](https://doi.org/10.1016/j.cej.2011.11.054).
- [279] Pangarkar, K.; Schildhauer, T. J.; van Ommen, J. R.; Nijenhuis, J.; Moulijn, J. A.; Kapteijn, F. Experimental and Numerical Comparison of Structured Packings with a Randomly Packed Bed Reactor for Fischer-Tropsch Synthesis. *Catal. Today*. **2009**, *147*, S2–S9. DOI: [10.1016/j.cattod.2009.07.035](https://doi.org/10.1016/j.cattod.2009.07.035).
- [280] Lešnik, J. Univerza v Novi Gorici, Heat Transfer in Structured Packings for Fischer-Tropsch Synthesis; University of Nova Gorica, Faculty of Environmental Sciences, Slovenia, **2010**.
- [281] Wiryadinata, S.; Jenkins, B.; Kornbluth, K.; Erickson, P. Experimental and Numerical Study into the Effects of Passive Flow Disturbance on Conversion and C_{7+} Yield of the Packed Bed Fischer Tropsch Reaction. *Fuel*. **2019**, *254*, 1–11. DOI: [10.1016/j.fuel.2019.05.154](https://doi.org/10.1016/j.fuel.2019.05.154).
- [282] Krishna, R.; Sie, S. T. Strategies for Multiphase Reactor Selection. *Chem. Eng. Sci.* **1994**, *49*(24, Part A), 4029–4065. DOI: [10.1016/S0009-2509\(05\)80005-3](https://doi.org/10.1016/S0009-2509(05)80005-3).
- [283] Moulton, S. A.; Weimer, A. W. Patent, WO2016081513A1, **2016**.
- [284] Wang, Y.; Tonkovich, A. L.; Mazanec, T.; Daly, F. P.; VanderWiel, D.; Hu, J.; Cao, C.; Kibby, C.; Li, X. S.; Briscoe, M. D. US Patent, US7084180B2, **2012**.